POLYMER-SUPPORTED METAL-ORGANIC FRAMEWORKS FOR ADSORPTION AND CATALYSIS

A Dissertation
Presented to
The Academic Faculty

by

Jacob Deneff

In Partial Fulfillment
of the Requirements for the Degree
Doctor of Philosophy in the
School of Chemical and Biomolecular Engineering

Georgia Institute of Technology
August 2019

POLYMER-SUPPORTED METAL-ORGANIC FRAMEWORKS FOR ADSORPTION AND CATALYSIS

Approved by:

Dr. Krista Walton, Advisor
School of Chemical and Biomolecular Engineering
Georgia Institute of Technology

Dr. Sven Behrens
School of Chemical and Biomolecular Engineering
Georgia Institute of Technology

Dr. Ryan Lively
School of Chemical and Biomolecular Engineering
Georgia Institute of Technology

Dr. Mark Losego
School of Materials Science and Engineering
Georgia Institute of Technology

Dr. Carson Meredith
School of Chemical and Biomolecular Engineering
Georgia Institute of Technology

Date Approved: May 20, 2019

ACKNOWLEDGEMENTS

I would first like to thank my academic advisor Dr. Krista Walton. She cultivated an environment of intellectual freedom and cooperation in her group that allowed all members to work and grow together. Without her guidance and the group dynamic she fostered I would not have been able to so effectively improve my skills as an independent researcher and contributing member of a research group. The Walton research group itself has been a welcoming, friendly place, and I am particularly thankful to all of its members for their contributions both to my research and to my enjoyment of my time at Tech.

I would also like to acknowledge the other members of the Tech community who contributed to this work. My PhD committee members, Dr. Lively, Dr. Meredith, Dr. Behrens, and Dr. Losego offered advice on areas outside of my or my group's expertise. The Kohl, Jones, and Koros group offered the use of their instruments and, often, their liquid nitrogen without which I would never have been able to characterize all of my materials. Rod Sefton the building manager for Bunger-Henry and his staff kept everything running and made sure we always got our packages on time.

Finally, I would like to acknowledge my family. My parents are responsible for sparking my interest in science, math, and technology. They were supportive throughout my education, and always gave me the encouragement and resources I needed to excel. My brother has been supportive as well and has provided stiff competition in the race to graduation that has helped me complete the program. Finally, my wife who has been endlessly supportive throughout my PhD studies and without whom I would never have made it this far.

TABLE OF CONTENTS

LIST OF TABLES

LIST OF FIGURES

LIST OF SYMBOLS AND ABBREVIATIONS

BET	Brunauer-Emmett-Teller
BET SA	BET Surface Area
CWA	Chemical Warfare Agent
DMF	Dimethylformamide
DMNP	Dimethyl Nitrophenylphosphate (methyl paraoxon)
HEMA	2-Hydroxyethyl Methacrylate
HIPE	High Internal Phase Emulsion
IGA	Intelligent Gravimetric Analyzer
MMM	Mixed Matrix Membrane
MOF	Metal-Organic Framework
Mw	Molecular Weight
NIPS	Nonsolvent Induced Phase Separation
polyHIPE	Polymerized HIPE
PSA	Pressure Swing Adsorption
PSM	Post-Synthetic Modification
PVDF	Polyvinylidene Difluoride
PXRD	Powder X-Ray Diffraction
RH	Relative Humidity
SBS	Solution Blow Spinning
SEM	Scanning Electron Microscopy
TGA	Thermogravimetric Analysis
THF	Tetrahydrofuran

TIC	Toxic Industrial Chemical
TMEDA	Tetramethylethylene Diamine
TOF	Turnover Frequency
TSA	Temperature Swing Adsorption
XRD	X-Ray Diffraction

SUMMARY

Metal-organic frameworks (MOFs) are hybrid materials with a variety of applications, including adsorption and catalysis. They have been proposed as new materials for use in industrial processes, including carbon capture, natural gas purification, and gas separation via temperature or pressure swing adsorption. They have also been examined for protection against toxic chemicals, including both toxic industrial chemicals like ammonia and chlorine, and chemical warfare agents like Soman and VX. In particular, a significant amount of research has coalesced around zirconium MOFs like UiO-66, which combine stability and chemical tunability making them suited for a wide variety of target adsorbates and for applications in organophosphate hydrolysis.

MOFs and other materials like them suffer in real applications because of their form as fine powders, which are prone to high pressure drop and maldistribution of flow in packed beds and are ill-suited to any applications in adsorption beyond packed beds. In order to apply them more broadly and effectively, MOFs must be combined with supporting material to create structured composites optimized for the form and transport requirements of a specific application.

This dissertation examines two broad categories of composites. The first is high internal phase emulsion templated foams. In these, a polymeric support is created via a cast of the external phase of an emulsion. This process creates a stiff, open cell foam that can be molded based on the shape of the container it was cured in and which allows access to MOF particles embedded within the bulk of the composite via diffusion through the macroporous foam. These composites could be structured for applications in pressure

swing or flow-through adsorption in ways not possible for bulk polymers, which would create insurmountable diffusion limitations within the structure.

The second category of composites examined in this dissertation is MOF-bearing polymeric fibers. For applications in personal protection, self-detoxifying fibers are a significant step in creating uniforms and equipment resistant to chemical threats. Incorporating MOFs with the desired capacity or catalytic characteristics into fibers could create such textiles. The solution blow spinning process outlined here provides a method for rapid synthesis and direct application of fibers to a desired surface, making it possible to supplement existing equipment or seal gaps that may exist in current protective measures.

This dissertation examines the structured composites outlined above, and the effects of the polymeric support material on the ability of the MOF to adsorb target chemicals or catalyze chemical reactions. In general, the inclusion of polymer diminishes the ability of the MOF to accomplish these tasks. However, alterations to the synthesis procedures were found that significantly improved MOF accessibility within the composite, restoring or nearly restoring the full capacity of the MOF while retaining the mechanical and transport related benefits of the structured polymeric support.

CHAPTER 1. INTRODUCTION

1.1 Toxic Chemicals

Chemical warfare agents (CWAs) are chemicals whose primary purpose is to be deployed aggressively during wartime. Their use on a large scale began with chlorine gas in World War I and has progressed to include blistering agents like sulfur mustard and choking agents like phosgene. After World War I a new class of CWAs called nerve agents were developed based on organophosphate pesticides.[1] These affect acetylcholinesterase binding sites in the body, and can cause paralysis, suffocation, and cardiac arrest. These nerve agents have been used both against military and civilian targets in the past, although they are officially being demilitarized after 1993.[2-3] They remain a potential threat both to the military and to the general public through the possibility of terror attacks.

Because of their toxicity, CWAs are subject to regulations that make them difficult to obtain and deploy. They may also have delivery mechanisms that make them difficult to deliver aggressively. However other chemicals are more easily obtained, including toxic industrial chemicals (TICs). TICs are substances that have industrial applications and are toxic enough to pose threats to human life or property.[4] They include ammonia, chlorine, carbon monoxide, and sulfur dioxide.[5] While their toxicity is lower than that of CWAs, TICs are manufactured and transported on a massive scale and, while regulated, are under less scrutiny than traditional CWAs. Their quantity and relative ease of access make TICs an equal or greater threat both from accidental release and from deliberate, targeted attack.

Both CWAs and TICs remain a threat to military and public safety in the modern era. As insurgency and asymmetrical warfare continue to rise, TICs in particular may become an even larger threat given their greater quantity and vulnerability. Materials to supplement or replace existing protective equipment in order to provide accessible, broad spectrum protection from toxic chemicals are needed to address this potential hazard.

1.2 Adsorbents

Adsorbent materials are well established within the field of personal protection. The current standard filtration system is a particulate filter paired with ASZM-TEDA, a porous carbon sorbent impregnated with additional elements to provide active sites for adsorption of chemicals that do not interact strongly with the carbon.[6-7] Beyond personal protection, adsorbents have drawn interest in a variety of processes including natural gas purification and carbon capture. Adsorbents have gained interest as alternatives to solvent based processes for gas separation in fields like carbon capture and natural gas purification. This is primarily because of the significantly lower energy costs of regeneration for adsorbents compared to solvents, which often contain large amounts of water as a diluent. Adsorbents are also much less corrosive than many commonly used solvents, making them attractive for reducing equipment costs as well.[8-9] Pressure and temperature swing adsorption in packed beds or fluidized reactors are commonly proposed for industrial applications and are based on a difference in adsorbent capacity between two different operating conditions. Adsorbent capacity and selectivity are determined by the surface area of the material, chemical functionality of the surface, and molecular sieving effects based on the average pore size. The overall performance of the material is based on a combination of its equilibrium properties, e.g. capacity and selectivity, the kinetics of transport and adsorption

in the material, and the regeneration cost. Both personal protection and industrially relevant applications require adsorbents suited to the specific gases or vapors being targeted for separation, as well as forms suited to the required transport and mechanical characteristics of the system.

1.3 Metal Organic Frameworks

Metal-organic frameworks (MOFs) are hybrid porous solids made up of metal or metal oxide clusters connected by multidentate organic linkers.[10] They are crystalline, with narrow pore size distributions in the micro to mesoporous range, large surface areas, and high pore volumes, making them attractive for a variety of applications including catalysis[11-13], gas storage[14-15], separations[16-18], and sensing[19-21]. MOFs are conventionally synthesized in solvothermal reactions by combining metal salts and linkers, which then self-assemble at moderate temperatures (25-250 °C). The solvent occupying the pore space after synthesis can be removed via heat and vacuum, leaving the crystalline structure with empty pore space, termed an "activated" MOF. A conceptual diagram of MOF synthesis is shown in Figure 1. Most actively studied MOFs are stable even after guest removal, and MOFs in general are typically stable up to at least 300 °C, although MOF stability in general remains an active area of study.

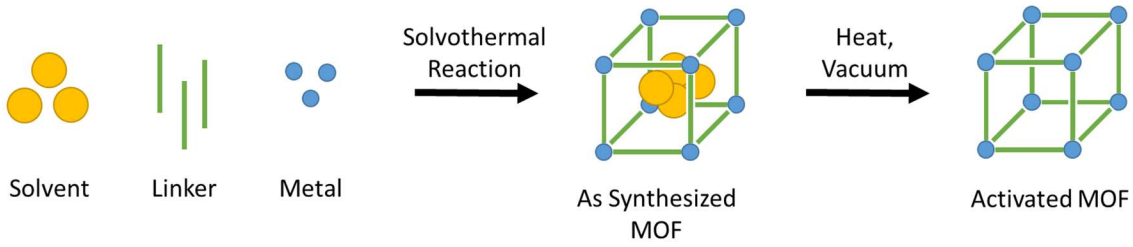

Figure 1 MOF synthesis conceptual diagram

Because of their hybrid structure, MOFs have significant chemical versatility, with thousands of different structures reported using many different metals and linkers. Several families of MOFs exist that retain their overall structure even with different metal centers or chemical functionalities created by pendant groups covalently bonded to the linker, making these MOFs modular in terms of their chemistry.[22-25] Their porosity, structural diversity, and chemical tunability make MOFs ideal for adsorptive or catalytic applications that require specific chemical environments or active sites.

1.3.1 UiO-66

One widely studied MOF of interest in this work is UiO-66. UiO-66 is a zirconium MOF with terephthalic acid linkers.[26] Each metal cluster is 12-connected, and the MOF is remarkably stable and can survive exposure to most common solvents and temperatures up to 520 °C.[27] Its water stability in particular makes UiO-66 interesting, as water is known to degrade or contribute to the degradation of a significant number of other MOFs, limiting their potential applications in real-world situations.[28] UiO-66 can also be easily functionalized via the inclusion of pendant groups on the linker molecule and by defect modulation, often with little modification of the overall synthetic procedure.[23, 29-34] The structure of the MOF itself and an example of an amino-functionalized linker are shown in Figure 2. The functionalized variants of UiO-66 retain the overall structure of the parent

MOF, including its stability and high surface area. Functionalization allows UiO-66 to be tailored to target specific adsorbates based on their chemistry, making it a platform MOF that can enable many different separation processes. In addition to its potential as an adsorbent, UiO-66 has also been shown to catalyze the hydrolysis of organophosphate compounds, a category of chemicals including pesticides and nerve agents like sarin and VX.[2, 11, 35] Its stability, tunability, and potential for catalysis make UiO-66 an ideal material for removal or detoxification of toxic chemicals, including both toxic industrial chemicals like ammonia[29, 36] and nitrogen dioxide[16, 32], as well as chemical warfare agents. It could supplement existing protective equipment to provide additional, broad spectrum protection.

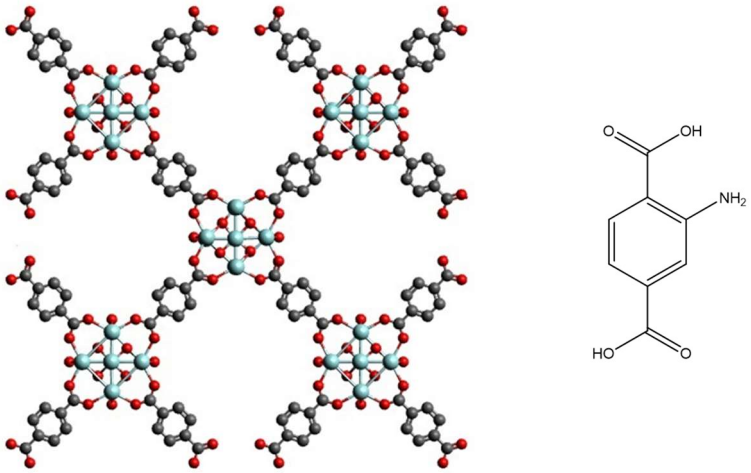

Figure 2 Structure of UiO-66 (left), and the amino functionalized 2-aminoterephthalic acid linker

1.4 Structured Adsorbents

MOFs are typically synthesized and studied at the lab scale as fine powders. This form becomes a drawback as the processes are scaled up and specific applications are

targeted, however. Powdered materials are limited to packed beds for separations, as they must be contained to be utilized. Powder in a packed bed is prone to channeling and maldistribution of the gas flowing through it and may fluidize at high flow rates. Pressure drop across the bed also becomes a problem as the length of the bed increases, making scale up beyond the lab difficult.[37] Other applications are affected by the difficulty of handling powders, the mechanical stability of the packed beds, or the prevention of attrition and loss through dust formation. To be utilized efficiently and at larger scales, powders must be processed into forms that are more suited to the process they are to be used for.

One common form for processed powders is pellets or beads. Their larger size prevents dense packing and can reduce pressure drop, channeling, and fluidization. However, beads introduce the problem of intra-particle diffusion.[38] The time scale of diffusion into large beads can be unacceptably long for rapid, cyclical separations or for single pass filtration, resulting in a significant quantity of unused adsorbent. As bead size is reduced to compensate, pressure drop and the other issues with powders become significant again. In addition to these general problems, many MOFs cannot be pelletized without altering their structure and lowering their adsorption capacity or reducing their chemical and thermal stability.[29, 39-40] For these reasons non-particulate adsorbent structures are attractive as alternatives.

Non-particulate adsorbents can take several forms including monoliths, membranes or laminates, foams, and fibers. Their use is intended to improve mass transfer within the adsorbent bed, increase space efficiency, lower pressure drop, and allow efficient heat transfer.[37] They are also useful in applications that require specific formed structures beyond beds or flow through units.

1.4.1 Monoliths

Monoliths can refer to either solid bodies of polymer or other material[41-42] or to honeycomb monoliths, which are bundles of parallel channels, separated by thin walls.[43-44] Solid monoliths are used for chromatography and liquid phase separations and some have incorporated MOFs to improve their separation. They are rarely used for gases or high flow rates due to their low overall permeability and the high pressure drop that would result. Honeycomb monoliths are more suited to flow through applications involving gases or requiring high throughput. They allow flow only in the axial direction and reduce pressure drop compared to packed beds. Gas adsorption occurs only on the channel surfaces, and monoliths have been reported with as many as 16,000 channels per square inch[45], creating a large surface area in contact with the gas. MOFs have been incorporated into monoliths via growth on the monolith substrate[46] or by extrusion of the MOF with a binder into a monolith shape.[47-48] In the first case, the monolith substrate required pretreatment in order to ensure good adherence of the MOF film to the substrate but performed well in cyclical adsorption experiments. In the second case the synthesis method was simplified, but the addition of plasticizers was required to extrude the MOF-binder mixture, and the final composites were prone to manufacturing inconsistencies and a loss of MOF capacity due to the binder blocking the MOF.

1.4.2 Membranes

The synthesis of membrane composites is a well-explored field of study, and MOFs have been included in them both as selective surface layers and as fillers in mixed matrix membranes (MMMs).[49-51] Until recently, however, membrane studies were primarily

concerned with enhancing the membrane selectivity or permeability rather than with the performance of the MOF itself as an active adsorbent material. Newer studies have begun to examine the adsorptive properties of MOFs in membranes, particularly in MMMs, with the polymer existing primarily as a mechanical support and an added source of selectivity or chemical stability. In one study, the use of hydrophobic polymer materials was found to improve the stability of water sensitive MOFs in humid environments without a significant loss of MOF surface area.[52] For polymers with poor permeability, the performance of these composites as adsorbents was found to depend on the total MOF loading.[53] At low loadings the MOF is entirely contained in the polymer, and the composite surface area and adsorption capacity are reduced to zero. At higher loading, contact between MOF particles becomes more extensive and can form a percolating network, in which adsorbates can diffuse through the MOF network, bypassing the polymer entirely.[54] Membranes and laminates can be formed into corrugated or spiral-wound modules that function in the same way as honeycomb monoliths.

1.4.3 Fibers

Fibers are another possible form for MOF composites, both for traditional separation operations and because they may be incorporated directly into clothing, filters, or other protective equipment directly. Broadly, MOF may either be grown directly on the surface of prefabricated fibers or embedded in the fiber during its production.

In the case of surface growth on prefabricated fibers, the fibers are typically submerged in a solution of the metal salt and organic linker, and then allowed to go through one or more cycles of solvothermal synthesis.[55-57] The MOF is supported by a flexible fiber

core that provides nucleation sites and structural support. However, the loading produced by this method can be difficult to control, and the strength of MOF adherence to the surface depends on pretreatments or specific surface characteristics of the fiber. This limits the materials that can be used to fabricate these composites, and the solvothermal synthesis may limit the rate of composite production.

Embedding pre-made MOF into fibers as the fibers are being produced is a method that allows loading to be more finely controlled. One method for producing MOF-embedded fibers is extrusion of a polymer solution into a non-solvent bath.[58] The non-solvent induces phase separation, resulting in porous fibers containing accessible MOF particles. This method is similar to the one used to produce hollow fiber membranes, and the adsorbent fibers can be made hollow as well to allow heat transfer fluid to be flowed through their cores.[59] MOF bearing fibers have also been produced via electrospinning using a feed solution containing suspended MOF particles.[60-62] This method can produce nanofibers, rendering the MOF accessible to adsorbates through polymer permeability or by reducing fiber sizes to length scales similar to the MOF particle diameter. Like membranes, fibers produced in this way have shown utility as both structural supports and chemical supplements, improving the stability of the MOF by preventing chemicals that could destabilize or destroy it from entering the fiber.

1.5 Project Motivation

The goal of this thesis is to utilize polymer structures to provide mechanical support for MOF particles and to create structured adsorbent composites with forms suited to specific applications. Two broad categories of composite are examined: polymer foams

produced via emulsion templated polymerization and polymer fibers produced via solution blow spinning. Both composites contain embedded MOF particles, and methods to improve the adsorption performance of the composites by increasing MOF accessibility within the polymer matrix are explored. Foams provide a platform for producing large, three-dimensional composite structures molded to suit a specific application, like air purification or carbon capture, while fibers may be incorporated directly into clothing or deposited as a nonwoven barrier to toxic chemicals. In this dissertation, the primary focus is on the performance of MOF-polymer composites in adsorption, although the materials studied are also intended to be capable of organophosphate hydrolysis.

CHAPTER 2. HYDROPHILIC MOF@POLYHIPE COMPOSITES

2.1 Introduction

Metal-organic frameworks are hybrid materials with applications as catalysts and adsorbents. Their as-synthesized powder form is unsuited to traditional flow through applications because the small particle size would result in high pressure drop, channeling, and material loss via fluidization and mechanical attrition. A solid polymeric binder could provide mechanical stability to the powder and could be molded into shapes suited to specific applications. Because a solid polymer would create a significant diffusion barrier, this chapter focuses on polymer foams to provide support while creating a hierarchical structure that maintains access to the internal MOF.

2.1.1 High Internal Phase Emulsion Templated Polymers

A high internal phase emulsion (HIPE) is a mixture of two immiscible fluids in which the internal, or droplet, phase makes up 74% or more of the total volume of the mixture.[63] HIPEs consist of large droplets of the internal phase surrounded by a thin film of the external phase, stabilized by particles or surfactants. If monomers and crosslinkers are included in the external phase, polymerization can be initiated resulting in a rigid polymer structure that holds the shape of the external phase. Once polymerization is complete the internal phase can be removed and the resulting polyHIPE will retain its macroporous foam structure with the solidified external phase now surrounding empty voids.[64] This permanent porosity does not require solvent induced swelling to open and introduces tortuosity as opposed to the straight axial channels of a honeycomb monolith, making it attractive for

gas adsorption processes. PolyHIPE structure can be varied with voids ranging from 1 to 100 μm in diameter, different internal phase volume fractions, and open or closed cell foam. They may also be formed from a variety of monomers, including styrene[65-66], acrylamide[67], and acrylic acid[68]. PolyHIPEs take the shape of the container in which they are cured, and so are most commonly utilized as cylindrical or cubic monoliths although they could feasibly be molded into any desired shape.

2.1.2 MOF@polyHIPE

Composites of MOFs and polyHIPEs, termed MOF@polyHIPE materials, have been reported in the past. One study presented a monolithic polyHIPE that was modified with hydrophilic surface groups to allow the MOF HKUST-1 to be grown on its surface.[69] Another used polyacrylamide as a polyHIPE material in the form of beads, allowing the copper open metal sites in HKUST-1 to interact with the polyHIPE surface directly, without modification.[70] In both studies the polyHIPE was soaked in the MOF precursor solution during MOF synthesis, creating a layer of MOF on the internal surfaces of the polyHIPE. A third study utilized a polyurethane foam as the polyHIPE support for the MOF UiO-66 but noted that the MOF grew in the voids of the foam, rather than on its surfaces.[71] An alternate approach to growing the MOF on a polyHIPE support was examined by Calvez et al. who synthesized the MOF and polyHIPE together in a single step.[72] Finally, two groups examined the possibility of embedding the MOF directly in the polyHIPE by mixing it in before initiating polymerization. In one case the MOF itself was used as an emulsion stabilizer in place of a surfactant.[73] In the other case the MOF was simply mixed into a preformed emulsion before polymerization proceeded.[74] The second group observed that the BET surface areas of the composites were lower than expected,

however, and suggested that the polymer was blocking the pores of the MOF. They were able to alter the polymerization step to achieve higher surface areas in the final composites.

2.2 Materials and Methods

2.2.1 Materials

All chemicals were available commercially and were used as received: 2-hydroxyethyl methacrylate (Aldrich, 97% with ≤250 ppm monomethyl ether hydroquinone), N,N'-methylene bisacrylamide (Sigma-Aldrich, 99%), ammonium persulfate (Sigma-Aldrich, ≥98%), Kolliphor P 188 (Sigma), cyclohexane (Sigma-Aldrich, ≥99%), N,N,N',N'-tetramethylethylenediamine (TMEDA) (Aldrich, ≥99.5%), zirconium chloride (Aldrich, ≥99.5%), terephthalic acid (Aldrich, 98%), and 2-aminoterephthalic acid (Acros Organics, 99%).

2.2.2 PolyHIPE Synthesis

The polyHIPE was synthesized according to a previously reported procedure with 13% crosslinker.[74-75] 1.03 mL of 2-hydroxyethyl methacrylate, 200 mg of methylene bisacrylamide, 35 mg of ammonium persulfate, and 750 mg of Kolliphor P188 surfactant were added to 2.60 g deionized water and stirred for 10 minutes to combine. 11 mL of cyclohexane was added to the aqueous solution dropwise while stirring constantly, and the entire emulsion was left to stir for 30 minutes. After the formation of the emulsion, 0.15 mL of a 20% aqueous TMEDA solution was added, acting as a redox pair with the ammonium persulfate to induce polymerization at low temperatures. The emulsions were quickly transferred to syringes where they were cured for 24 hours at room temperature.

After being removed from the syringes the cured polyHIPE samples were washed in distilled water and dried at 80 °C in an isothermal oven.

2.2.3 MOF Synthesis

UiO-66-NH_2 was synthesized according to a modified version of the procedure presented by Peterson et al.[29] 5.448 mmol each of 2-aminoterephthalic acid and zirconium chloride were added to a mixture of 212 ml DMF and 0.8 ml distilled water. After complete dissolution of the reactants the mixture was divided into 8 glass vials and placed in an isothermal oven for 24 hours at 120 °C. The products were combined after being removed from the oven and washed 3x with DMF and 3x with methanol.

UiO-66 was prepared using a nearly identical procedure, replacing the 2-aminoterephthalic acid with an equimolar amount of terephthalic acid and omitting the water.

All MOF samples were sieved using a 40-mesh sieve to break up powder aggregates after drying. Before use in further synthesis MOF samples were re-activated at 110 °C under vacuum to remove adsorbed water and any remaining solvent.

2.2.4 MOF@polyHIPE

MOF@polyHIPE composites were prepared as follows. After preparing the emulsion as described above, 1000 mg of emulsion was placed in each of several syringes with their tapered tips cut off. Activated MOF was weighed and mixed into each syringe using a spatula until the mixture became homogenous. 0.05 mL of the 20% aqueous TMEDA solution was added to the composite mixture in each syringe and stirred using a

spatula for 30 seconds. The composites were then left to cure in the upright syringes for 24 hours, washed with distilled water, and dried at 80 °C in an isothermal oven. Composites containing both UiO-66 and UiO-66-NH_2 were synthesized. A summary of the synthesis is shown in Figure 3.

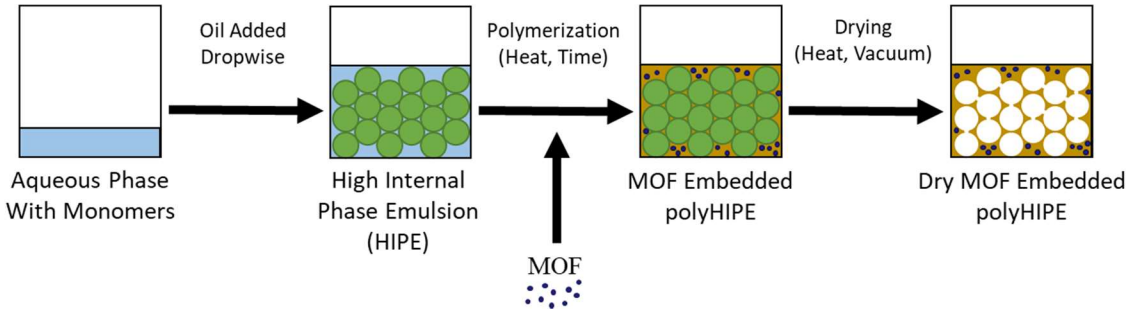

Figure 3 Diagram showing synthesis steps for MOF@polyHIPE composites

2.2.5 Catalysis

To examine the catalytic properties of the composites their behaviour toward the simulant dimethylnitrophenylphosphate (DMNP) was tested. 4 µL of DMNP was added to a 1 mL buffer solution of 0.45 M N-ethylmorpholine in water. 2.5 mg of sample was added, and the concentration of product monitored over 1 hour via UV-vis spectroscopy.

2.2.6 Characteriztion

Powder X-ray diffraction (PXRD) patterns were obtained using a Panalytical XPert PRO Alpha-1 XRD. SEM images were taken with a LEO 1530 FE-SEM. TGA measurements were taken using a NETZSCH STA 449 F1 Jupiter Instrument. Nitrogen physisorption data was obtained using a Quantachrome Quadrasorb Evo. An intelligent gravimetric analyzer (IGA-1) was used for carbon dioxide adsorption. Samples were outgassed at 80 °C before adsorption to remove residual solvent.

2.3 Results and Discussion

Composites were successfully synthesized containing both UiO-66-NH_2 and unfunctionalized UiO-66, to determine the effect of the functional group on the structure and performance of the composites. Each composite was given a nominal MOF content, determined by the mass of the MOF added to the emulsion before polymerization and the mass of the final, dry composite. The nominal loading varied slightly between batches but was averaged across batches for comparison.

The PXRD pattern for the MOF parent material matches the expected pattern for UiO-66 NH_2, confirming the MOF's identity and crystallinity. The pattern remains unchanged for the MOF@polyHIPE composites as shown in Figure 4, indicating no change in crystallinity due to incorporation into the polymer or reaction with the components of the unpolymerized emulsion. The polyHIPE parent material is amorphous and contributes no peaks to the patterns. IR spectra were used to confirm the identity of the polyHIPE by a comparison of the peaks measured to those reported by Wickenheisser and Janiak[74]. Based on this data, we conclude that the MOF was not structurally or chemically affected by the polymer or the polymerization, and the monomers were successfully and completely polymerized.

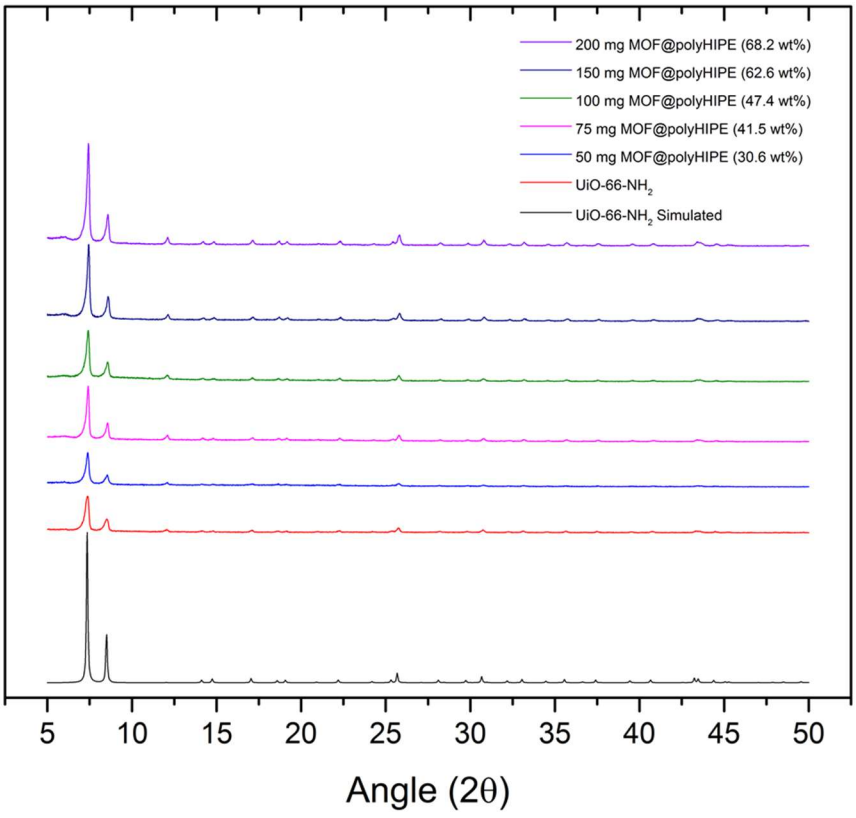

Figure 4 PXRD patterns for UiO-66-NH_2 and MOF@polyHIPE composites

SEM images of the composites containing UiO-66-NH_2 can be seen in Figure 5. The typical polyHIPE structure for this material consists of an open cell foam with large voids 10-30 µm in diameter connected by smaller pores 2-4 µm in diameter. At low MOF loadings, up to 47.4% MOF, the composites maintain that structure with the addition of small clusters of MOF embedded in the polymer of the void walls. The MOF appears to be well embedded in the polymer, rather than resting on the surface or in the voids. At higher loadings the polyHIPE structure is more disturbed by incorporation of the MOF. While macroporosity still exists, the voids deform, and large MOF aggregates are visible distorting the polymer structure. The change in structure is also noticeable in the mechanical stability of the composites, with higher loading composites being much more

brittle and granular compared to those with lower MOF content. It appears that, as the MOF volume in the composites approaches and exceeds the polymer volume, the polymer can no longer effectively bind the MOF together without distorting. The MOF ceases to be embedded in the polyHIPE structure's walls and instead aggregates and is covered by the polymer, with macropores mainly existing between the polymer coated aggregates.

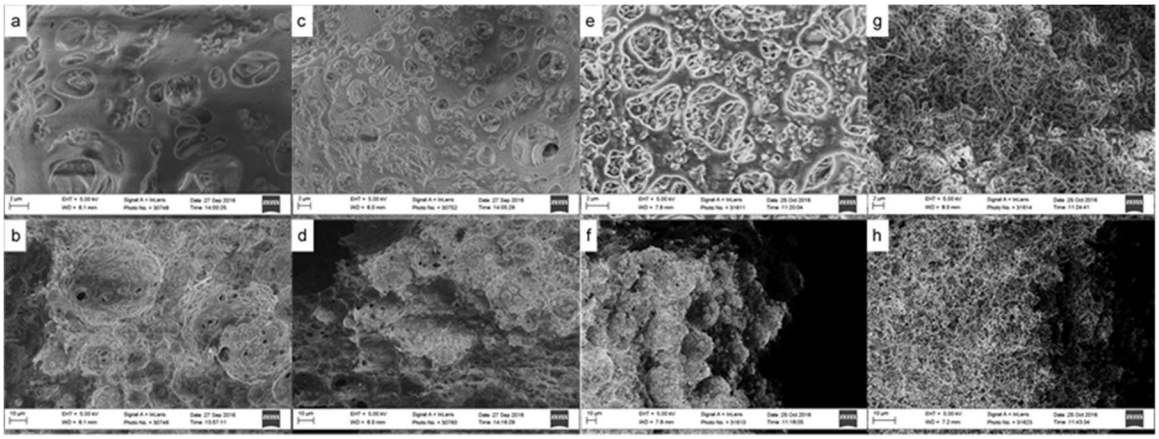

Figure 5 SEM images of MOF@polyHIPE composites. a,b 50 mg (30.6%); c,d 75 mg (41.5%); e,f 100 mg (47.4%); g,h 150 mg (62.6%)

Composites containing the un-functionalized parent UiO-66 can be seen in Figure 6. Morphologically these composites are identical to the ones containing the functionalized UiO-66-NH_2, with small MOF particles embedded in the walls of the large voids formed by the polymer. As the MOF content is increased, the same distortion of the polyHIPE structure occurs as well. The lack of an amine functional group and the slight increase in hydrophobicity it causes does not have an effect on the composite morphology.

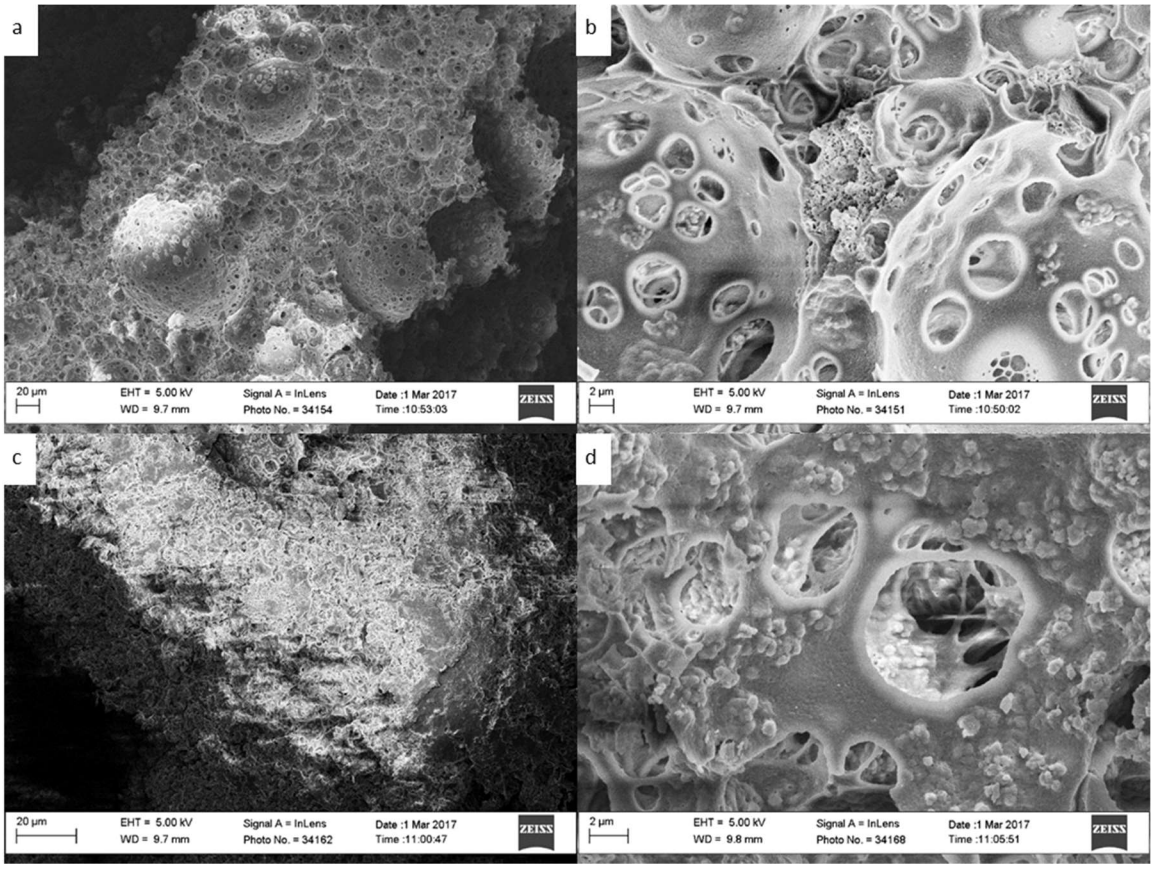

Figure 6 SEM images of UiO-66@polyHIPE composites. a,b: 50 mg (30.6%); c,d: 150 mg (62.6%)

2.3.1 BET

BET surface areas of both the parent materials and the composites were calculated based on nitrogen physisorption at 77 K, and can be seen in Table 1. The parent MOF is highly microporous and will contribute to the surface area of the composite while the polymer is only macroporous and has no consistently measurable BET surface area. Because of this the polymer can be expected to contribute only structural support and additional mass.

The MOF content of each sample based on the mass added during synthesis is termed the nominal MOF content. After measuring the BET surface areas of the composites, an apparent MOF mass percent can be calculated by comparing the values of the composite surface area and the parent MOF surface area. A comparison between the nominal MOF content and BET based MOF content for the composites is shown in Figure 7. For every sample the MOF content based on BET surface area was significantly lower than the nominal MOF content. This result indicates that a portion of the MOF is inaccessible to the nitrogen used in BET analysis and is not contributing to the surface area of the composites. While the composite surface areas were higher than the polymer alone, a significant amount of MOF does not participate in adsorption, and the efficiency of the composites is reduced as a result.

Table 1 BET data for MOF@polyHIPE composites

MOF Added [mg]	Nominal MOF Content	BET SA Measured [m^2/g]	MOF Content Based on BET
50	30.6 %	75.7	7.0 %
75	41.5 %	130.7	12.1 %
100	47.4%	196.6	18.2 %
150	62.6 %	245.1	22.7 %
200	68.2%	324.6	30.0 %

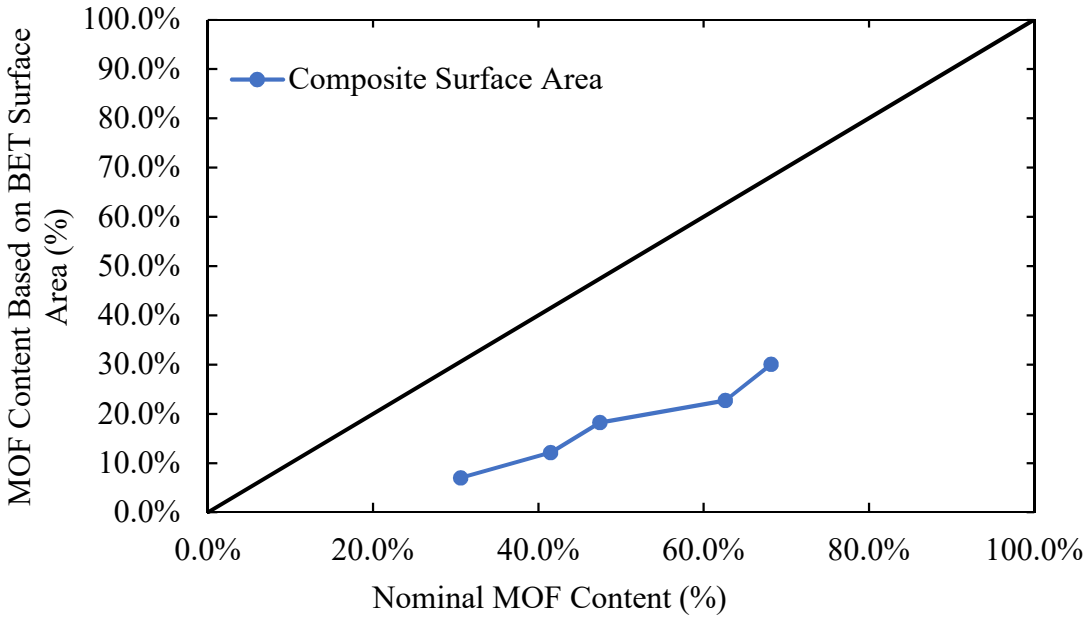

Figure 7 Comparison of nominal MOF content in MOF@polyHIPE composites with the calculated loading based on their BET surface areas. Black line is 1:1 ideal case

The lower than expected surface areas could be attributed to four factors: (i) degradation of the MOF structure on incorporation into the polymer, (ii) pore blocking within the MOF by monomers or other components of the polymer solution, (iii) interactions with the polymeric surfactant, or (iv) encapsulation by the polymer blocking the surface of the MOF and rendering it inaccessible to nitrogen. Based on PXRD patterns we conclude that the MOF's crystallinity is unchanged by incorporation into the polymer and no new peaks arise to indicate development of new crystal phases, suggesting that MOF degradation is not responsible for the lower surface areas. Pore blocking by monomers, surfactant interactions, and encapsulation in the polymer can be addressed through modifications to the polyHIPE composite synthesis. These possibilities are addressed further in the following chapter.

2.3.2 CO_2 Adsorption

To probe the accessibility of the MOF particles at higher temperatures, CO_2 adsorption was measured at 25 °C for composites fabricated with UiO-66-NH_2. Adsorption isotherms for the MOF, polymer, 30.6% MOF composite (low MOF content), and 62.2% MOF composite (high MOF content) are shown in Figure 8. The adsorption follows a type 1 isotherm and there is no hysteresis on desorption. At every pressure tested in the isotherm an ideal theoretical value for the composite CO_2 loading was calculated by a weighted average of the nominal loadings of the parent materials. A non-ideal theoretical value was also calculated using the loadings of parent materials based on the BET surface area.

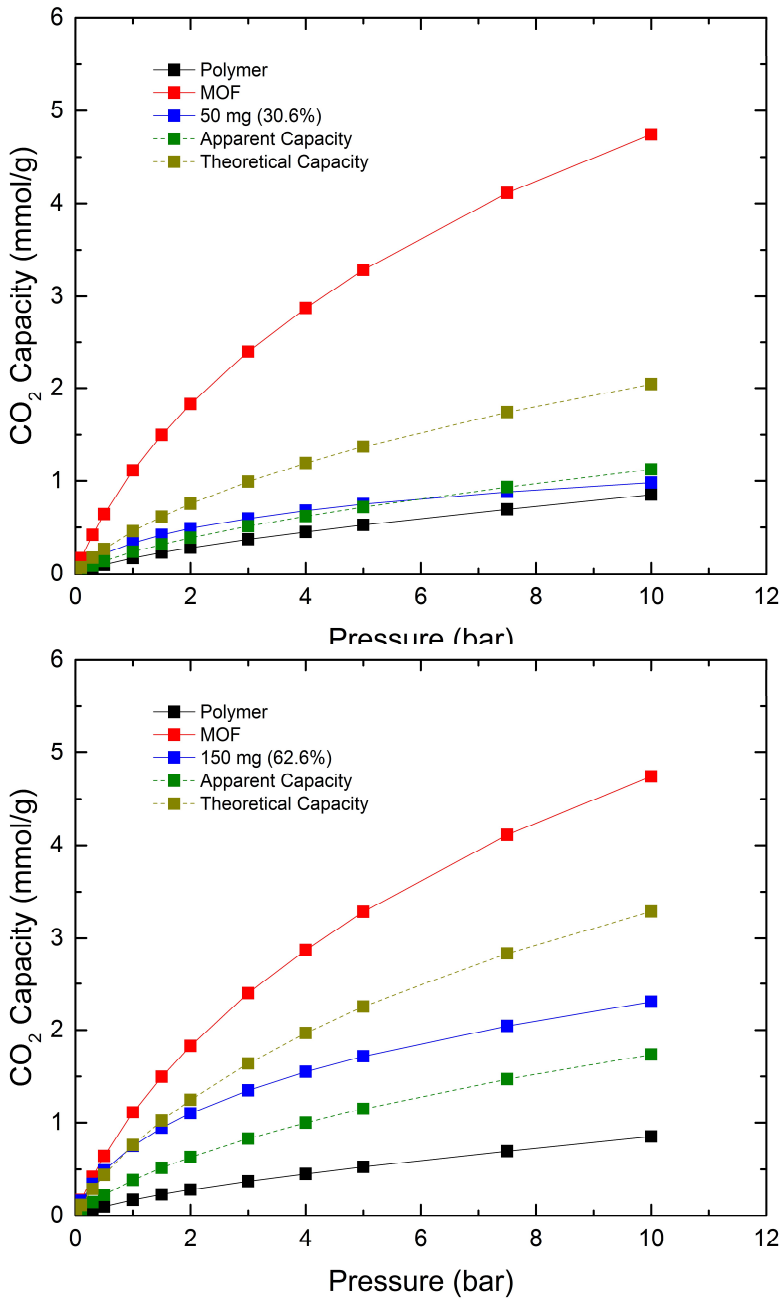

Figure 8 CO_2 adsorption isotherms for pure and composite materials. Top: Low loading composite (30.6 wt% MOF); Bottom: High loading composite (62.6 wt% MOF)

For the low MOF-content composite, the CO_2 capacity at low pressure is what would be expected based on the nominal MOF content. However, as the pressure increases the

deviation from the theoretical loading increases as well, reaching only 48% of the calculated ideal value at 10 bar. This composite exceeds its calculated BET-based capacities below 5 bar but tracks with those calculated values above that. The high MOF-content composite behaves similarly, agreeing with its ideal calculated capacities below 1 bar, and falling to 70% of its calculated capacity at 10 bar. This composite remains above its calculated BET-based capacities for the entire isotherm, always adsorbing more CO_2 than predicted based on BET surface area.

This CO_2 adsorption above the calculated BET-based capacity without exceeding the ideal calculated capacity is likely in part due to the polymer, which contributes nothing to the surface area of the composite but will add to the CO_2 capacity. It may also be an indication that the polymer is allowing CO_2 at room temperature to pass through abd reach MOF particles that could not be accessed by nitrogen at 77 K. Despite this, the composites generally did not reach their ideal calculated CO_2 capacities, particularly at high pressures. This suggests that there are either significant diffusion limitations for MOF particles embedded deeply in the polymer, or that these completely embedded particles are not accessible at all, even to CO_2 at room temperature. The significantly higher performance by the high loading composite over the low loading composite may be explained by the creation of percolative pathways between aggregated or otherwise contacting MOF particles. It has been observed that permeability to CO_2 increases significantly at high MOF loadings in mixed matrix membranes, as an interconnected network of MOF crystals is formed, allowing the gas to move more efficiently to and between them.[53-54] The low loading composite is below this threshold, and it is assumed that the MOF is more isolated and more likely to be covered completely by polymer.

2.3.3 DMNP Catalysis

The catalytic performance of the composites was evaluated using the half-life ($t_{1/2}$) values determined by the experiments assuming first order kinetics and the turn-over frequency (TOF) of the material, which could be normalized based on MOF content. TOF is calculated by dividing the rate of product production by the concentration of active sites in the catalyst multiplied by the mass of the catalyst. The TOF for the samples examined here could be determined from the actual MOF loading or from the effective MOF loading calculated based on BET surface area. The data is summarized in Table 2. UiO-66-NH_2 had a $t_{1/2}$ of 20 min, while the 30.6% and 62.2% composites had $t_{1/2}$ of 726 min and 155 min respectively. The catalysis of DMNP by the composites is significantly slower than that by the MOF, even accounting for the lower mass of MOF present in the composites. The TOF values for the composites are also much lower than for the parent MOF when normalized by the mass of the MOF present in the tested sample. Both values confirm the assumptions based on the composite adsorption performance, that a portion of the MOF is inaccessible. However, when the MOF content is back-calculated using the BET surface area, the TOF values agree closely between the MOF and the composites. The BET surface area appears to correlate with the amount of MOF in the composite taking part in catalysis. This is consistent with the idea that some part of the polymer or emulsion mixture is blocking the MOF active sites, and that the DMNP cannot diffuse through whatever barrier is present. Based on this result, the BET surface area is used as the primary metric of performance for future composites. This shortcut is necessary given the difficulties of testing a large number and variety of composites for catalytic activity using DMNP.

Table 2 DMNP catalysis data for MOF@polyHIPE composites and parent materials

MOF Content (wt%)	Percent of MOF Surface Area	$t_{1/2}$ [min]	TOF from MOF Content [min^{-1}]	TOF from BET Surface Area [min^{-1}]
0.0	0.0	90,798	-	-
30.6	7.0	726	15.1	64.5
62.6	22.7	155	30.1	78.5
100	100	20	78.3	78.3

2.4 Conclusions

We have successfully created composites of the MOF UiO-66-NH_2 in a hydrogel polyHIPE by mixing the MOF into the monomer solution and allowing it to become embedded during polymerization. PXRD and IR confirmed the identity of the MOF and polymer and that they were not degraded in the synthesis. The polyHIPE maintained its macroporous structure up to 62.6% MOF loading as seen in SEM images of the composites. BET surface areas were lower than expected for these composites, likely because large portions of the MOF were inaccessible to nitrogen due to embedding. Prepolymerization of the polyHIPE and use of unfunctionalized UiO-66 in additional syntheses confirmed that simple embedding is the likely cause of the reduction. CO_2 adsorption isotherms of the composites and their parent materials suggests the MOF is accessible at room temperature to gases that can pass through the polymer, though there are diffusion limitations. For both nitrogen and CO_2 the composites represented an improvement in performance over the polymer alone.

Our findings suggest that MOF@polyHIPE materials may be useful as structured adsorbents for gases, with their permanent macroporosity making them more effective than un-templated MOF@polymer composites. More study into the polymer-particle interactions and the polymerization conditions may increase MOF accessibility and uptakes. An examination of the catalytic properties of the composites is also desirable, as the swelling behavior of the poly(2-hydroxyethyl methacrylate) may render the MOF much more accessible to chemical species in aqueous mixtures. With their ability to bind powders together and retain a rigid shape, these composites could be used in the future to fabricate macroporous, three-dimensional adsorbent and catalytic structures in applications where powders would be disadvantageous or rapid diffusion throughout the structure is necessary.

CHAPTER 3. MORPHOLOGY MODIFICATIONS TO HYDROPHILIC

3.1 Introduction

Based on the results of the previous chapter, particularly the lower than expected BET surface areas of the composites based on their actual MOF content, it is apparent that the MOF is being obstructed by some component of the polymer material. This phenomenon has been observed in many studies of MOF@polyHIPE composites. Several possible causes exist and will be explored in this chapter. The first possibility is that the pores of the MOF are being blocked by monomers small enough to enter them. A second possibility is that the polymer is covering the surface of a portion of the MOF too completely to allow adsorbates to penetrate. A third possibility is that interactions between the surfactant, a long chain triblock co-polymer, and the surface of the MOF are causing the pores to become obstructed. Potential solutions are presented below.

3.1.1 Prepolymerization

Beginning the polymerization of the high internal phase emulsion is one method for preventing the MOF pores from being blocked by small molecules entering the framework. By forming larger oligomers before incorporating the MOF, small molecules will be less likely to enter the MOF pores and cause surface area reductions. In the past this method was used with MIL-101(Cr) to produce MOF@polyHIPE composites with increased surface area.[74] That study found that at higher MOF loadings the composite surface area could be doubled via prepolymerization, although the theoretical maximum surface area

was still unattainable. Prepolymerization was accomplished by adding a small amount of the polymerization catalyst and allowing it to react before incorporating the MOF and adding the remaining catalyst.

3.1.2 Post-Synthetic Modification of MOF Surface

To address the polymer covering the surface of the MOF, modifications to that surface may be necessary. A large amount of work has been done on post-synthetic modification (PSM) of MOFs.[76-77] Because pendant groups can easily be included on their linkers, reactions using click-chemistry or other methods to directly modify these linkers are relatively common. MOFs containing amine pendant groups like IRMOF-3 and UiO-66-NH_2 have been targeted in the past because of their ability to form amide bonds. A study by Cohen et al found that the extent of modification could be controlled by controlling the size of the molecule used for PSM.[78] They found that alkyl anhydrides could be reacted with amine groups on MOFs to form amides, and that the length of the alkyl chain determined the extent of the reaction. An example of this reaction is shown in Figure 9. Chains up to 6 carbons long resulted in conversions of 90% or higher of the amine functional groups to amides with grafted alkanes. At 12 carbons the conversion was reduced to 31%, and at 18 carbons to 11%. They also observed that the BET surface area of the modified MOF initially decreased with increasing alkyl chain length but was recovered after a threshold length was reached. These observations suggest that the longer chains preferentially functionalized the surface of the MOF particles because of the diffusion limitations of the large molecules. Using this method, the MOF particles can be modified without significantly sacrificing porosity or surface area.

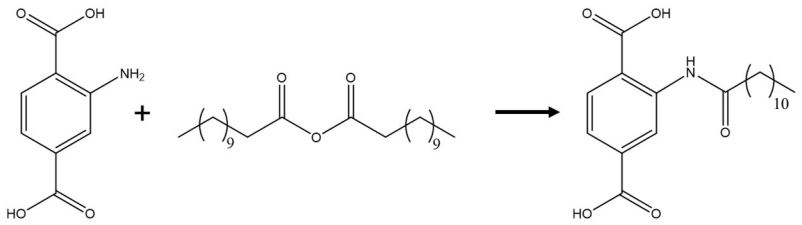

Figure 9 PSM reaction diagram using dodecanoic anhydride and 2-aminoterephthalic acid

Because UiO-66-NH_2 is hydrophilic, it will preferentially partition into the aqueous phase of the high internal phase emulsion. After polymerization of the monomers in that aqueous phase, the MOF will be embedded in the polymer that results, potentially creating a barrier to adsorbates. By selectively functionalizing the surface of the MOF particles with long alkyl chains the particles can be made hydrophobic without significantly reducing their surface area, preventing them from partitioning into the aqueous phase and being completely covered by the polymer.

3.1.3 Pickering Emulsions

A method for addressing both MOF embedding in the polymer and potential interactions between the MOF and the surfactant is the use of Pickering emulsions in polyHIPE synthesis. A Pickering emulsion is stabilized by particles rather than a surfactant, resulting in a more stable emulsion due to the stronger absorption of the particles at the oil-water interface.[79-80] The location of the MOF at the oil-water interface will also allow the walls of the resulting porous polymer to be completely functionalized with MOF particles, significantly reducing the diffusion barrier caused by the polymer. Because little to no surfactant is required, any interactions between the MOF and the surfactant will also be reduced.

Pickering emulsions have been created with a variety of materials.[81-83] Recently the use of the MOF UiO-66 was reported to successfully stabilize high internal phase emulsions with up to 90 vol% internal phase.[73] When solidified using a polymer additive, the MOF particles were bound together and remained at the surface of the resulting polymeric structure. This study did not examine the use of these composites as adsorbents, however, and was limited in the maximum loading of MOF that could be achieved.

3.2 Materials and Methods

3.2.1 Materials

All chemicals were available commercially and were used as received: 2-hydroxyethyl methacrylate (Aldrich, 97% with ≤250 ppm monomethyl ether hydroquinone), N,N'-methylene bisacrylamide (Sigma-Aldrich, 99%), ammonium persulfate (Sigma-Aldrich, ≥98%), Kolliphor P 188 (Sigma), cyclohexane (Sigma-Aldrich, ≥99%), N,N,N',N'-tetramethylethylenediamine (TMEDA) (Aldrich, ≥99.5%), zirconium chloride (Aldrich, ≥99.5%), terephthalic acid (Aldrich, 98%), and 2-aminoterephthalic acid (Acros Organics, 99%).

3.2.2 UiO-66

UiO-66-NH_2 was synthesized according to the procedure given in Chapter 2 of this thesis. 5.448 mmol each of 2-aminoterephthalic acid and zirconium chloride were added to a mixture of 212 ml DMF and 0.8 ml distilled water. After complete dissolution of the reactants the mixture was divided into 8 glass vials and placed in an isothermal oven for

24 hours at 120 °C. The products were combined after being removed from the oven and washed 3x with DMF and 3x with methanol.

UiO-66 was prepared using a nearly identical procedure, replacing the 2-aminoterephthalic acid with an equimolar amount of terephthalic acid and omitting the water. To limit particle size and prevent aggregation, 30 molar equivalents of acetic acid were added to the synthesis as a modulator.

All MOF samples were sieved using a 40-mesh sieve to break up powder aggregates after drying. Before use in further synthesis MOF samples were re-activated at 110 °C under vacuum to remove adsorbed water and any remaining solvent.

3.2.3 Prepolymerization

The synthesis followed the polyHIPE procedure from Chapter 2 of this thesis with some modification. 1.03 mL of 2-hydroxyethyl methacrylate, 200 mg of methylene bisacrylamide, 35 mg of ammonium persulfate, and 750 mg of Kolliphor P188 surfactant were added to 2.60 g deionized water and stirred for 10 minutes to combine. 11 mL of cyclohexane was added to the aqueous solution dropwise, and the entire emulsion was left to stir for 22 hours. After this time, 60 µL of a 20% aqueous solution of TMEDA was added to the emulsion and stirred for 3 minutes. The emulsion was divided into 1000 mg portions in separate syringes, mixed with activated MOF using a spatula until homogeneous, and then combined with an additional 30 µL of the TMEDA solution and stirred using a spatula. The emulsions were left to polymerize for 24 hours before being removed washed in deionized water. The composites were dried at 80 °C for 24 hours in an isothermal oven.

3.2.4 Post-Synthetic Modification

UiO-66-NH_2 was used for PSM experiments. 78 mg of dodecanoic anhydride was dissolved in 8 mL of chloroform. 60 mg of activated UiO-66-NH_2 was added to the solution and allowed to stand for 24 hours. The solid MOF was recovered via filtration, rinsed three times with chloroform, then soaked in chloroform for 72 hours, with the solvent replaced every 24 hours. The final solid product was activated at 100 °C under vacuum for 24 hours before use.

The composites were prepared using the standard MOF@polyHIPE synthesis from Chapter 2 of this thesis. The modified MOF described above was substituted for the original parent material, but otherwise no modifications were made.

3.2.5 Pickering Emulsions

Unfunctionalized UiO-66 was used to synthesize the Pickering emulsion composites. Pickering emulsions were synthesized via a modified version of the procedure described in Chapter 2 of this thesis. 0.28 mL of 2-hydroxyethyl methacrylate, 58 mg of methylene bisacrylamide, and 10 mg of ammonium persulfate were dissolved in 0.72 g of deionized water. 4 mL of cyclohexane was added over 1 minute while mixing at 15,000 rpm using a homogenizer. 50 µL of 20 vol% aqueous TMEDA was added to the emulsion and mixed again with the homogenizer for 15 seconds. The completed emulsion was transferred to a syringe and left to cure at room temperature for 24 hours before being rinsed in water and dried at 80 °C for 24 hours. Based on this procedure, the MOF loading in the final dry composite was 13 wt%.

To examine the effects on the morphology of the composites, some surfactant (Kolliphor P188) was included in a set of Pickering samples. The amount of surfactant is given as a percentage of the concentration in the standard synthesis, and samples containing 0.1%, 1%, 10%, and 25% were synthesized.

3.2.6 Characterization

Powder X-ray diffraction (PXRD) patterns were obtained using a Panalytical XPert PRO Alpha-1 XRD. SEM images were taken with a LEO 1530 FE-SEM. Nitrogen physisorption data was obtained using a Quantachrome Quadrasorb Evo. Samples were outgassed at 80 °C before adsorption to remove residual solvent.

3.3 Results and Discussion

3.3.1 Prepolymerization

Prepolymerization of the polyHIPE composites did not change any of their macroscopic characteristics of the final product relative to the standard synthesis. SEM images showing the microscopic structure of the composites are shown in Figure 10. While the average void size is the same as the standard synthesis for low MOF loadings, the size distribution is much more uniform. This can be attributed partially to the significantly longer stirring time, and partially to the prepolymerization. The longer stirring time will create more uniform droplet size, and prepolymerization will ensure that those droplets do not have time to coalesce or ripen, resulting in a much more uniform foam after polymerization. At low MOF loadings, the structure of the emulsion is not significantly affected by the MOF particles, and they can be seen embedded in the walls of the polymer

in the same way as they appear in the standard synthesis. At higher loadings the structure is significantly affected by the incorporation of the MOF. While the composite is still macroporous, the polymer separates into strands connecting MOF aggregates rather than forming a cast of the emulsion. The prepolymerization may make the polymer more prone to deformation when exposed to shear, with the MOF dragging the polymer out of place rather than becoming embedded in it.

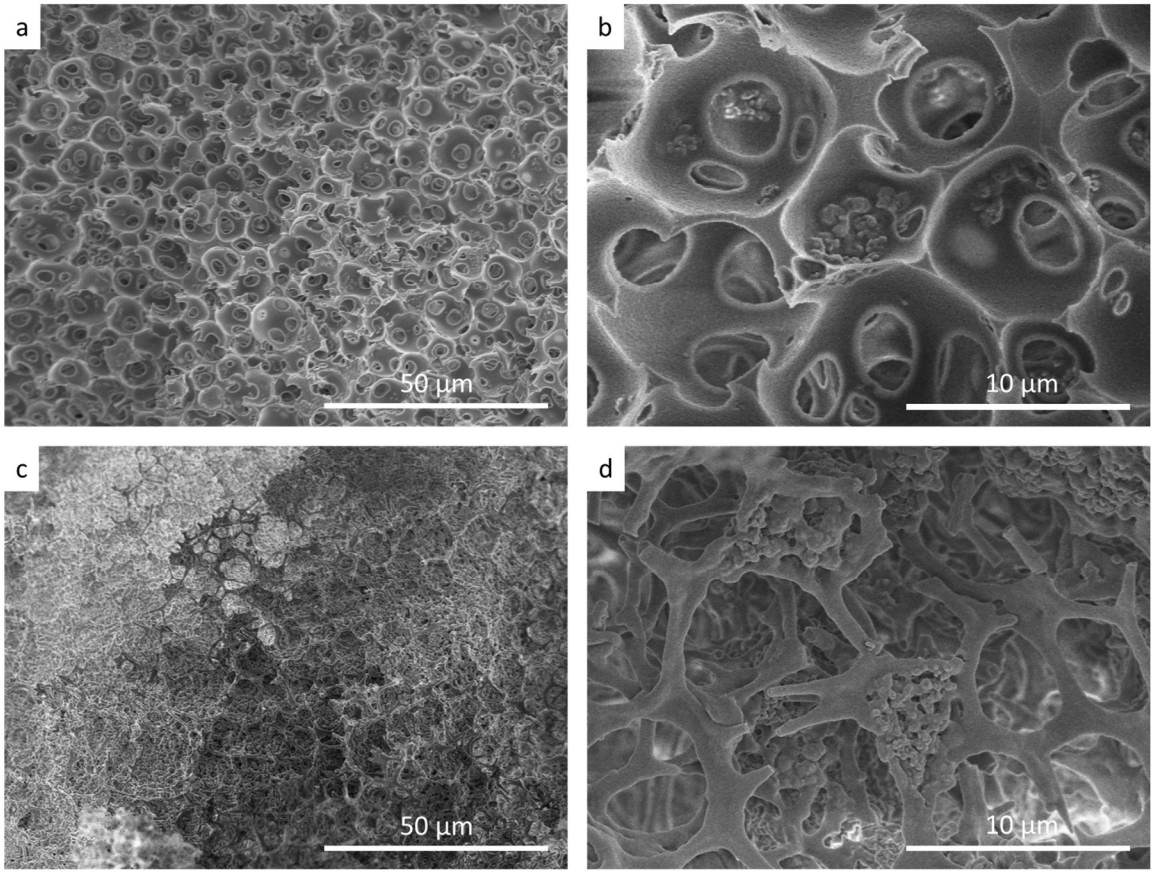

Figure 10 SEM images of prepolymerized MOF@polyHIPE composites containing UiO-66-NH_2. a,b: 50 mg (30.6%); c,d: 150 mg (62.6%)

As in the previous chapter, nitrogen physisorption and BET analysis was used to determine MOF accessibility within the composites. As shown in Figure 11, prepolymerization had no significant effect on the surface area of the composites. This

result contradicts previously reported data for the MOF MIL-101. Prepolymerization may result in higher surface areas for MIL-101 composites because both the MOF particle size and the MOF pore size are larger, making it more difficult for the polymer to completely cover individual particles and easier for monomers to enter and block the MOF pores. UiO-66 particles are smaller and have much smaller pore sizes, making them less affected by the changes created by prepolymerization.

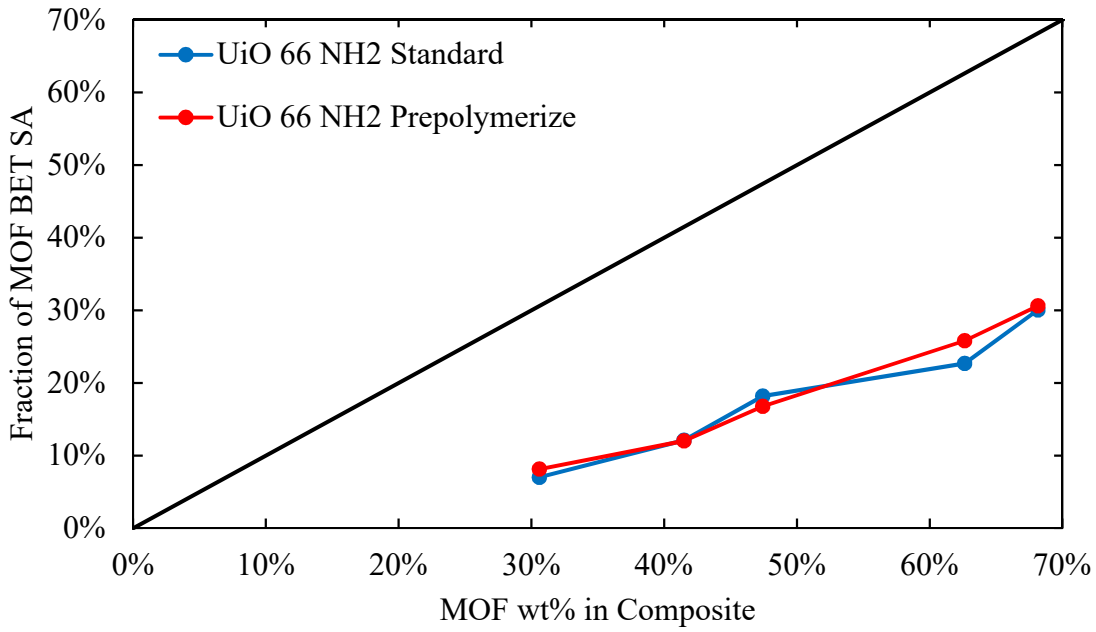

Figure 11 Comparison of actual MOF content in standard and prepolymerized MOF@polyHIPE composites with the percent of MOF surface area their measured surface areas represent. Black line is 1:1 ideal case

3.3.2 Post-Synthetic Modification

PolyHIPE composites containing alkane modified MOFs were significantly more brittle and prone to dust formation than composites produced from the original MOF. The cause is apparent in the SEM images, shown in Figure 12. While some portions of the

polyHIPE retain the foam structure seen in the original synthesis, a significant portion of the structure has collapsed or is dominated by MOF aggregates. In areas with relatively low MOF loading some MOF particles can be seen on the surface of the polymer, rather than embedded in it, and the polyHIPE structure is unchanged. However, in MOF rich areas the inclusion of the hydrophobic particles broke the emulsion, creating structures similar to what is expected in a bulk polymer composite. Because the polymer does not interact closely with the MOF based on the hydrophobicity of the particles, and the MOF rich areas create weak points in the structure that can easily form cracks and breaks, resulting in overall lower mechanical stability.

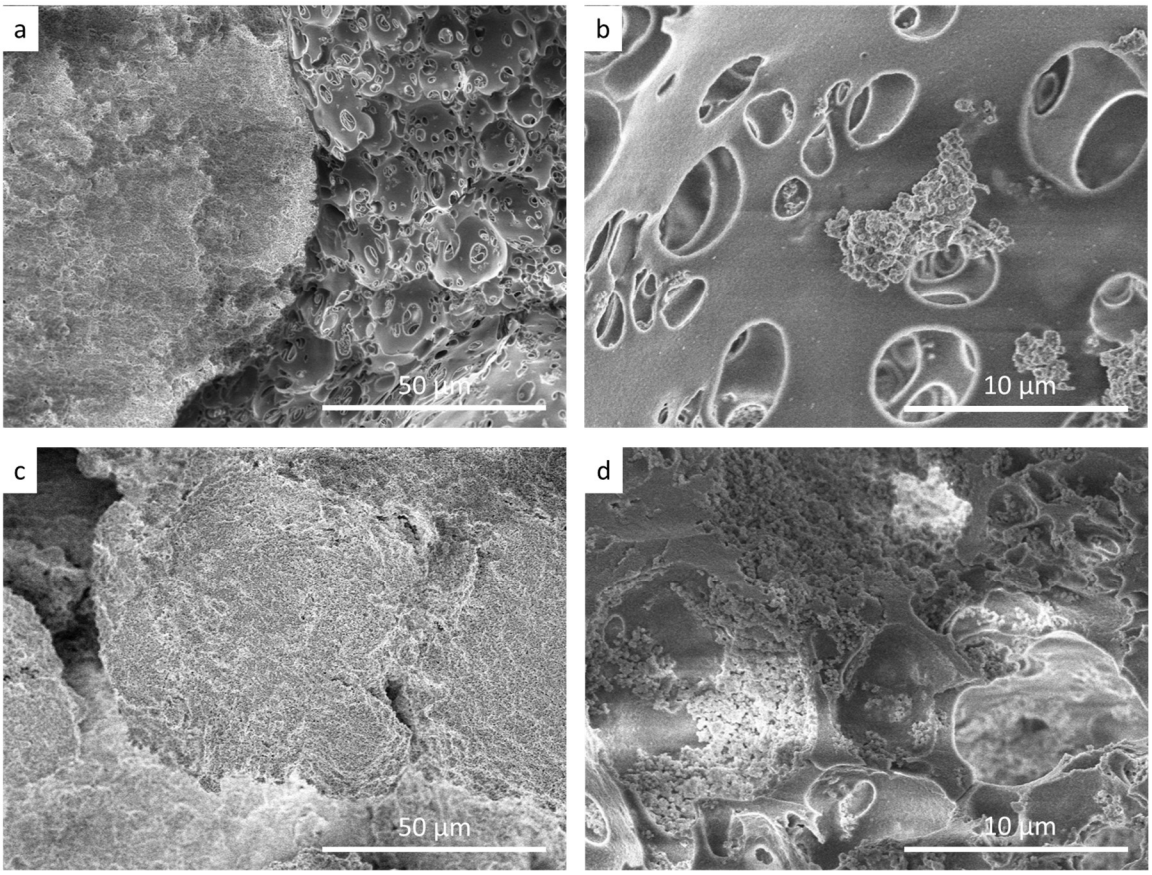

Figure 12 SEM images of MOF@polyHIPE composites containing amide-modified UiO-66-NH_2. a,b: 50 mg (30.6%); c,d: 150 mg (62.6%)

Despite the hydrophobicity of the particles, no significant change was seen in BET surface area for the PSM composites, at both low and high MOF loading as shown in Figure 13. While the hydrophobicity of the particles prevents them from becoming embedded in the polymer, in areas where the emulsion appears to have broken it is likely that the shell of polymer created around the aggregates creates adsorption behavior similar to what is seen in bulk composites. Even though the polymer and the MOF do not interact significantly at the interface, as seen in other, previous studies bulk or membrane style composites require a threshold loading of MOF before any surface area is measured. In membranes this loading was 70 wt%, whereas the composites presented here were capped at 60 wt%. It appears that the structure altering effects of the hydrophobic particles either balance or confound the fact that the particles are not embedded in the polymer to the extent that they are in the standard synthesis.

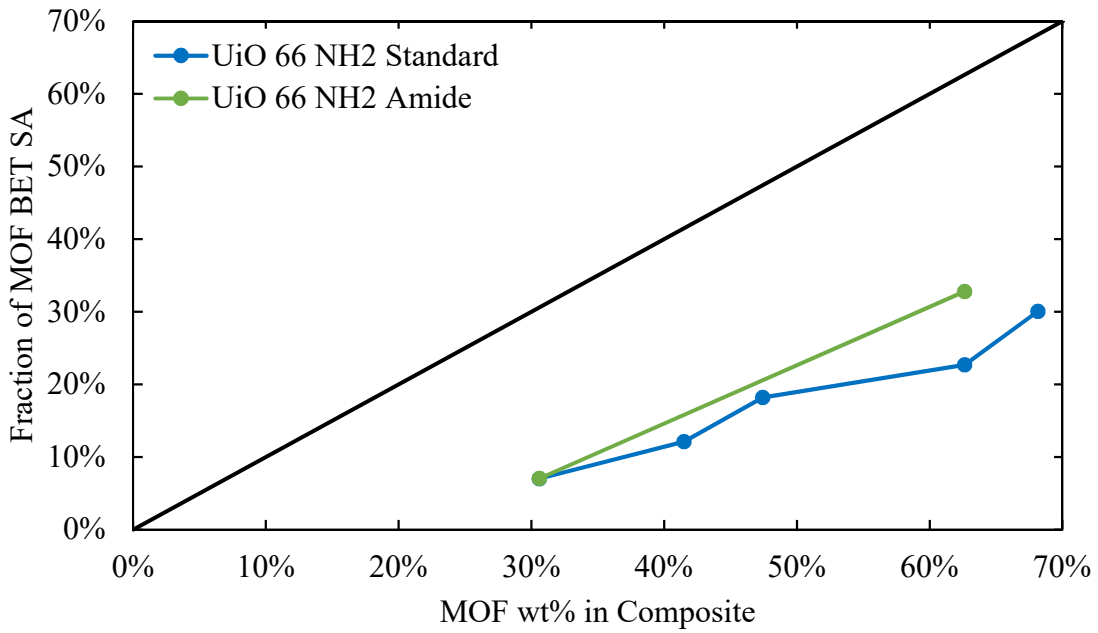

Figure 13 Comparison of actual MOF content in standard and amide modified MOF@polyHIPE composites with the percent of MOF surface area their measured surface areas represent. Black line is 1:1 ideal case

3.3.3 Pickering Emulsions

Composites produced from Pickering emulsions did not appear significantly different from those created in the standard synthesis from a macroscopic point of view. They differed significantly in their microscopic structure, as shown in Figure 14. The voids formed by the internal phase were significantly larger for the Pickering emulsions, from 50 to 100 µm in diameter. The walls between the voids were also significantly thicker, resembling bulk polymer rather than the thin walls seen in the standard synthesis composites. Another significant morphological difference was the presence of MOF particles lining the internal faces of the voids. The particles appear to completely cover the inner surface of the voids in a single layer, reflecting their position at the oil-water interface before polymerization. No MOF particles were visible apart from what was on the surfaces,

and the particles did not appear to be embedded in the polymer. The most significant change in the overall morphology of the emulsions using the Pickering synthesis was that the structure transitioned from an open-cell foam seen in the standard synthesis to a closed cell foam for Pickering composites. This change is caused by the thicker walls of the Pickering composite. Even at their thinnest point between two droplets, the walls were not thin enough for contraction during polymerization to open up windows between them.

When small amounts of surfactant were included in the Pickering synthesis the open-cell morphology was recovered. The morphology changes are shown in Figure 14. With only 1% of the original surfactant content windows between adjacent voids become present again, with some very large voids lined with MOF particles still present. At 10% of the original surfactant content the foams appear nearly identical to those produced using the standard synthesis, although areas still exist where the MOF is at the inner surface of a void, indicating that some of the MOF remained at the oil-water interface despite the inclusion of the surfactant. At 25% of the original surfactant content the polymer structure appears to collapse, remaining macroporous but losing the well-defined structure of the previous samples. Based on the morphology changes, we can conclude that the surfactant allows the external phase present between two internal phase droplets to become thinner than it could when stabilized by particles alone.[82] These thin areas can open into windows between the voids of the foam after polymerization, recovering the open-cell structure that was lost when the emulsions were stabilized by particles alone.

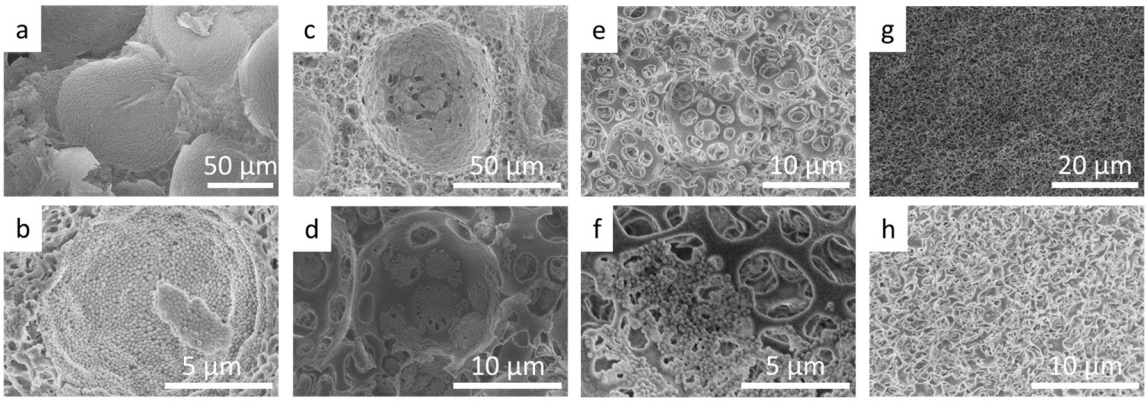

Figure 14 SEM images of Pickering MOF@polyHIPE composites with increasing amounts of added surfactant expressed as a percent of the concentration in the original standard synthesis. a, b: 0%; c, d: 1%; e, f: 10%; g, h: 25%

The BET data for the Pickering polyHIPE composites is shown in Table 3. Each composite was 13 wt% MOF based on what was included in the synthesis. The Pickering composite with no surfactant had a surface area of 41 m^2/g, about 3% of the MOF value in spite of the MOF being almost entirely located at the oil-water interface. This is explained by the closed-cell morphology of the foam, which creates layers of polymer surrounding the voids containing the MOF and preventing diffusion into them. Performance is slightly improved by the addition of a small amount of surfactant but is reduced again upon adding more surfactant. Based on this behavior it appears that the limits of the closed-cell foam morphology can be slightly mitigated through surfactant use, but that excessive surfactant can cause the MOF to become embedded in the polymer in the same way as in the standard synthesis, reducing the accessibility of the MOF to adsorbates.

Table 3 BET data for Pickering MOF@polyHIPE composites. MOF surface area is 1352 m^2/g, MOF loading is 13 wt%

Percent of Original Surfactant	BET Surface Area [m^2/g]	Percent of MOF Surface Area
0.0	41	3.0
0.1	70	5.2
1	6	0.4
10	8	0.6
25	7	0.5

Attempts to increase the MOF loading in Pickering emulsions lead to emulsion instability and separation of the oil and water phase. It is possible that performance could be improved with higher loading, which could create more internal phase droplets and thinner polymer walls between them, but this could not be achieved using the synthetic method presented here.

3.4 Conclusions

A number of different methods were examined with the goal of increasing the MOF accessibility within 2-hydroxyethyl methacrylate polyHIPE supports. Prepolymerization

of the monomers to prevent pore blocking in the MOF did not improve the surface areas of the composites, in contrast to observations in a previous study involving the MOF MIL-101. The smaller pore diameter of UiO-66 relative to MIL-101 makes it less likely that UiO-66 pores will be blocked by small molecules, making prepolymerization ineffective at improving MOF accessibility. Hydrophobic MOF modification successfully prevented the MOF from being fully embedded in polymer, but also resulted in broken emulsions, creating the same structure as bulk polymer casting and losing the benefits of the emulsion templating. Pickering emulsions were successfully formed and successfully controlled the location of the MOF particles, but created stable, thick walls between internal phase droplets, preventing openings from forming between them and resulting in a closed cell foam. Despite the MOF location, this resulted in poor surface areas compared to loadings, even lower than expected from the standard synthesis.

Based on the results of experiments with these composites we conclude that the low MOF accessibility in the composites results from a combination of MOF interactions with the surfactant and the MOF being too well embedded in the polymer walls, creating a barrier to diffusion into the MOF particles. Determining the extent to which each factor contributes to the loss of surface area has proven impossible, given the confounding factors of structure changes in the amide and Pickering emulsion samples.

CHAPTER 4. HYDROPHOBIC MOF@POLYHIPE COMPOSITES

4.1 Introduction

Gas separation via adsorption has drawn increasing interest as an alternative to membrane, solvent, or distillation separation processes, with the potential for greater efficiency and lower energy costs.[8] Pressure swing adsorption and temperature swing adsorption have both been proposed as potential separation processes, often with the research focused on the behavior of particular adsorbents in gas adsorption isotherms. However mass transfer within the adsorption module also contributes significantly to the overall performance of PSA and TSA. Conventional systems use adsorbents in the form of beads or granules, presenting a problem of mass transfer within the particles themselves. As faster cycling times are beneficial to throughput, these mass transfer limits can be reduced by reducing particle size. This reduction can create higher pressure drop, and therefore energy costs, and if taken to the extreme may even result in fluidization of the bed and potentially in maldistribution of flow through channeling. Because of these problems there is an interest in non-particulate adsorbent materials that can be structured to optimize performance within PSA and TSA systems.[37, 84]

Several structured adsorbents have been examined in literature, including honeycomb monoliths, membranes, and fibers. Honeycomb monoliths are bundles of coaxial channels either supporting or completely made up of the active material.[46, 48, 85] Monoliths are excellent at minimizing pressure drop but are limited by the amount of

exposed surface area within their channels. The geometric surface area, and therefore the capacity, can be improved by increasing the number of channels per square inch, although this makes manufacturing more complex and the resulting structure more fragile. Monoliths have also been produced from MOF particles extruded with a clay binder, but this is a relatively unexplored area.[47-48]

Mixed matrix membrane research has traditionally focused on the incorporation of small amounts of supplementary material to improve the permeability or selectivity of the membrane.[49] Some recent work has been more focused on the adsorbent qualities of the membrane. One study found that membranes produced using the polymer PVDF provide full access to the MOF surface area, but another found that within other polymers the MOF is accessible to adsorbates only if the loading is high enough to form a percolating network within the polymer support.[52-53] Similarly, fiber composites as adsorbents have been found to be effective if the fibers are sufficiently thin or porous to allow adsorbate gases to reach the MOF.[60-61]

Emulsion templated polymers may offer another support for adsorbents, particularly in applications where the adsorbing module can be cast into shape. High internal phase emulsions (HIPEs) are emulsions in which the droplet phase makes up 74% or more of the total emulsion volume.[64] By including monomers and crosslinkers in the external phase of the emulsion a cast of the emulsion can be formed during polymerization, with polymerization induced contraction opening windows between the voids left by the droplet phase. Adsorbents can be introduced to the polymeric structure by physical mixing with the external phase or by growth on the cured polymer. These polyHIPE materials are open cell foams with up to 90% of their volume left empty by removal of the droplet phase after

polymerization, making diffusion of gases throughout the structure possible. They can be cast into a variety of shapes, like the monoliths described above, but by allowing rapid radial diffusion they would eliminate the need for thin walls and many parallel channels, which may make manufacturing easier.

This chapter examines the viability of styrene-based polyHIPE materials as supports for adsorbents for gas separation applications. The metal organic framework (MOF) UiO-66 and its functionalized variant UiO-66-NH_2 are used as model adsorbents because of their chemical and thermal stability and because they can be modified easily in terms of particle size and chemical functionality. MOF@polyHIPE composites could provide cast adsorbent structures tailored for specific applications like PSA and TSA by casting a highly permeable polymer structure into a shape optimized for that purpose. While MOF-bearing polyHIPEs have been examined before they have tended to focus on using the polymer as an anchor for growing MOF particles.[69-71] This method ensures that the polymer will not obstruct the MOF but provides little control over loading or the strength of the bond between polymer and MOF. To our knowledge only one prior study has examined embedded MOF@polyHIPEs using a hydrophilic polymer that interfered with the adsorption capacity of the MOF.[74] This work uses a styrene based polyHIPE that can be easily manipulated in terms of crosslinker, internal phase volume, and inclusion of porogenic solvents, making it a better platform for examining ways to preserve MOF accessibility and capacity within the composites.

4.2 Materials and Methods

4.2.1 Materials

All chemicals were available commercially and were used as received: styrene (Sigma-Aldrich, ≥99% with 4-tert-butylcatechol as stabilizer), divinylbenzene (Sigma-Aldrich, 80%), Span 80 (Sigma-Aldrich), potassium persulfate (Sigma-Aldrich ≥99%), calcium chloride dihydrate (Sigma-Aldrich ≥99%), zirconium chloride (Aldrich, ≥99.5%), terephthalic acid (Aldrich, 98%), and 2-aminoterephthalic acid (Acros Organics, 99%).

4.2.2 MOF Synthesis

UiO-66 and UiO-66-NH_2 were synthesized according to the procedure outlined in Chapter 2 of this thesis. 5.448 mmol each of linker (2-aminoterephthalic acid or terephthalic acid) and zirconium chloride were added to a mixture of 212 ml DMF. For UiO-66-NH_2, 0.8 ml distilled water was added as well. After complete dissolution of the reactants the mixture was divided into 8 glass vials and placed in an isothermal oven for 24 hours at 120 °C. The products were combined after being removed from the oven and washed 3x with DMF and 3x with methanol.

The products of several syntheses were mixed together to create large, homogeneous samples of both functionalized and unfunctionalized MOF. MOF samples were activated at 110 °C before use and characterization to remove residual solvent and adsorbed water.

4.2.3 PolyHIPE

0.2 g of potassium persulfate and 1.0 g of calcium chloride were first dissolved in 90 mL of water. A total of 10 mL of styrene and divinylbenzene were mixed with 3 mL of Span 80 in a large beaker. The aqueous phase was added dropwise to the oil phase while stirring constantly at 300 rpm. The total mixing time was 1 hour, after which the emulsion was transferred into Teflon cups and left to cure for 48 hours at 60 °C. After curing the polymer was removed from the Teflon vessels and rinsed in a Soxhlet extractor with ethanol for 48 hours. Finally, the polymer was dried in an oven at 60 °C for 48 hours.

4.2.4 MOF@polyHIPE Composites

MOF@polyHIPE composites were first synthesized using UiO-66-NH_2. Both the MOF and the HIPE were prepared as above, but the polymer was not cured. Instead it was divided between several Teflon cups and mixed with activated MOF using a spatula until achieving a homogeneous appearance. Added MOF masses were chosen to result in composite loadings of 10, 30, and 60 wt% MOF. The composites were then cured, washed, and dried in the same way as the pure polymer samples.

A second synthesis method was used to better distribute the MOF throughout the polyHIPE material. This method used a quarter of each component for a scaled down synthesis. In this method the activated MOF was first suspended in the water making up the aqueous phase of the polyHIPE via sonication. Synthesis then continued as above, with the MOF now incorporated along with the aqueous phase. UiO-66-NH_2 could not be used in this method because it interfered with the curing of the polymer, but UiO-66 could be used without issue.

4.2.5 Characterization

Powder X-ray diffraction (PXRD) patterns were obtained using a Panalytical XPert PRO Alpha-1 XRD. SEM images were taken with a Hitachi SU8010 SEM. TGA measurements were taken using a TA Instruments Q50. Nitrogen physisorption data was obtained using a Quantachrome Quadrasorb Evo. Samples were outgassed at 80 °C before adsorption to remove residual solvent.

4.3 Results and Discussion

The polyHIPE composites produced both with and without embedded MOF solidified completely and retained the shape of the container they were polymerized in. Visually the MOF appeared to be distributed throughout the entire polymer body, although some large grains of MOF were visible, indicating that some MOF aggregates remained even after mixing. The polymer retained its texture and structural stability regardless of MOF content, and dust formation was minimal. The presence of MOF aggregates appears to have had no effect on the overall stability of the composites, and the MOF is well-contained within the polymer matrix. Varying the extent of crosslinking had a more significant effect on the materials, with higher crosslinker percentages yielding stiffer polymer samples regardless of MOF content.

The crystallinity of the MOF within the composites was probed by examining XRD patterns. The patterns, seen in Figure 15 XRD patterns of polyHIPE composites and parent materials, show that the crystallinity of the MOF is unchanged after incorporation into the polymer, with no significant additional or missing peaks. The peak intensity was reduced,

and a broad peak between 15° and 25° was visible at low MOF concentrations, reflecting the presence of amorphous polymer material in the samples.

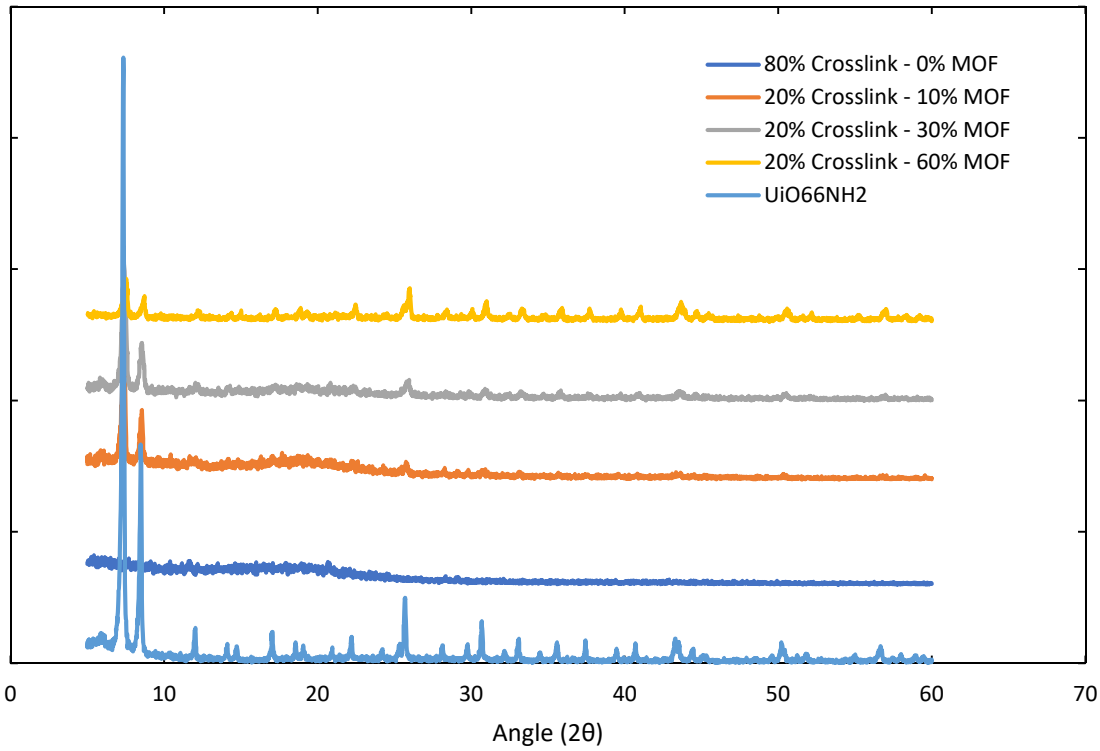

Figure 15 XRD patterns of polyHIPE composites and parent materials

TGA was used to confirm the MOF content of each composite sample. The values obtained this way match with the expected trend but deviated by 10 to 15% from their expected values for some samples. This likely reflects the aggregation of MOF within the sample, in combination with the relatively small sample size evaluated in TGA. While not desirable, the aggregation did not appear to have any effect on the other characterization methods, or on the overall quality of the composites.

SEM images of the parent polyHIPE material with varying crosslinker content are shown in Figure 16. The emulsions consisted of 90% internal phase by volume before

polymerization, and this proportion was assumed to be unchanged in the final, polymerized materials. The polyHIPE had a low-density sponge-like morphology with spherical voids left by the removal of the internal phase and windows between the voids created by shrinking during polymerization. The void diameters ranged from 10 to 50 μm with windows ranging from 5 to 15 μm. The average void size decreased with increasing crosslinker percentage. Larger internal phase droplets, and therefore void sizes in the final material, are linked to droplet coalescence or Ostwald ripening which have larger effects over time. A lower crosslinker content may result in a longer period before a stiff, fully crosslinked cast of the emulsion is formed, giving more time for the droplets to grow while the polymer is flexible enough to allow it. It may also reflect contraction and collapse of the stiffer polymer that results from a high crosslinking content.

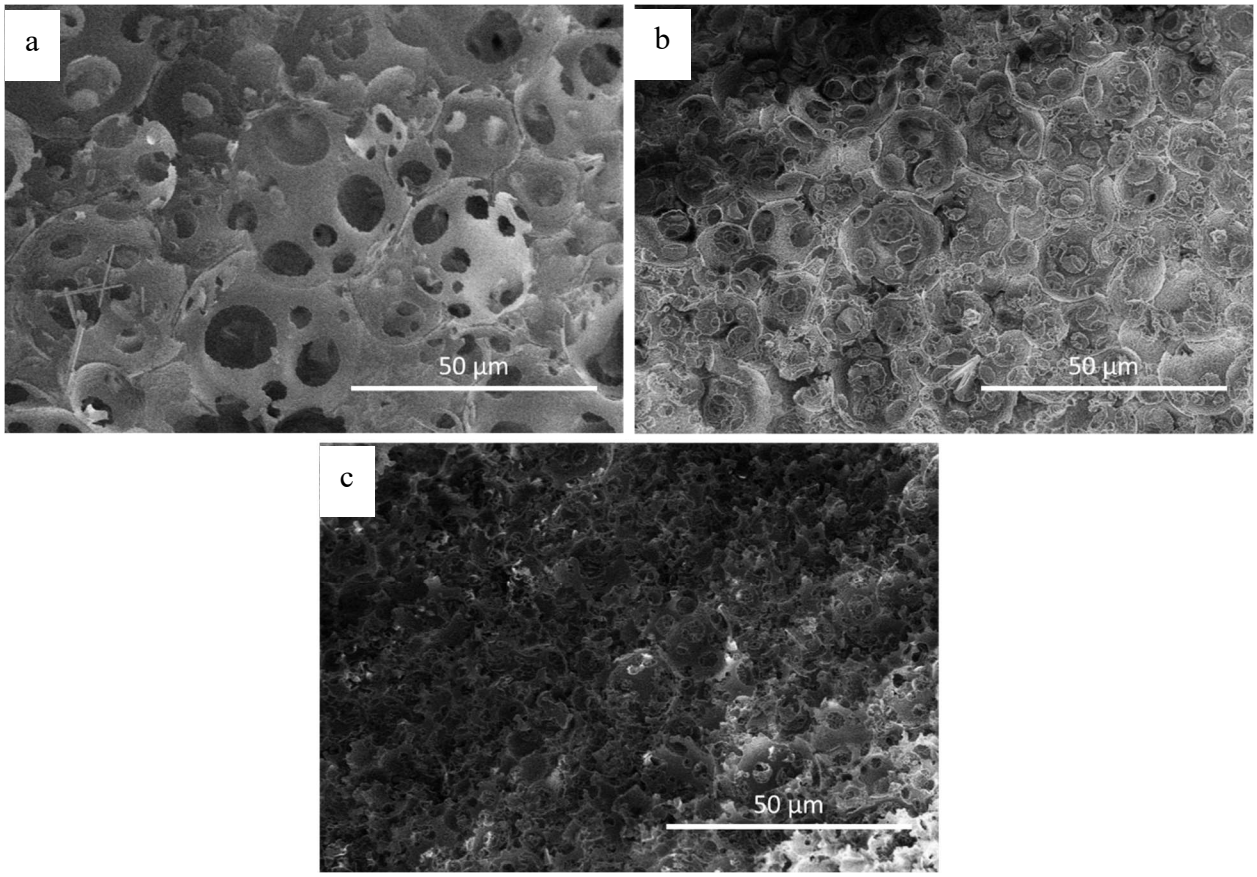

Figure 16 SEM images of polyHIPE samples with no added MOF and varying levels of crosslinking. a. 20% crosslinker; b. 50% crosslinker; c. 80% crosslinker

The addition of MOF to the polyHIPEs did not significantly affect the structure of the polyHIPE itself at the microscopic level. SEM images of MOF-bearing samples with 20% crosslinker can be seen in Figure 17. The SEM images show that the MOF tends to aggregate rather than become fully distributed throughout the polymer. Large areas of dense, concentrated MOF crystals can be seen, connected by MOF-poor regions that retain the open pore polyHIPE structure. Although it is not well distributed, the MOF appears to be securely embedded in the polymer matrix. The polymer appeared to be in contact with the MOF aggregates rather than forming voids around them, and no loose MOF was

observed in SEM. Additionally, the aggregates were larger than the average size of the voids, making it unlikely that the MOF would be lost from the structure.

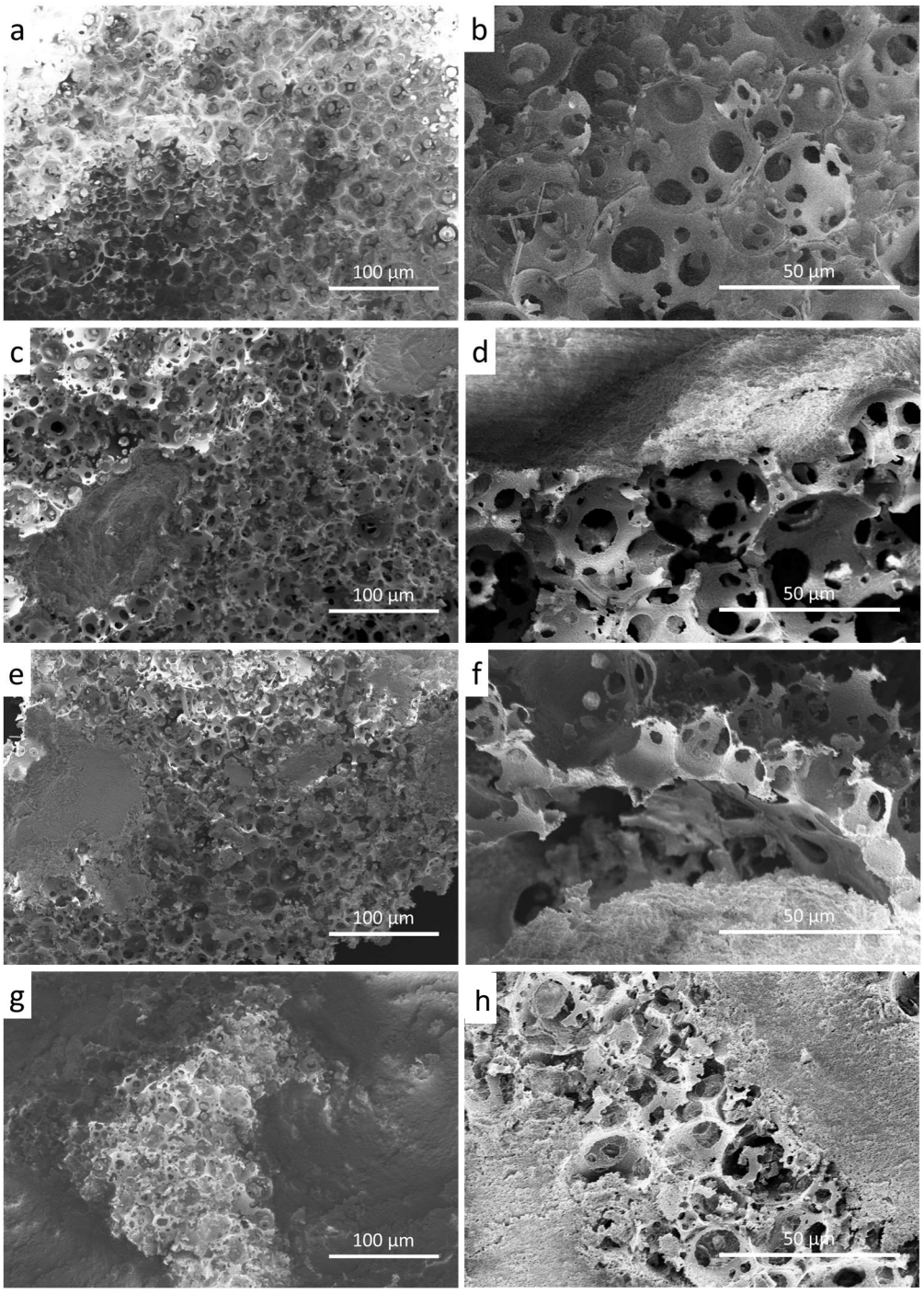

Figure 17 SEM images of UiO-66-NH_2 MOF@polyHIPE composites with 20% crosslinker. a, b: 0% MOF; c, d: 10% MOF; e, f: 30% MOF; g, h: 60% MOF

4.3.1 BET

Nitrogen physisorption at 77 K and BET analysis was used to probe the accessibility of the MOF within the polymer matrix. The BET data as well as the TGA data is shown in Table 4 Summary of TGA and BET data for MOF@polyHIPE composites. The UiO-66-NH_2 had a surface area of 1080 m^2/g, and the polymer varied from 9 to 40 m^2/g, with higher crosslinker content corresponding to higher surface areas. The measured surface areas of the composites were compared to estimates based on the surface areas of the parent components, with the results shown visually in Figure 18. While there is variation between samples, the composite surface areas are close to what would be expected based on their composition, with an average difference of 4%. In general, the measured surface areas were slightly lower than expected. This result indicates that the majority of the MOF particles were accessible to adsorbates despite being embedded in the polymer matrix, with only a small amount being entirely obstructed by the polymer. This behavior can be attributed to a combination of the slight hydrophilicity of the MOF relative to the hydrophobic polymer, to the large void volume of the polymer, and to the formation of MOF aggregates during mixing. The difference in hydrophobicity makes the non-aqueous phase less likely to wet the MOF particles before polymerization, preventing the polymer from forming a continuous skin over the particles. The large void fraction in the polymer matrix creates polymer walls with very short length scales, increasing the chances that MOF particles will be located at polymer-air interface. The aggregates contribute as well, as they are larger than the average size of the walls between the polyHIPE voids, making it unlikely that they would be completely covered by polymer. Because the particles in the aggregates are close together, if a portion of the aggregate is accessible then it is likely that the entire aggregate

will be as well, with adsorbates diffusing between particles that might otherwise be obscured by the polymer.

Table 4 Summary of TGA and BET data for MOF@polyHIPE composites

Extent of Crosslinking	Nominal MOF Content (wt%)	MOF Content by TGA (wt%)	BET SA (m^2/g)	MOF Content Based on BET (wt%)
80%	0%	0%	40	0%
	10%	11%	99	6%
	30%	35%	268	22%
	60%	60%	641	58%
50%	0%	0%	32	0%
	10%	5%	99	6%
	30%	13%	356	31%
	60%	69%	527	47%
20%	0%	0%	9	0%
	10%	15%	107	9%
	30%	31%	282	25%
	60%	72%	537	49%

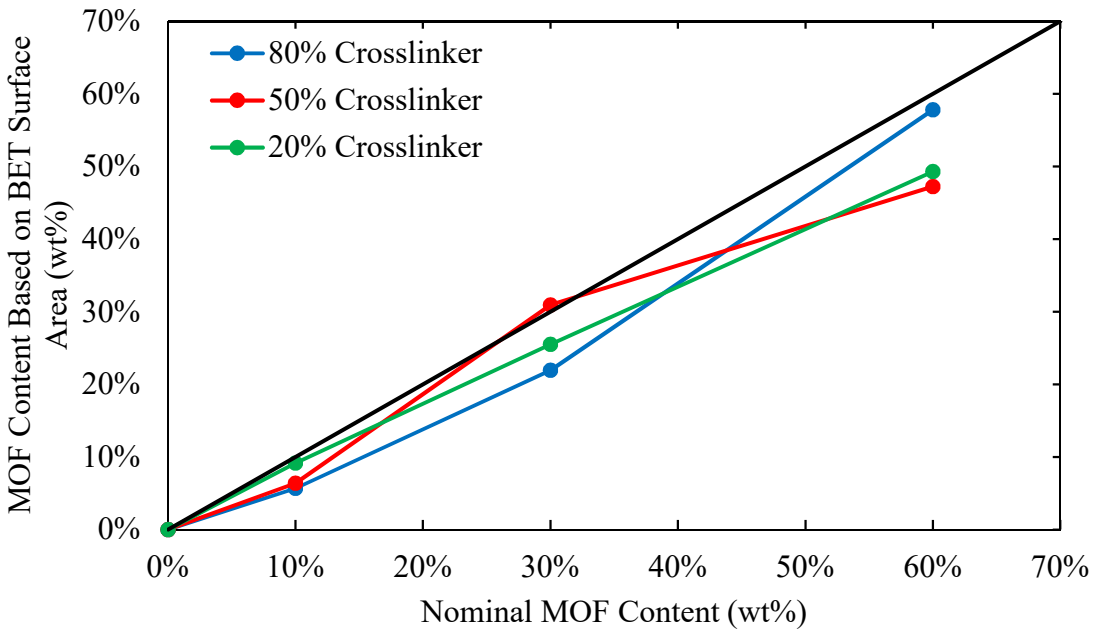

Figure 18 Comparison of nominal MOF content and MOF content calculated based on measured BET surface areas in MOF@polyHIPE composites. Black line is 1:1 ideal case

4.3.2 MOF Distribution

In order to produce composites with more well distributed MOF, a second set of samples was synthesized using unfunctionalized UiO-66 dispersed via sonication in the aqueous phase before the formation of the emulsion. Morphologically these composites were identical to those produced by the original synthesis, with the most significant difference being the lack of color due to the absence of amino pendant groups, and the lack of apparent MOF grains. SEM images of the composites shown in Figure 19 show significantly less aggregation of MOF particles compared to the original synthesis, and the MOF appears to be more evenly distributed through the structure. BET data taken for this second set of composites shows the same trends as the original synthesis, with the MOF maintaining the same level of accessibility despite the absence of MOF aggregates. That

data is shown in Figure 20. This performance confirms the MOF's accessibility within the polystyrene matrix even when more evenly distributed. It suggests that the high accessibility is related to the high void volume of the polymer and the different hydrophobicity of the two materials rather than the size of the MOF aggregates.

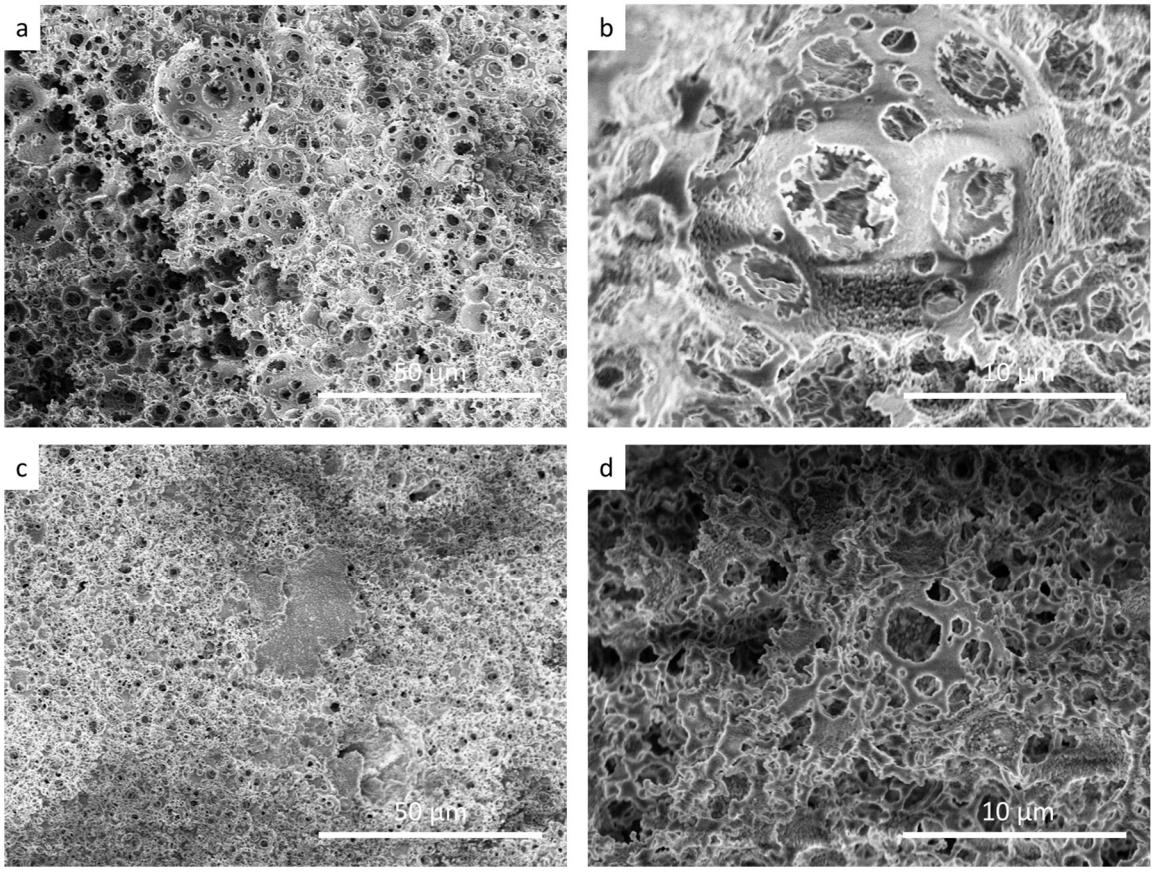

Figure 19 SEM images of UiO-66 MOF@polyHIPE composites in which the MOF was sonicated with the aqueous phase before emulsion formation. a, b: 10% MOF; c, d: 30% MOF

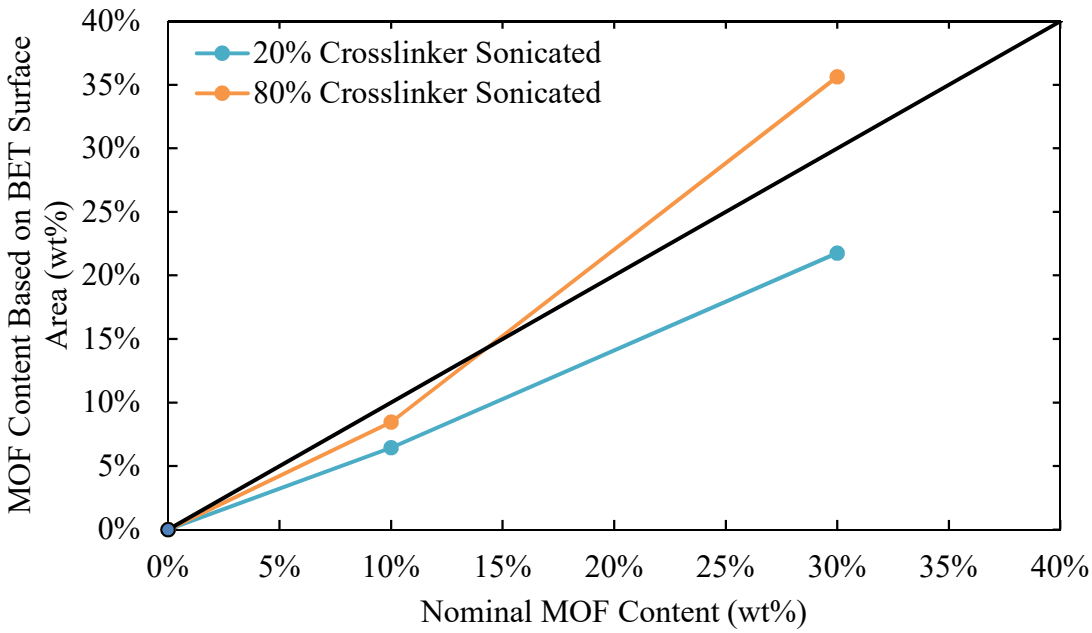

Figure 20 Comparison of nominal MOF content and MOF content calculated based on measured BET surface areas in MOF@polyHIPE composites with the MOF dispersed in the aqueous phase before emulsion formation. Black line is 1:1 ideal case

4.4 Conclusions

We have successfully synthesized polystyrene foam composites containing embedded MOF with full accessibility as determined by surface area. Loadings of up to 60 wt% could be achieved without significantly compromising the macroscopic structure or stability of the polymeric materials. Using simple mechanical mixing, the MOF was found to aggregate within the polymer before polymerization, resulting in the presence of MOF rich and MOF poor regions. This did not appear to affect the overall quality of the composites, and experiments intended to more evenly distribute the MOF throughout the polymer did not significantly change the surface area for equivalent MOF loadings. Based on these results we conclude that a combination of the high internal phase volume, and therefore the void fraction of the final composite, and the hydrophobic nature of the

polymer create a composite where the MOF can be accessible to adsorbates even while securely embedded in the polymer matrix.

MOF@polyHIPE materials with high MOF accessibility have potential applications in a wide variety of processes, including pressure or temperature swing adsorption. Their hierarchical pore structure allows gases to reach the MOF even through relatively thick structures via diffusion in the macropores. It is possible to mold them into forms based on the shape of the polymerization vessel. Work to create appropriately shaped structures, incorporating additional hierarchical pore structures, and to test them in specific applications is ongoing. In the future these applications may include pressure or temperature swing adsorption and single pass filtration, both of which require excellent MOF accessibility and fast diffusion throughout the structure.

CHAPTER 5. SOLUTION BLOW SPUN MOF-FIBER COMPOSITES

5.1 Introduction

Because of their potential for adsorption and catalysis of toxic chemicals, MOFs have been proposed for use in personal protection applications.[2] However, they are poorly suited to this application in their as-synthesized powder form. Fibers supporting MOF particles are of growing interest in toxic gas applications because they can be incorporated directly into filters and clothing to protect against a variety of harmful particulates and gases, creating self-detoxifying textiles.[61, 86] The fibers themselves may be produced by a variety of methods or can be derived from natural sources like cotton. In previous work, fibers were used as anchors for growing the MOF, resulting in a MOF surface layer with the fiber as a flexible core.[57, 87] MOF-bearing fibers have also been produced directly from MOF suspensions in polymer solutions via electrospinning and extrusion into a non-solvent.[58, 60] These methods can circumvent problems with the stability of the fibers in MOF precursor solutions, while ensuring that the MOF is held strongly by the polymer. Fiber composites have been produced with several polymers, and their effectiveness has been demonstrated in applications as catalysts, adsorbents, and particulate filters.

5.1.1 Current Methods

Two common methods that can produce polymer fibers with diameters in the nanometer range are melt-blowing and electrospinning. Melt-blowing is a common industrial process that uses a high velocity gas stream to draw out fibers from an extruding

spinneret and can be scaled up by using multiple spinnerets.[88-89] Melt-blowing can produce both micro and nanofibers but obtaining fibers with diameters below 800 nm can be difficult. Additionally, melt-blowing is poorly suited to the production of MOF-bearing fibers both because of the relatively high heats required and the rheology of particle-melt mixtures. Electrospinning is a heavily researched technique which uses an electric field to draw out a jet of polymer melt or solution from a spinneret to a collector. Electrospinning can produce nanofibers with diameters in the hundreds of nanometers, smaller than can typically be achieved with melt-blowing but is more difficult to scale up because of the electrical requirements and interference between jets.[90-92] Electrospinning has been used to produce MOF-bearing fibers, but requires a solvent with particular electrical properties, and is relatively slow compared to melt-blowing. To obtain fibers with smaller diameters, a combination of the two techniques is used called gas assisted electrospinning. The addition of a high velocity gas stream further thins the jet produced by electrospinning, creating finer fibers.

5.1.2 Solution Blow Spinning

A relatively new method known as solution blow spinning (SBS) is an alternative to electrospinning and melt-blowing for making fibers from MOF suspensions. SBS is like melt-blowing, using a similar concentric nozzle design with the outer nozzle blowing high velocity gas and the inner nozzle extruding a polymer solution rather than a melt. The gas blowing past the inner nozzle draws the polymer solution out into strands that rapidly dry as they fly toward a target.[93-96] SBS fibers are similar in size and morphology to electrospun fibers but can be produced at a faster rate from a single nozzle. SBS also requires no electric field to draw the solution into fibers, making it possible to use a much wider variety of

solvents in the polymer solutions and making scale up simple using a multi-headed nozzle with several concentric nozzles.[97-98] SBS enables direct application of fibers to a surface through in-situ fabrication, rather than by incorporating MOF-bearing fibers into a manufactured item. In-situ fabrication would facilitate use by supplementing rather than replacing existing protective equipment and requires no new equipment to be produced beyond MOF-bearing polymer solutions and spray devices.

The purpose of this work is to examine SBS fibers as a platform for MOF composites for in-situ applications. Because the technique is easily scalable and relatively agnostic toward solvent, polymer, and active materials embedded in the fibers, SBS can be used with non-toxic solvents and polymers to provide a temporary protective layer of clothing for an individual exposed to chemical hazards. The protective layer could be tuned based on the active material included in the fibers and adjusted to address expected threats or provide supplemental protection for those without adequate protective equipment. This work presents a detailed study of polystyrene fibers bearing UiO-66-NH_2. This system combines a low-hazard, low-cost polymer and a highly stable MOF to enable a systematic evaluation of the effects of the process on the accessibility of active materials.

5.2 Materials and Methods

5.2.1 MOF

UiO-66-NH_2 was chosen for its robust chemical and thermal stability, as well as its high capacity for several toxic gases. 5.448 mmol each of terephthalic acid and zirconium chloride were added to a mixture of 212 ml DMF and 0.8 ml distilled water. After complete dissolution of the reactants the mixture was divided into 8 glass vials and placed in an

isothermal oven for 24 hours at 120 °C. The products were combined after being removed from the oven and washed 3x with DMF and 3x with methanol. The products of several syntheses were mixed together to create a homogeneous sample used for all composites. This procedure produced MOF crystals with diameters of approximately 200 nm, which are typically intergrown and clump together as larger aggregates.

5.2.2 Solution Blown Fibers

The solution blowing device is depicted in Figure 21. The nozzle itself is made of two concentric tubes. The outer tube bearing compressed nitrogen is 2 mm in diameter, and the inner tube is a blunt-tipped 18-gauge needle protruding 1 mm from the plane of the outer tube. A syringe pump is connected to the needle to control the flow rate of the polymer solution through the needle. The fibers were collected on a flat, stationary aluminum foil target placed 35 cm from the nozzle.

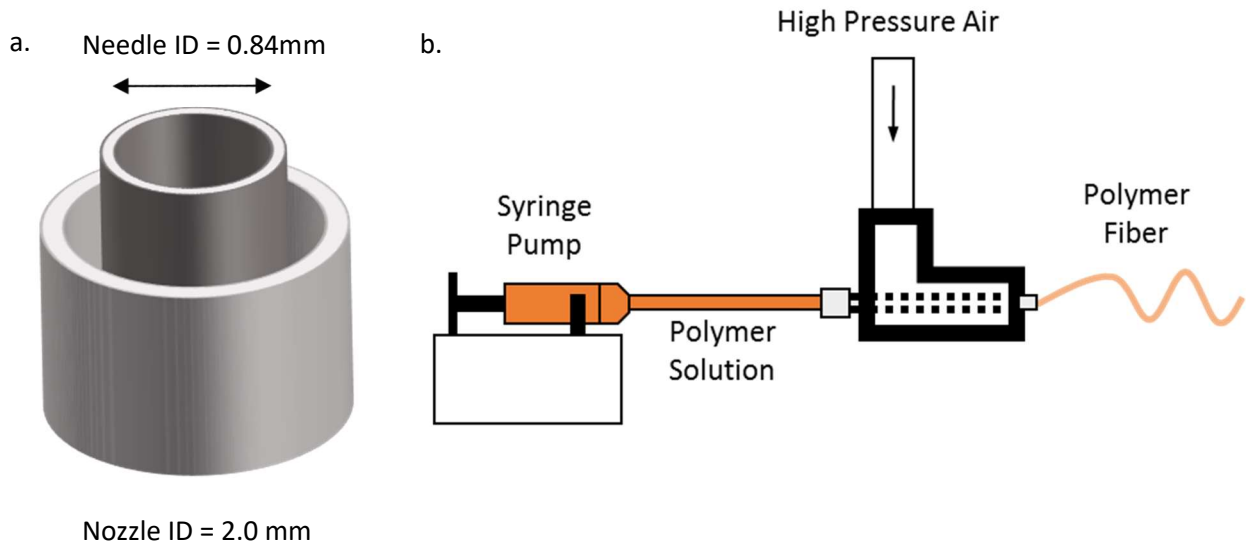

Figure 21 a: Simplified diagram illustrating the concentric nozzle and b: the overall SBS apparatus

5.2.2.1 Polymer Fibers

Polymer solutions were prepared by dissolving polystyrene (Mw = 192 kDa and 350 kDa) pellets in a solvent overnight by stirring constantly at room temperature. The homogeneous solutions were loaded into 10 mL syringes and spun immediately. Ethyl acetate, chloroform, THF, DMF, and toluene were used as solvents during initial tests of the SBS system. Ethyl acetate was ultimately chosen as the primary solvent for data collection due to its relatively low hazard and the quality of the fibers it produced.

The variables examined using ethyl acetate solutions and their values in each experiment are outlined in Table 1. Polymer concentration, propelling gas pressure, and solution flow rate were each varied independently for both low (192 kDa) and high (350 kDa) molecular weight polystyrene, with all other variables held constant. This resulted in three sets of fibers for each molecular weight of polymer, 24 samples total.

Table 5 SBS variables examined for pure polymer fibers

Experiment	Polymer Concentration (wt%)	Gas Pressure (psi)	Solution Flow Rate (mL/h)
1	10	20	60
	12.5		
	15		
	17.5		
	20		
2	15	10	60
		20	
		30	
3	15	20	30
			60
			90
			120

5.2.2.2 Composite Fibers

The MOF UiO-66-NH_2 was activated for 24 hours at 110 °C under vacuum to remove any residual solvent or water. After activation the MOF was immediately suspended in a predetermined volume of ethyl acetate via sonication. The polymer and solvent mixture compositions are reported here based only on the polymer and solvent content, using the same weight percent (wt%) mixtures as the pure polymer fibers outlined above. Once the MOF was suspended, the polymer pellets were added to the solution and stirred overnight at room temperature. Solutions were visually inspected for homogeneity before being loaded into syringes and then were spun immediately to avoid settling.

Final MOF content, polymer concentration in solution, and polymer molecular weight were varied. Samples with projected final MOF content of 10%, 30%, and 50% were prepared for polymer solutions with 10%, 12.5%, and 15% polymer of each molecular weight. A total of 18 samples were needed to examine all possible combinations.

5.2.3 Characterization

Powder X-ray diffraction (PXRD) patterns were obtained using a Panalytical XPert PRO Alpha-1 XRD. SEM images were taken with a Hitachi SU8010 SEM. TGA measurements were taken using a TA Instruments Q50. Nitrogen physisorption data was obtained using a Quantachrome Quadrasorb Evo. An intelligent gravimetric analyzer (IGA-1) was used for carbon dioxide adsorption, and a second model (IGA-3) was used for water vapor adsorption. Samples were outgassed at 80 °C before adsorption to remove residual solvent.

5.3 Results and Discussion

5.3.1 Initial Tests – Solvent Variation

The first tests conducted were to determine which solvents could be used in the SBS process with polystyrene. Polymer concentrations ranging from 2 wt% to 20 wt% were examined using ethyl acetate, chloroform, THF, DMF, and toluene. DMF and toluene produced layers of polymer on the surface of the collector rather than fibers, indicating that the solvent did not evaporate quickly enough during the fibers' flight. Increasing the working distance significantly resulted in fiber formation but was impractical based on available fume hood space. THF, chloroform, and ethyl acetate produced fibers, and required polymer concentrations of between 10 wt% and 25 wt%. THF produced light fibers that did not adhere well to the collector. Chloroform and ethyl acetate produced well-formed fibers that adhered to the collector and dried before reaching it. For identical concentrations, SEM images showed that THF produced the finest fibers, followed by chloroform, and ethyl acetate produced the thickest. Beyond this, the fibers appeared morphologically identical. Ethyl acetate was chosen for further experiments based on the formation of fibers and because it is less hazardous than the other solvents tested.

5.3.2 Polymer Fibers

The fibers produced via SBS were randomly oriented on the surface of the collector and resembled a cotton ball in texture. From observation of the spraying process we found that fibers were formed from many solution streams propelled by the gas rather than a single continuous stream. The fibers range from 1 to 10 μm in diameter, depending on spinning conditions and solution concentration. They exhibit morphologies ranging from

wrinkled cylinders to flat or distorted ribbons which can be seen in Figure 22. The wrinkling and distorted shapes are due to the evaporation of solvent as the fibers fly toward the collector. Rapid evaporation from the fiber surface produces a polymer-rich skin and a solvent-rich core, which then collapses as solvent continues to evaporate and the fibers shrink to their final size. Beads and larger polymer structures are seen in the SEM images along with fibers, and in many cases are significantly larger than the fibers themselves. Beads-on-a-string morphology is typically explained as resulting from surface tension forming droplets as the fibers dry, with viscosity as an opposing force. In this system large beads and polymer chunks may also be formed because of the failure of the gas stream to break up and stretch out the polymer solution uniformly, occasionally allowing droplets and larger volumes of solution to leave the needle without forming fibers. Fiber bundles are also observed in the imaged samples along with individual fibers, and the fibers have no discernable orientation but are distributed randomly.

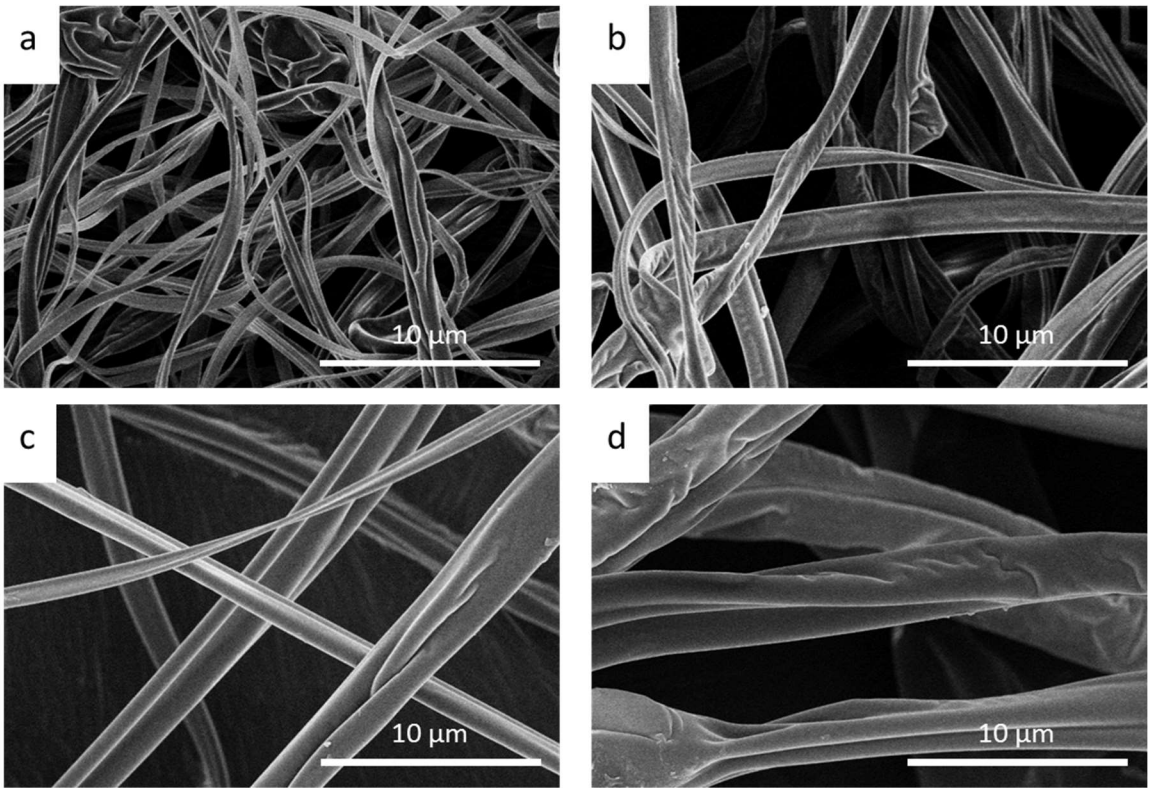

Figure 22 SEM images of SBS polymer fibers made from varying concentrations of 192 kDa polystyrene in ethyl acetate. Polymer concentrations in wt%, average fiber diameters and standard deviations of fiber diameters follow: a. 10% (0.59 ± 0.26 µm); b. 12.5% (1.08 ± 0.30 µm); c. 15% (1.96 ± 0.84 µm); d.17.5% (2.51 ± 0.99 µm).

No visible porosity is observed in SEM images of the fibers regardless of the solution composition and spinning conditions. Breath figures do form due to rapid evaporation and cooling, particularly on larger fibers and on beads, resulting in golf-ball-like dents on the fiber surfaces. However, these breath figures do not extend into the fibers or create porosity. Fibers that broke before imaging are observed to have a thin, solid outer layer with a less dense core, caused by rapid evaporation of solvent from the fiber surface during flight.

5.3.2.1 Effect of Polymer Concentration

The variable with the largest effect on fiber morphology, texture, and size is polymer concentration in the solution (Figure 2). Fiber size data for the range of concentrations examined is also presented numerically in Figure 3, which shows that higher concentrations produced both higher diameter fibers and a larger distribution of fiber sizes. Solutions with lower polymer concentrations do not produce fibers, instead breaking up into droplets and depositing as a thin film on the surface of the collector. Solutions with higher polymer concentrations produce fibers, but they do not dry fully in the air and form a film when the wet fibers join together on the surface. The samples made from high molecular weight polystyrene have uniformly larger average diameters than those made from low molecular weight polystyrene at each concentration.

Fiber diameter appears to be primarily determined by solution viscosity. As noted in previous studies, at low viscosities the surface tension of the solution tends to cause the formation of droplets rather than fibers. As the viscosity increases, the solution resists this tendency and remains a continuous stream long enough to solidify, moving from droplets to beads-on-a-string to continuous fibers. Increasing the viscosity of the solution further makes it progressively more difficult for the force exerted by the air to move and thin the fluid, creating thicker fibers. At high viscosities the fibers are thick enough to hinder solvent evaporation during their flight to the collector, or the spray becomes large drops of solution that cannot be easily broken up by the air stream.

Concentration also affects fiber adherence to the surface of the collector. Lower polymer concentrations produce fibers that do not stick well due to their smaller diameters

and quantity. These smaller fibers tend to blow off the collector before accumulating enough to form a cohesive layer. Higher concentrations produce larger fibers that accumulate on the collector and can be removed as a single sheet. Fiber deposition, adherence, and removal are all optimized at 15 wt% polymer loadings when using ethyl acetate solutions.

5.3.2.2 Effect of Gas Pressure and Solution Flow Rate

Gas pressure was found to have very little effect on fiber diameter, as shown in Figure 3. However, higher pressures cause fibers to blow off the collector preventing the formation of a coherent layer. Solution flow rate also has very little effect on fiber diameter, which confirms that the polymer stream breaks into many ribbons that then solidify into fibers, rather than a single ribbon drawn out from the tip. Flow rate does affect the texture of the composite on the surface. As the flow rate increases, the fibers begin to fuse together on the surface of the collector. While the solution breaks up in a similar way and into fibers of similar diameter regardless of flow rate, evaporation of the solvent is too slow to allow large volumes of solution to solidify before reaching the collector. The conditions that consistently produce large amounts of easily removed fibers without film formation are 20 psi and 60 mL/h.

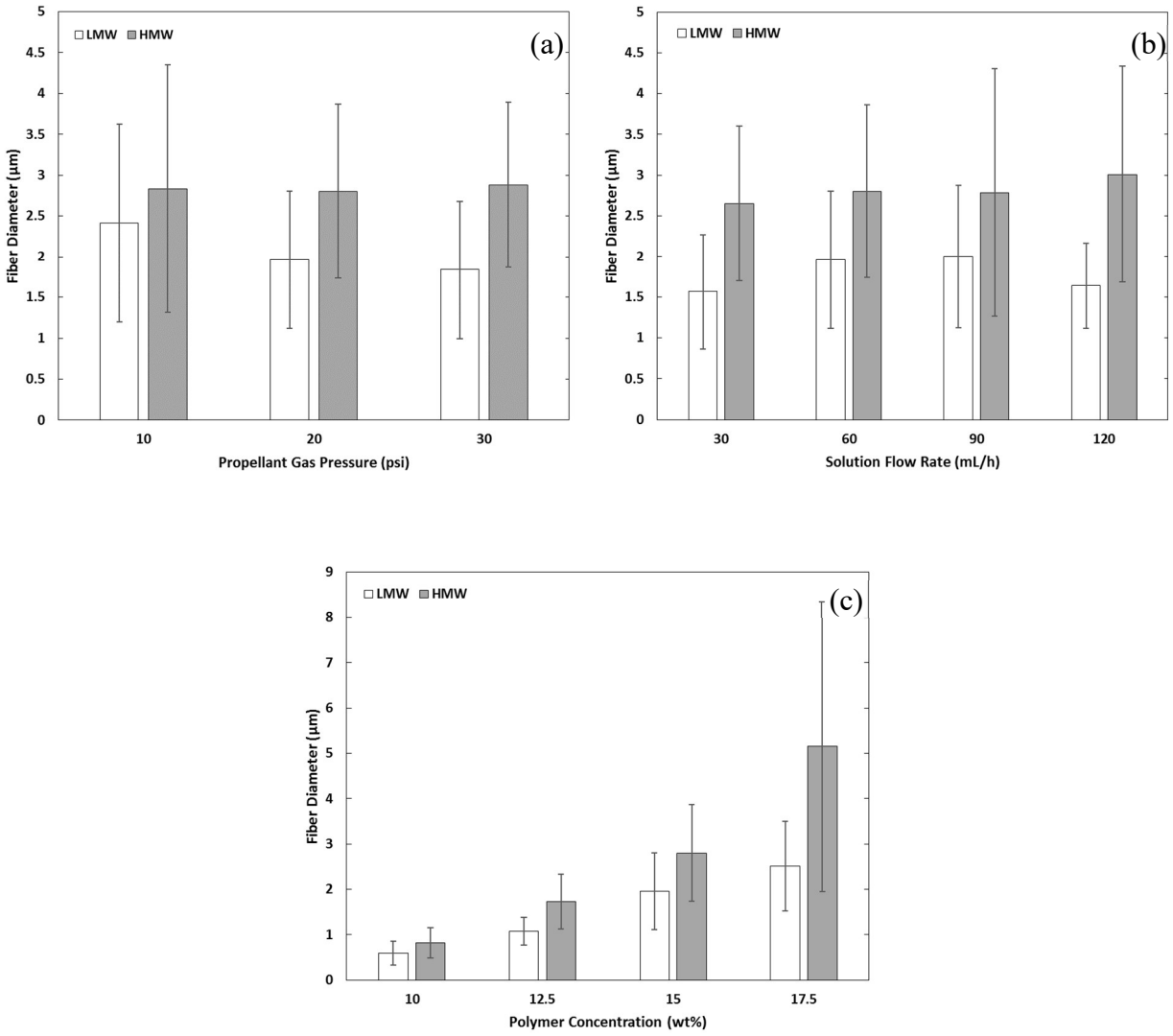

Figure 23 Fiber diameter as a function of gas pressure (a), solution flow rate (b), and polymer concentration (c). White and gray bars represent average fiber diameters for 192 and 350 kDa polystyrene respectively, and error bars represent the standard deviation of each sample set

5.3.3 Composite Fibers

Fibers spun with MOF suspended in the polymer solution do not differ significantly in morphology or texture from pure polymer fibers regardless of MOF content, aside from the visible inclusion of the MOF shown in Figure 24. The MOF tends to form small, widely

distributed aggregates when present at low concentrations (Figure 24a). The aggregates grow larger and are more prevalent as the MOF concentration increases, and at 50 wt% MOF they make up almost the entire fiber (Figure 24c). The MOF is contained in the fibers regardless of composition, and no unattached MOF is observed visually or in SEM. Despite the size of some of the MOF aggregates they always appear covered in some amount of polymer and bound to one or more fibers.

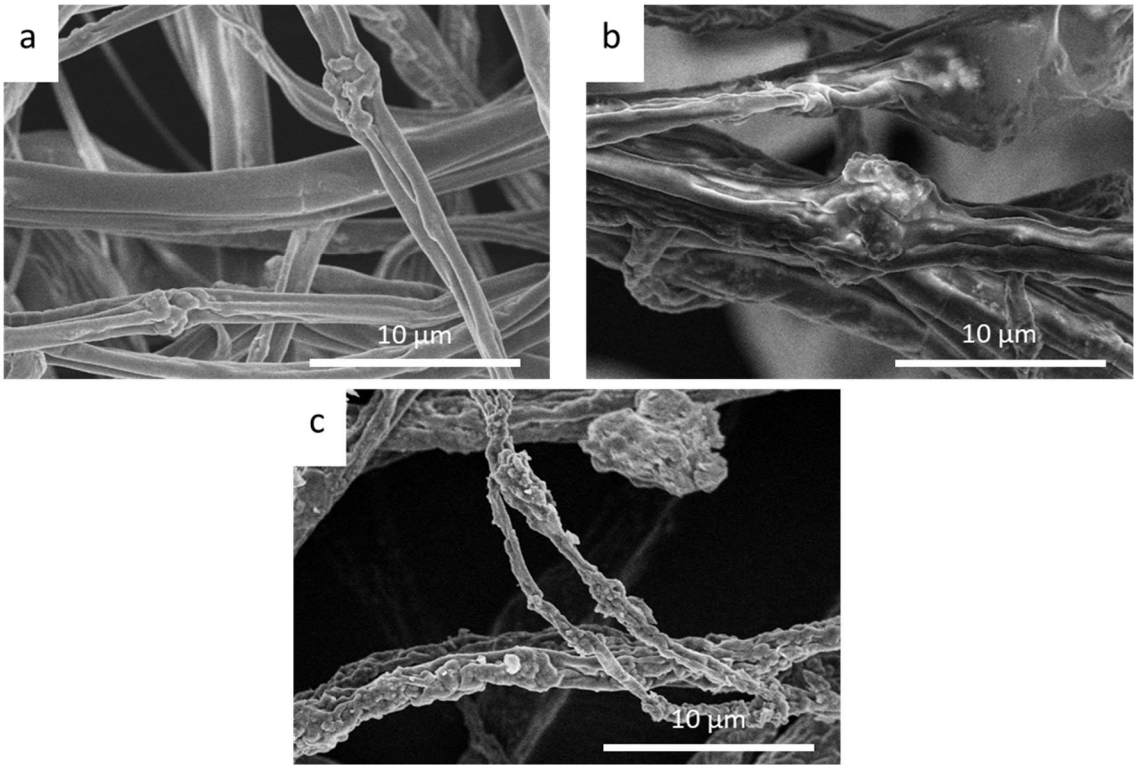

Figure 24 SEM images of MOF-bearing fibers. MOF content in wt%, average fiber diameter, and standard deviation of fiber diameter follow: a. 10 wt% (2.04 ± 1.67 µm); b. 30 wt% (1.62 ± 0.77 µm); c. 50 wt% (2.23 ± 0.86 µm)

The viscosity of the solution has the greatest impact on composite fiber diameter, and the average diameters are relatively unchanged from the pure polymer fibers with the same polymer concentration. Above 50 wt% MOF, the solutions become very viscous and do not form fibers when spun.

XRD patterns were used to confirm the identity of the MOF and any structural changes from incorporation into the composite and are shown in Figure 25. Measurements confirm the formation of UiO-66-NH_2 by comparison to previously reported crystallographic data. XRD patterns of the composite fibers show that the MOF is unchanged in terms of its crystallinity by incorporation into the fibers. This was expected given the stability of UiO-66 and its functional varieties, as well as the relatively benign solution components and spinning conditions.

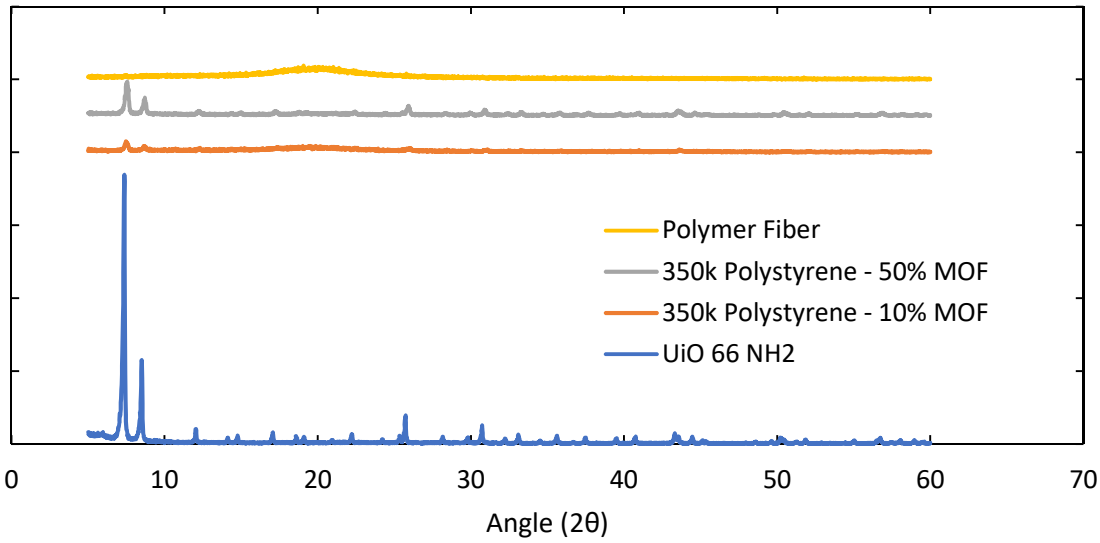

Figure 25 XRD patterns of SBS fiber composites and parent materials

The MOF content of a subset of composites was calculated from thermal gravimetric analysis. The amount of MOF calculated by this method matches the amount of MOF added to the original solution. This confirms that the spinning solutions are homogeneous and not affected by settling during the time between when they are mixed and when they are spun.

5.3.3.1 BET

The UiO-66-NH_2 used in the composite fibers has a surface area of 950 m^2/g, while the fibers themselves have no consistently measurable surface area based on BET calculation from nitrogen adsorption data measured at 77K. This indicates that all of the measurable surface area of the composites is due to its MOF content. We can judge the performance of the composite in terms of MOF accessibility by comparing its measured BET surface area as a percent of the pure MOF surface area to the amount of MOF we know to be in it. The results of the surface area analysis are presented in Table 6. These results show that in composites with 10 wt% MOF, the MOF is almost completely inaccessible, which yields composites with almost no measurable surface area. For the 192 kDa polystyrene samples, surface area is observed to increase with MOF content but is consistently lower than expected based on the actual MOF content. 350 kDa samples follow similar trends, although with lower surface areas for comparable concentrations and MOF contents.

Table 6 BET surface area derived from nitrogen adsorption isotherms at 77K for MOF-fiber composites

Polymer Concentration (wt%) & Mw (kDa)	MOF Content (wt%)	BET SA (m^2/g)	Percent of MOF SA
0% (Pure MOF)	-	950	100%
10% 192 kDa	10	11	1%
	30	62	7%
	50	242	25%
10% 350 kDa	10	8	0%
	30	57	6%
	50	149	16%
12.5% 192 kDa	10	22	2%
	30	101	11%
	50	275	29%
12.5% 350 kDa	10	2	0%
	30	18	2%
	50	104	11%
15% 192 kDa	10	6	1%
	30	118	12%
	50	111	12%
15% 350 kDa	10	4	0%
	30	23	2%
	50	82	9%

In studies of MOF-bearing polystyrene membranes, it was found that the MOF is largely inaccessible to nitrogen when present at low concentrations relative to the polymer. Only when the MOF percentage rises above 70 is surface area again measurable. This sudden increase can be explained by the formation of a percolating network by the MOF. At low concentrations the particles are isolated within the polymer bulk. They begin to cluster and to come into contact with each other at higher concentrations, allowing gas to

be transferred from the surface through the bulk via the connections between particles.[53-54] Because of the small fiber diameters and the tendency of the MOF to form clusters within the fibers, many small percolating networks can form along the length of the fiber at lower loadings than were used in the membrane study. This allows small gaps in the polymer skin to give access to entire MOF clusters rather than single particles. Given the poor polymer permeability at BET conditions, the lack of polymer porosity, and the MOF aggregates observed in SEM, the formation of connected networks of MOF particles explains the high surface area at low loadings. We observe an increase in surface area for the composites over the plain fibers even at relatively low MOF percentages compared to what we would expect in membranes or bulk polymer structures. More MOF results in higher surface areas, while polymer solutions that produce thicker fibers generally produce composites with lower surface areas. Some portion of the MOF is always rendered inaccessible by being embedded fully in the polymer, but the extent of its accessibility can be tuned based on MOF content and solution composition.

5.3.3.2 CO_2 and H_2O Adsorption

To expand our characterization of the system, carbon dioxide adsorption measurements were carried out at 25 °C. A subset of the composite samples was tested, with the results summarized in Table 7. All samples exhibit a higher capacity for carbon dioxide at 1 bar and 25 °C than their BET surface area predicts. This higher than expected capacity is likely due to increased polymer permeability at higher temperatures. While the carbon dioxide capacities of these composites are not particularly notable, these results show that BET surface area may not provide a complete picture of MOF accessibility, particularly for higher temperature applications where polymer permeability may play a

larger role. Despite greater accessibility, the carbon dioxide capacity for most samples is lower than would be expected given their actual MOF content. These results indicate that some of the MOF is still fully obstructed within the polymer matrix. Because the polymer is not distributed uniformly over the surface of the MOF particles it creates a greater barrier to diffusion of gas for some portion of the MOF.

It has been suggested in several studies that a hydrophobic polymer matrix may improve the stability of MOFs that break down in the presence of water.[52] While the MOF used in this study is water stable, its adsorption behavior towards water vapor when embedded in polystyrene gives an indication of the polymer's effectiveness as a moisture barrier. The isotherms are shown in Figure 26, and the numerical results are summarized in Table 1Table 7.

For every composite sample the water loading at 80% relative humidity is higher than the BET surface area predicts, suggesting that polymer permeability is relevant to water adsorption at 25 °C. When given as a percentage of the pure MOF capacity, the composite capacities are close to what was observed in the carbon dioxide adsorption experiments. This suggests that the same amount of MOF is accessible in each composite for each gas, and that some of the MOF is completely inaccessible within the polymer. It also indicates that, while polystyrene does prevent some amount of water from reaching the MOF, it is likely that it does reach the portion that contributes to adsorption of other gases. Based on this, we conclude that polystyrene in the fiber form examined here is not an effective moisture barrier.

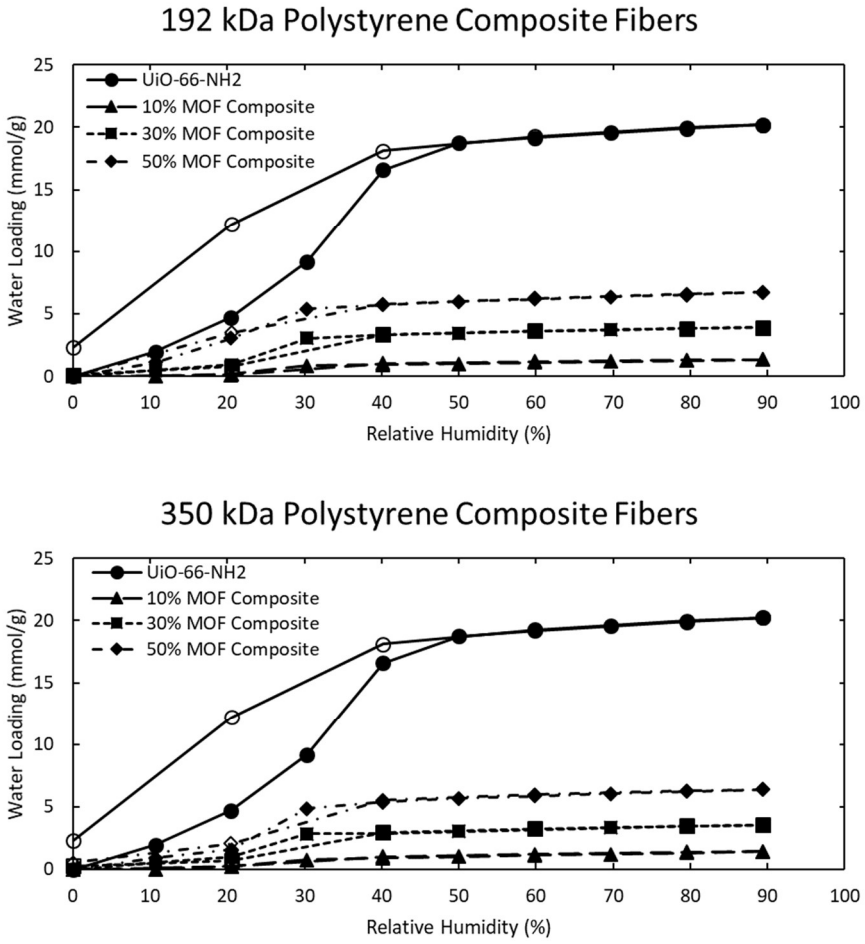

Figure 26 Water adsorption isotherms for MOF powder and MOF-fiber composites. Closed symbols are adsorption points, open points are desorption points

Table 7 Carbon dioxide and water vapor adsorption capacities measured at 25 °C

Sample	MOF Content from TGA	CO_2 Capacity at 1 bar (mmol/g)	Percent of MOF CO_2 Capacity	H_2O Capacity at 80% RH	Percent of MOF H_2O Capacity	Percent of MOF BET Surface Area
UiO-66-NH_2	100%	2.00	100%	19.91	100%	100%
192 kDa – 10% MOF	9%	0.17	8%	1.23	6%	1%
192 kDa – 30% MOF	30%	0.46	23%	3.82	19%	12%
192 kDa – 50% MOF	48%	0.78	39%	6.50	33%	12%
350 kDa – 10% MOF	12%	0.20	10%	1.32	7%	0%
350 kDa – 30% MOF	30%	0.49	25%	3.43	17%	2%
350 kDa – 50% MOF	48%	0.78	39%	6.23	31%	9%

5.4 Conclusion

We have reported the synthesis of a set of MOF-polymer composite fibers synthesized via SBS. Initial experiments with polymer fibers confirmed that SBS could produce fibers with diameters in the micron range with solution flowrates of up to 120 mL/h. The polymer concentration was determined to be the critical variable in determining fiber diameter and the texture of the fibers overall. This is primarily due to the increasing viscosity of the solutions as the polymer concentration increases. Composite fibers were produced from MOF suspension in polymer solutions and examined for both MOF stability and accessibility. SEM images and XRD patterns confirmed the presence of the MOF in the fibers and its stability toward synthesis conditions. Accessibility was first examined by N2 physisorption measurements, but the BET surface areas of the composites were found to be lower than expected for their MOF content. The onset of measurable surface area for

the composites is at 30 wt% MOF, whereas previous studies have suggested that up to 70 wt% is required to form an accessible percolating network in membranes made of similar materials.[53] This increase in composite surface area is due to the smaller length scales for polymer thickness present in the fibers, as well as the size of the MOF aggregates relative to the fibers. Examination of carbon dioxide adsorption at 25 °C showed a much higher accessibility for the MOF than the BET surface areas predicted due to an increase in polymer permeability at higher temperatures. Water adsorption isotherms at 25 °C agree with the carbon dioxide isotherms in terms of composite capacity, showing that while the polymer may provide an additional diffusion barrier for water vapor, it will not ultimately serve as an effective long-term moisture barrier for water unstable MOFs. MOF-polymer fibers produced by SBS provide an interesting platform for delivery of different MOFs to target a variety of applications, particularly those requiring scale-up or in-situ production.

CHAPTER 6. CONTROLLING POROSITY IN SOLUTION BLOWN MOF-FIBER COMPOSITES

6.1 Introduction

Metal-organic frameworks (MOFs) are hybrid materials composed of metal or metal oxide clusters connected by organic linkers.[10] A variety of functional groups can be incorporated into the MOF structure by anchoring them to the organic linkers, and the metal clusters can serve as open metal sites or catalytic sites depending on their chemistry and post-synthetic modification.[11, 23, 99] MOFs have been found to active as adsorbents or catalysts for a variety of toxic chemicals. These properties have drawn attention to MOFs as potential supplements to or replacements for existing materials in the field of personal protection and decontamination. One well studied MOF for this application is the zirconium MOF UiO-66 which, along with its functionalized variants, has been shown to adsorb toxic industrial chemicals like ammonia[29] and nitrogen dioxide[16], and to neutralize organophosphate chemical warfare agents like sarin.[35] However, MOFs are typically synthesized as fine powders, and must be processed into a form that can be used in a practical setting. A form that has drawn increasing interest is fiber-supported MOFs, which could be used to create self-detoxifying textiles for integration into protective clothing.

MOF-bearing fibers have been synthesized in several different ways. One method is to grow MOF crystals on the surface of pre-made fibers.[55, 57, 100] Surface growth generally involves immersing the fibers in a solution of MOF precursors and carrying out the typical solvothermal MOF synthesis. While it allows the use of naturally occurring fibers like

cotton or wood pulp as well as synthetic materials, surface growth often depends on specific chemistry present on the fiber surface and may require additional pretreatments to ensure MOF growth and successful anchoring. In addition, MOF crystals may form without attaching to the fiber surface, decreasing the efficiency of the synthesis, and the fibers must be able to withstand the conditions of the synthesis. A second common method for MOF-fiber synthesis is to create a slurry of MOF in a polymer solution, then spin fibers from that solution. This method has been used to produce microfibers and hollow fibers via extrusion into a solvent bath[58], and to produce nanofibers via electrospinning.[60-62] Composites produced from slurries have MOF particles embedded in them and can more easily control loading and prevent MOF loss through dust formation. One common factor for all the above methods however is that they require the composite to be produced well in advance of use because of the equipment and synthesis conditions required. This may allow time for the composite to degrade, or for the MOF to be lost, and would require current equipment production to be altered significantly to accommodate the new materials. A gap exists for in-situ synthesis of similar fibers to supplement existing equipment.

6.1.1 Solution Blow Spinning

Solution blow spinning (SBS) is a relatively new method for producing micro and nanofibers that may fill this in-situ gap. It uses compressed air to spray out a polymer solution from a nozzle.[93, 97] The droplets are elongated into jets by the shear forces, and the jets solidify in flight due to solvent evaporation and deposit as fibers onto a collector. Because it requires no heat, electrical field, or special equipment, SBS fibers can serve as a platform for delivering MOFs within nonwoven textiles as required by the presence of toxic chemicals without modifying existing equipment. In a previous study we examined

MOF-bearing SBS fibers for adsorption and found that the surface area and capacities of the fibers were lower than would be expected based on MOF content. This was explained by the formation of a glassy, non-porous polymer skin on the outside of the fibers, rendering a large portion of the MOF inaccessible.

6.1.2 Phase Separation

In order to improve MOF accessibility in SBS fiber composites, porosity must be introduced into the fiber to allow adsorbates to reach the MOF inside the fibers. Studies of electrospun systems have shown that the solvent used can significantly affect the morphology of the fibers[101-102], as can humidity[103] which results in the formation small pores called breath figures during the evaporation of the solvent from the fiber surface. However, this behavior has not been explored in SBS, and is difficult to achieve because of the specific conditions required. A potentially more reliable method to induce porosity is via non-solvent induced phase separation (NIPS), a technique commonly used to fabricate membranes and extruded polymer fibers.[104-105] NIPS relies on spinodal decomposition, using a non-solvent to destabilize a polymer solution and cause it to form polymer rich and polymer poor regions. The polymer poor regions become pores once the membrane solidifies. A conceptual phase diagram is shown in Figure 27. For membranes and extruded fibers the phase separation is induced by immersing the material in a bath of non-solvent before it can solidify through evaporation. The same process has been used in electrospun composites by incorporating the non-solvent into the fiber spinning solution and using a volatile solvent which changes the solution composition as it evaporates.[106-107] In this case the phase separation relies on a significant difference in evaporation rate between the solvent and nonsolvent.

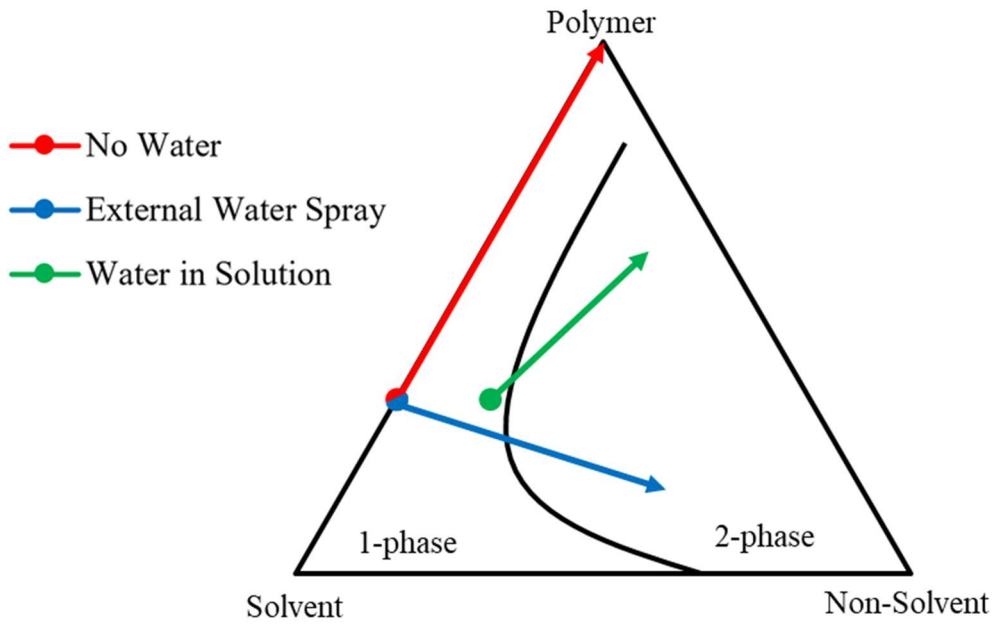

Figure 27 Conceptual ternary phase diagram showing the composition trajectories of three possible polymer solutions: binary solvent/polymer, binary with simultaneous non-solvent spray intersecting the SBS fiber spray, and ternary solvent/non-solvent/polymer

6.1.3 Motivation

This study will examine the incorporation of a nonsolvent directly into the polymer solution and simultaneous spraying of aerosolized nonsolvent in order to achieve porosity through nonsolvent induced phase separation. THF and water were selected as the solvent and non-solvent respectively because of their miscibility and their relatively large difference in volatility. Polystyrene was chosen as the polymer because of its low cost, ready availability and a significant quantity of prior data, and UiO-66-NH_2 was chosen as the MOF for its chemical stability and capacity to adsorb or break down several different toxic chemicals.

6.2 Materials and Methods

6.2.1 MOF

UiO-66-NH_2 was synthesized according to the procedure in Chapter 2 of this thesis. 5.448 mmol each of 2-aminoterephthalic acid and zirconium chloride were added to a mixture of 212 ml DMF and 0.8 ml distilled water. After complete dissolution of the reactants the mixture was divided into glass vials and placed in an isothermal oven for 24 hours at 120 °C. The products were combined after being removed from the oven and washed 3x with DMF and 3x with methanol. Before use in further synthesis, MOF samples were re-activated at 110 °C under vacuum to remove adsorbed water and any remaining solvent.

6.2.2 SBS Fibers

The solution blow spinning device consists of a nozzle made from two coaxial tubes. The inner tube was an 18-gauge needle protruding 1 mm from the outer tube, which had a diameter of 2 mm. Nitrogen at 20 psi was blown through the outer tube, and a polymer solution was flowed through the inner tube at 60 mL/h using a syringe pump. A flat aluminum foil collector was positioned 35 cm from the tip of the nozzle.

Three sets of fibers were created using different components and conditions. The first was produced from a binary mixture linear polystyrene (Mw = 192 kDa) dissolved in THF. The second was produced from the same binary mixture, but an artist's spray brush was used to create a spray of aerosolized water that intersected with the fiber jet from the SBS nozzle. In this case the water was driven by a flow of nitrogen at 30 psi and the flow rate

was not regulated. The third was produced from a ternary mixture of polystyrene dissolved in THF with 5 wt% water added.

MOF bearing fibers were produced from a MOF-polymer slurry. First the MOF was suspended in the solvent via sonication before dissolving the polymer. The mass of the added MOF was determined based on the mass of the polymer included in the solution and the desired MOF content of the final, dry fibers.

6.2.3 Characterization

Powder X-ray diffraction (PXRD) patterns were obtained using a Panalytical XPert PRO Alpha-1 XRD. SEM images were taken with a Hitachi SU8010 SEM. TGA measurements were taken using a TA Instruments Q50. Nitrogen physisorption data was obtained using a Quantachrome Quadrasorb Evo. Samples were outgassed at 80 °C before adsorption to remove residual solvent. Mercury porosimetry was used to determine macropores and mesopores of the polymer fibers. The measurement was taken by an AutoPore IV (Micromeritics) porosimeter. The pore size distribution was calculated via Washburn equation.

6.3 Results and Discussion

6.3.1 Polymer Fibers

SEM images of the polymer fibers without MOF are shown in Figure 28. Fibers spun without water had morphologies ranging from cylindrical to ribbon-like, but always appeared to have smooth, non-porous surfaces. When water was added by simultaneous spray during fiber spinning the overall morphology of the fibers remains the same, and no

significant change in fiber diameter can be seen in the SEM images. However, the surface of these fibers appears to be much more porous. This porosity may be attributed partially to phase separation, but also to significant formation of breath figures. Because the secondary spray saturates the air with water and water vapor, more condensation is expected to form on the surface of the drying fibers as rapid solvent evaporation cools them. The pores for these samples all appear to be round, consistent with the formation of breath figures after the jet has formed, but before it is fully dried into a fiber.

When a small amount of water was added directly to the polymer solution before fiber spinning, the morphology of the fibers changed much more significantly than in the previous cases. The average fiber diameter rose, and the fibers tended to be more irregularly shaped. This morphological change is likely due to the addition of water, resulting in an increase in solution viscosity which was shown in a previous study to control fiber diameter and shape. In addition, more extensive surface irregularity is visible in SEM. In these samples, breath figures appear, but the majority of the pores are elongated to a significantly higher degree than in the samples discussed above. This points to their formation occurring while the solution jet is still forming and being thinned by the air flow from the nozzle, suggesting that phase separation is playing a much greater role. The polymer rich and poor regions form almost immediately as the solvent rapidly evaporates, and both are stretched by the shear into the shapes visible in the SEM images.

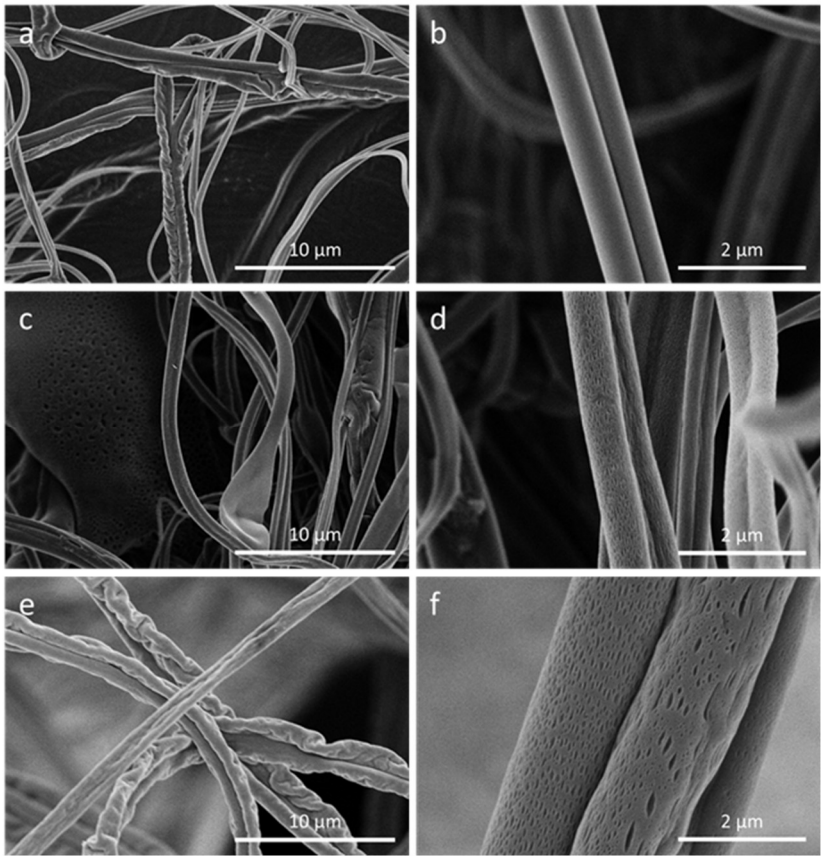

Figure 28 Polystyrene fibers produced via SBS. Fibers contain no MOF. a,b: binary solution; c,d: binary solution with simultaneous water spray; e,f: ternary solution

Although the surface morphology visibly changes with the addition of a non-solvent it is difficult to tell from images alone whether the pores permeate the polymer skin on the surface of the fibers, or significantly impact the overall porosity of the fibers. Mercury porosimetry data, shown in Figure 29 can provide a more quantitative approach to evaluating fiber porosity. Adding water in an external spray results in an increase in pores between 7 nm and 20 nm compared to the control with no water. This corresponds to the diameter of many of the small breath figures seen in the SEM images. When water is added directly to the spinning solution the effect is magnified and continues to pore diameters of 50 nm. This data confirms the formation of new pores with the addition of water and

suggests that the pores penetrate the polymer skin rather than simply forming indentations in the fiber surface.

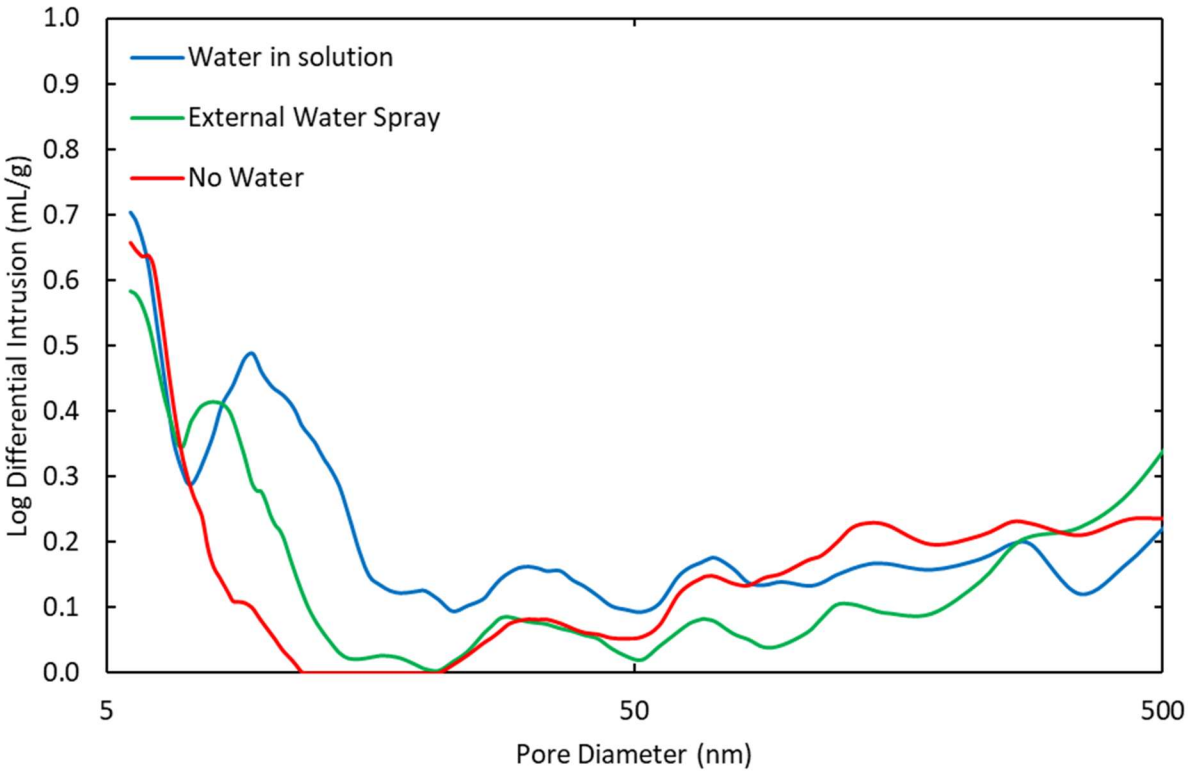

Figure 29 Mercury porosimetry data showing increase in porosity with water (non-solvent) inclusion

6.3.2 Composite Fibers

TGA measurements were used to confirm the MOF loading of each composite sample. The MOF loading for each sample was found to be what was expected based on the initial composition. The MOF suspension was stable, and the MOF appears not to have significantly aggregated or settled before spinning. XRD measurements confirmed that the crystallinity of the MOF was unaffected by the SBS process.

SEM images of the composite fibers are shown in Figure 30. MOF aggregates are clearly visible in every composite sample and appear to be well distributed throughout the fibers. With increasing MOF loading the aggregates grow larger and more frequent, and at 50 wt% the MOF appears to be distributed throughout the fibers continuously. The morphology trends with respect to water inclusion were unchanged from the pure polymer fibers, with breath figures, pores, and changes to fiber diameter. In composites produced with added water, MOF particles visible through some of the larger pores, adding further evidence that the pores penetrated the polymer skin to reach the interior of the fibers. Regardless of water inclusion, the MOF appeared to be contained within the fibers in every sample, with no loose or unattached MOF particles.

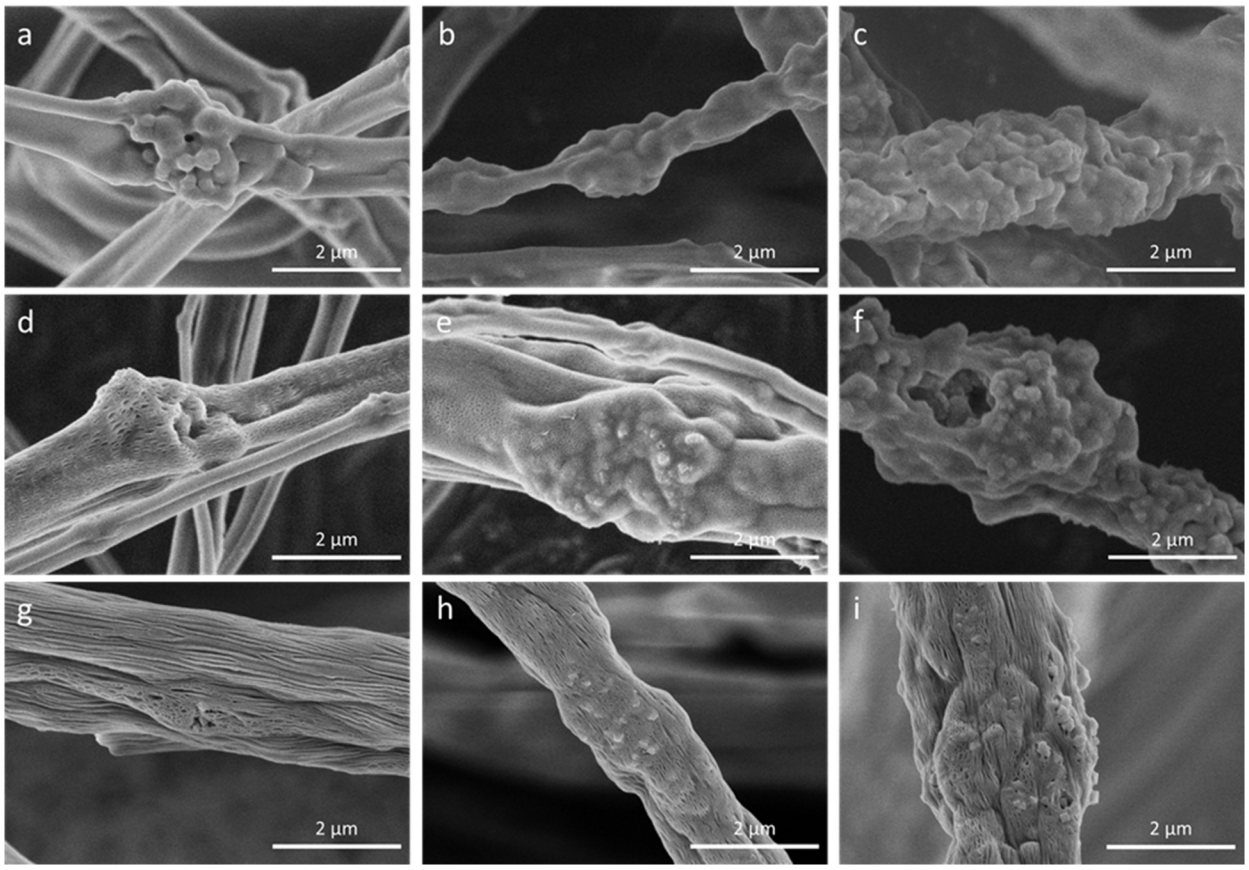

Figure 30 SEM images of fiber composites with different UiO-66-NH_2 loadings. a,b,c: binary solution with 10%, 30%, and 50% MOF respectively; d, e, f: binary solution with simultaneous water spray with 10%, 30%, and 50% MOF respectively; g, h, i: ternary solution with 10%, 30%, and 50% MOF respectively

6.3.2.1 BET

Nitrogen physisorption and BET analysis were used to measure the accessibility of the MOF within the composites. The MOF UiO-66-NH_2 had a surface area of 816 m^2/g, and the fibers had no measurable surface area regardless of water inclusion. The composite surface areas can be used to estimate MOF loading by comparing them to the surface area of the parent MOF. Comparing this loading estimate to the actual loading determined by TGA provides a metric for MOF accessibility in the composite. The results for the composites are summarized visually in Figure 31 and numerically in Table 8.

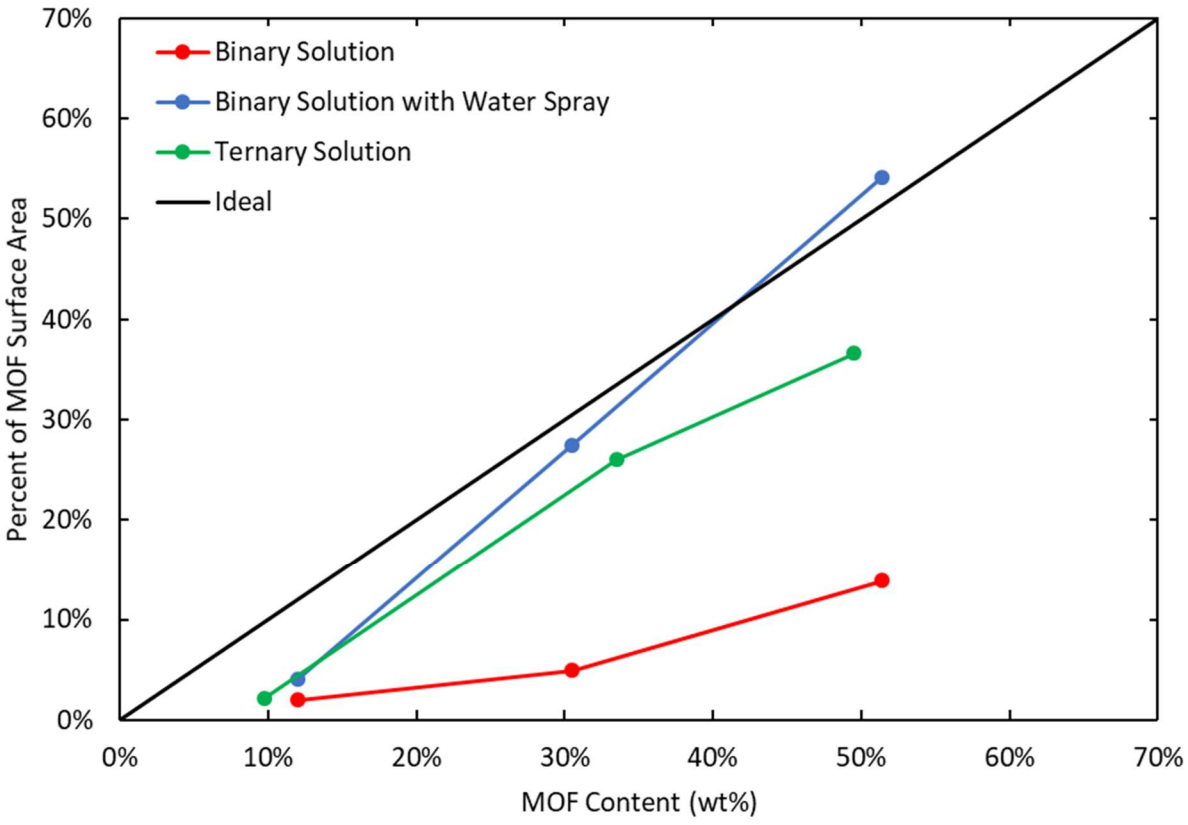

Figure 31 Comparison of MOF content in fiber composites with the percent of the MOF surface area represented by the surface area of each composite. Ideal performance with completely accessible MOF is represented by the diagonal black line

Table 8 Numerical BET data for fiber composites with phase separation

Solution Composition	MOF Content (wt%)	BET SA (m^2/g)	Percent of MOF SA
0% (Pure MOF)	-	816	100%
Binary Solution	0	5	1%
	10	16	2%
	30	40	5%
	50	113	14%
Binary Solution with Water Spray	0	6	1%
	10	33	4%
	30	224	27%
	50	442	54%
Ternary Solution	0	3	0%
	10	18	2%
	30	212	26%
	50	299	37%

Fibers spun from binary THF/polystyrene solutions performed poorly in terms of their BET surface area relative to their MOF loading. Even at a loading of 50 wt% MOF the composite surface was only 14% of the parent MOF surface area, indicating that much of the MOF is inaccessible to the nitrogen used in BET analysis. This is explained by the formation of a non-porous polymer skin around the outside of the fibers when the volatile THF rapidly evaporates from the surface of the solution jet. Adding water to the fiber spinning solution significantly increases the surface area of the MOF-fiber composites produced. Both the simultaneous spray and solutions that include water directly in the spinning solution give surface areas that match much more closely to what we would

predict based on actual MOF content. This increase in accessibility is more pronounced at higher MOF loadings due to larger MOF aggregates visible in SEM. At low loadings the more distributed MOF particles may still be significantly covered by the polymer, but if one portion of a large aggregate is accessible via pore formation then the rest of the aggregate will be as well. The heightened MOF accessibility confirms that the porosity induced by water inclusion penetrates the surface of the fibers and disrupts the formation of the impermeable polymer skin.

6.4 Conclusions

We successfully produced fibers from solutions of polystyrene in THF via SBS. Incorporating water by mixing it into a ternary solution or by simultaneous spraying created porous fibers via non-solvent induced phase separation and breath figure formation. The presence and extent of the porosity was probed via SEM and mercury porosimetry. The primary pore formation mechanism for the simultaneous spray samples appears to be breath figure formed during solvent evaporation from the water saturated air. The ternary solutions appear to develop pores based on phase separation, which are then stretched as the solution jet elongates. Spinning MOF suspensions created MOF-bearing composite fibers with the same morphological characteristics as the pure polymer fibers. Composite fibers with water incorporated had BET surface areas close to what was expected based on their MOF loading, suggesting that the pores penetrated the polymer skin of the fiber and allowed the adsorbate to reach the MOF more easily. With their high MOF accessibility, these composite fibers could be used to produce clothes, coatings, or masks to efficiently decontaminate or protect individuals exposed to toxic chemicals.

CHAPTER 7. CONCLUSIONS AND RECOMMENDATIONS

7.1 Hydrophilic PolyHIPEs

7.1.1 Work Completed

Composites were successfully synthesized by mixing MOF powder into a high internal phase emulsion containing 2-hydroxyethyl methacrylate monomer and methylene bisacrylamide crosslinker before polymerization. The resulting MOF@polyHIPE materials retained the morphology of the emulsion, creating foams with approximate void volumes of 74% with the MOF particles distributed through and embedded in the polymer. PXRD patterns revealed that the process did not alter the crystallinity of the embedded MOF, and TGA meausrements showed MOF loadings between 30 wt% and 70 wt%.

Nitrogen adsorption isotherms taken at 77 K yielded BET surface areas for the composites lower than what was expected based on their known MOF content. This indicated that the MOF was being obstructed by some part of the emulsion mixture, due to (i) pore blocking by monomers, (ii) embedding under a layer of polymer, (iii) interaction with the polymeric surfactant, or some combination of the three. Higher capacities for water and CO_2 at room temperature suggested that permeability played a role in MOF accessibility, and that higher temperatures increased permeability. Catalysis experiments using the CWA simulant DMNP revealed that the rate of catalysis corresponded to the BET surface area, further confirming that the MOF is obstructed, and showing BET surface area as a metric of performance both for adsorption and for catalysis in these composites.

Several methods were explored to determine the source of the relatively low surface areas and capacities of the MOF@polyHIPE composites. Pre-polymerization was used to convert monomers into oligomers before incorporation of the MOF, preventing pore blocking by small molecules. This had no significant effect on the composite surface area and resulted in significant distortions of the foam structure at high MOF loading. Post-synthetic modification to create hydrophobic MOF particles was used to prevent the MOF from becoming completely embedded in the polymer, but this also had little effect on composite surface area. The failure of PSM may be related to the distortion or collapse of the emulsion caused by the hydrophobic particles, leading to a composite that resembles a bulk MOF-polymer composite rather than a MOF@polyHIPE composite after polymerization. Finally, Pickering emulsions were examined both to eliminate the surfactant entirely and to force the MOF to the oil-water interface of the emulsion, resulting in it being located at the air-polymer interface of the polymerized foam. This also had little to no positive effect on the composite surface areas and created closed-cell foams rather than the open-cell foams seen in the original synthesis. The structure of the Pickering emulsions and the relatively low loadings lead to low surface areas compared to the MOF loading.

Based on the results of the experiments conducted here, the MOF is concluded to be obstructed by a layer of polymer covering it and by interactions with the surfactant. It appears as though both contribute, but to deconvolute the effects has proven difficult given the other morphological changes that occur when attempting to eliminate either factor. Despite this poor performance, the composites still outperformed what would be expected from similarly formulated membranes or bulk polymers containing MOF particles.

7.1.2 Proposed Future Work

7.1.2.1 Alternative Separation Applications

While the hydrophilic MOF@polyHIPE composites underperformed in gas phase separations, it is possible that they would be more suited to aqueous separations. Potential applications in this field include heavy metal removal and dye adsorption. Because the crosslinked 2-hydroxyethyl methacrylate is a hydrogel it can take up a significant amount of water. The macroporous structure of polymer contributes to the uptake volume and provides pathways for diffusion into the body of the composite. MOF@polyHIPE composites would be expected to provide structure, mechanical support, and ease of recovery not found in MOF powders in aqueous applications. Because the hydrogel would be swollen by water, it is possible that the composites would display more ideal performance for separation of water-soluble materials, facilitating access to the MOF via diffusion through the swollen polymer rather than blocking diffusion as observed with gases.

One significant problem found with MOF@polyHIPE composites using a hydrogel is shrinkage and distortion caused by the removal of water after synthesis. This causes a loss of mechanical stability, formation of cracks, and inability to cast composites into exact shapes. If used in aqueous separations, however, the drying could be avoided and the polymer used in its as-synthesized, water-swelled state. This use would rely on diffusion through the water laden composite, and on the MOF affinity for the adsorbate to displace water within the pores rather than uptake into a dry polymer matrix. By avoiding completely drying the composites, their shapes could be maintained without distortion, and

the MOF accessibility could be preserved because of the significantly swollen polymer. Alterations to crosslinker identity and content could provide additional levels of control to the swelling of the polymer, and higher internal phase fractions could be explored if shrinking based on water removal were not a factor in synthesis.

7.1.2.2 Alternative Additives to Pickering Emulsions

Using MOF particles rather than surfactant to stabilize the high internal phase emulsions results in the void walls of the resulting polyHIPE being lined with MOF particles. This has the potential to eliminate both surfactant interactions with the MOF and the polymer layer covering the embedded MOF particles, resulting in higher MOF accessibility. However, in reality it creates a polyHIPE with walls too thick to be ripped by contraction during polymerization, and so the resulting foam has a closed cell morphology, essentially creating a polymer membrane around each void and the MOF particles in them.

In this project small amounts of added surfactant were explored as a means to overcome the closed cell morphology. Other methods exist however that could accomplish the same goal. One potential method is to utilize both small and large particles in the formation of the emulsion. If the large particles were significantly larger than the length scale of the polymer layer between internal phase droplets, it is possible that they could bridge the polymer layer and create links between the voids in the dry polyHIPE composite. The larger particles might also be chosen to be soluble in some solvent or vulnerable to a chemical reaction that would break them down, allowing them to be completely removed to leave an additional level of hierarchical porosity that might create a more open-cell structure. Another potential method is to utilize a secondary polymer system in addition to

the 2-hydroxyethyl methacrylate chosen to be selectively removed after polymerization. Like the particle process described above, this could also result in regions of removed polymer that bridge the layer between voids in the MOF@polyHIPE composite, recovering the open-cell structure and allowing access to the MOF without any surfactant required.

7.2 Hydrophobic PolyHIPEs

7.2.1 Work Completed

MOF@polyHIPE composites were created with styrene crosslinked by divinylbenzene as the polymer matrix, with a final void fraction of approximately 90%. These composites were synthesized both by mixing the MOF directly into a preformed emulsion before polymerization, as with the hydrophilic materials, and by suspending the MOF particles in the aqueous phase before forming the emulsion. The MOF loadings ranged from 10 wt% to 60 wt%, and the distribution of the MOF within the matrix depended on the method for dispersing it in the emulsion. Simply mixing it into the emulsion resulted in an uneven distribution on a microscopic level, with aggregates forming MOF-rich areas within the polymer matrix, while distribution in the aqueous phase resulted in more evenly distributed MOF. In either case the mechanical properties of the composites were not altered to a noticeable extent, and the polymer does not shrink or distort after washing and drying, instead retaining its cast shape.

The accessibility of the MOF within the polymer for these composites was found to be nearly ideal across a range of crosslinker percentages. Accessibility was determined by comparing predicted BET surface areas to measured BET surface areas for the composites. This can be explained by the relative hydrophilic nature of the MOF particles relative to

the hydrophobic polymer, preventing it from entirely covering the particles, by the much higher internal phase volume of the hydrophobic composites (90% vs 74%), and by the aggregation of the MOF. Because the composites do not warp or shrink during or after curing and drying, they can be cast into a variety of shapes and sizes to suit specific applications.

7.2.2 Proposed Future Work

7.2.2.1 Composition Alterations

This thesis work was restricted primarily to the crosslinker content and MOF content of the MOF@polyHIPE composites. In previous works on similar systems with pure polymers, it was found that the extent of crosslinking could have an effect on the surface area of the composites, a trait confirmed by this work. Additionally, it was assumed that the crosslinker content would have a significant effect on the stiffness and mechanical stability of the composites. However, several other variables could be altered to change the characteristics of the composites.

Internal phase volume is one such variable that could have a significant effect on the composites and their performance. High internal phase emulsions have internal phase volumes higher than 74%, and in this work a 90% internal phase polymer was used. This provides significant macropore space for diffusion but may weaken the structure and decreases the volumetric efficiency or capacity of the composite. Decreasing the internal phase volume could strengthen the composites and create denser structures with more active material in the same area. Conversely it could lead to a lower MOF accessibility

based on thicker polymer walls between voids. Systematically varying the internal phase volume is a significant next step in examining these composites.

A second potential variable is secondary polymeric additives. In prior work involving polystyrene crosslinked by divinylbenzene, it was found that a small amount of a different monomer could significantly affect glass transition temperature of the composites, affecting their stiffness and mechanical properties depending on the temperature. By adding small amounts of monomers other than styrene and divinylbenzene, the properties of the composite could be tuned beyond what can be achieved through crosslinker content alone.

A third variable to examine is the inclusion of different solvents in the internal or external phase of the emulsion. Some solvent, like toluene, have been found to be porogenic in the styrene-divinylbenzene system. Because of their effect on nucleation during polymerization, inclusion of these porogenic solvents can create additional porosity in the polymer itself at the micropore level, potentially increasing the BET surface area of the polymer and providing additional adsorption sites or pores to access embedded MOF particles. Should a lower internal phase volume reduce MOF accessibility, porogenic solvents may provide a method to recover accessibility by improving the permeability of the polymer itself through porosity. Added solvents can also have an effect on the stability of the emulsion, resulting in faster or slower droplet coalescence or Ostwald ripening and ultimately affecting the size of the voids in the final polymer structure and the windows between them. An examination of the effects of these alterations, and specifically of their effects on MOF surface area is an excellent next step.

7.2.2.2 Additional Pore Hierarchies

Work done with these composites has shown a combination of micropores provided by the MOF, macropores provided by the polymer, and larger channels or openings provided by the casting mold. An extension to this work would be to incorporate additional, intermediate pore structures, and to create gradients within single composite bodies. This could be accomplished through several methods, the simplest of which is to create molds with finer features, providing gradients through the shape the polymer is cast in. Incorporating intermediate sized particles into the emulsion which can be removed via dissolution or reaction after polymerization could also provide an additional level of intermediate porosity without the need for specially fabricated molds. Finally, aging the emulsions may result in larger internal phase droplets via coalescence and Ostwald ripening. By utilizing one or more of these methods additional pores and channels could be created with sizes not present in the composites examined in this work. If a large composite body was created by layering together several emulsions, each with increasingly fine pores, a gradient could be created within a single, continuous material, suited for both gas transport and reaction or adsorption in the finest pores.

7.2.2.3 Extended Adsorption and Mechanical Testing

This work did not extend beyond qualitative observations of the mechanical strength of the composites produced and was primarily focused on their characteristics as adsorbents under laboratory conditions similar to those examined for pure MOF samples. In order extend this work and use these composites in real world applications, quantitative mechanical tests will be required to determine the effects of composition and structure on

their mechanical stability. This will allow further optimization of the structures to match specifications for particular processes. Additionally, characterization of the composites beyond the isothermal adsorption measurements examined here will be required as well. Examination of the kinetics, transport limitations, and regeneration costs for processes like pressure swing adsorption that we have proposed for these composites will provide a more accurate prediction of performance in actual applications. Evaluation of the composites in more realistic adsorption unit operations will also allow changes in the shape and structure of the composite to be evaluated beyond their effect on the adsorption capacity alone.

7.3 SBS Fiber Composites

7.3.1 Work Completed

Beginning from the goal of a MOF-fiber composite that could be applied directly to a person or surface as required for protection against toxic gases, this work examined fibers produced via SBS. Polystyrene was chosen for the fiber material because of its low cost, non-hazardous characteristics, and because of the work that has been done using it in electrospinning in the past. Fibers were successfully produced from a number of different solvents, and those spun from ethyl acetate were systematically examined to determine the optimal conditions for production. When MOF was added, the performance was similar to what was observed in the hydrophilic polyHIPEs: low surface areas and adsorption capacities compared to predictions based on loadings. This was determined to be an effect of the polymer forming an impermeable skin layer over the MOF inside the fibers.

To improve adsorption performance a nonsolvent was added to the solution to induce phase separation during fiber spinning. It was found that including the nonsolvent in the

polymer solution and spraying it simultaneously from a separate nozzle both created additional porosity and disturbed the formation of the skin layer, resulting in significantly improved performance based on BET surface areas.

7.3.2 Proposed Future Work

7.3.2.1 Expansion to Other Polymers and Solvents

While this work has provided an initial example of a polymer system that can support accessible MOF particles, advantages could be gained by expanding to include other polymers and solvents that provide different characteristics that may benefit specific applications and environments. Fiber formation through SBS is dependent on reaching a critical polymer concentration, with enough chain overlaps to produce a continuous fiber, while also preventing the solution from becoming too viscous to be spun. Cellulose acetate solutions, for example, were found to be too viscous to form fibers using the equipment from this work at the concentrations necessary for sufficient chain overlap. Each polymer/solvent system relies on a different balance of these variables and establishing which combinations can be used for fiber formation and the characteristics of the fibers formed would be valuable in the future. With enough experiments it is possible that a common relation between variables could be found to predict fiber formation without extensive experimentation in new systems.

7.3.2.2 Mechanical Testing and Improvement

One significant gap in this work is a lack of mechanical testing of the SBS fibers. This work focuses primarily on the adsorption performance of the composites, but in the

future the mechanical stability will be an important part of the overall characterization, including both qualities like tensile strength and resistance to abrasion.

One drawback to SBS fibers as they are currently synthesized is that they are oriented randomly on the surface of the collector. The fibers rely on only cohesion to remain in a single layer and are not strong in any particular direction. Aligning the fibers via a rotating collector or some other secondary step in the synthesis could provide additional strength and prevent the fibers from breaking or separating. Another possible solution is to incorporate a second polymer at a low concentration from a second spray source. A small amount of additional polymer could act as an adhesive, creating more bonds between fibers and helping to form an interconnected fiber network without compromising the accessibility of the MOF.

APPENDIX A. SUPPLEMENTAL DATA AND IMAGES FOR CHAPTERS 2 AND 3

Figure 32 Example of cured polyHIPE samples, without MOF on the left, with MOF on the right. Samples shown are ~1/2" in diameter.

A.1 Ammonia Adsorption

A.1.1 Method

Samples were broken down and sieved to 20x40 mesh particle size. The particles were packed into a vertically oriented quartz bed to a volume of 55mm^3 and activated at 80 °C for 2 h under 50 mL/min N_2 flow. After allowing the bed to cool, the gas stream was switched to a flow of 1500 ppm NH_3 in air at a rate of 20 mL/min. For humid runs, 16 mL/min of air was flowed through a water bubbler and then mixed with a 7155 ppm NH_3 stream flowing at 4 mL/min for a final concentration of 1431 ppm NH_3 and approximately 80% relative humidity. The effluent stream was analyzed using an Analytical Technology H10-15 ammonia electrochemical sensor taking data points at 30s intervals. When the ammonia concentration in the effluent reached 500 ppm the NH_3 flow was switched to N_2 at 50 mL/min to desorb NH_3 from the bed. The dead volume of the system was calculated

using a blank bed of sand, and no significant pressure drop was observed across the bed. Adsorption capacities were calculated based on a relative concentration of 10% in the effluent.

A.1.2 Results

Table 9 Data summary for dry ammonia breakthrough using HEMA polyHIPE composites

Sample	Assumed MOF Mass Percentage	MOF Mass Percent from BET	Measured Capacity (mmol/g)	Theoretical Assumed Capacity (mmol/g)	Theoretical Accessible Capacity (mmol/g)
Polymer	0 %	0 %	0.14	-	-
50 mg Composite	30.6 %	7.0 %	0.40	0.93	0.32
150 mg Composite	62.6 %	22.7 %	1.05	1.77	0.73
UiO-66-NH_2	100 %	100 %	2.74	-	-

Table 10 Data summary for humid ammonia breakthrough using HEMA polyHIPE composites

Sample	Assumed MOF Mass Percentage	MOF Mass Percent from BET	Measured Capacity (mmol/g)	Theoretical Assumed Capacity (mmol/g)	Theoretical Accessible Capacity (mmol/g)
Polymer	0 %	0 %	0.44	-	-
50 mg Composite	30.6 %	7.0 %	1.26	1.02	0.57

150 mg Composite	62.6 %	22.7 %	1.08	1.63	0.87
UiO-66-NH_2	100 %	100 %	2.34	-	-

A.2 TGA

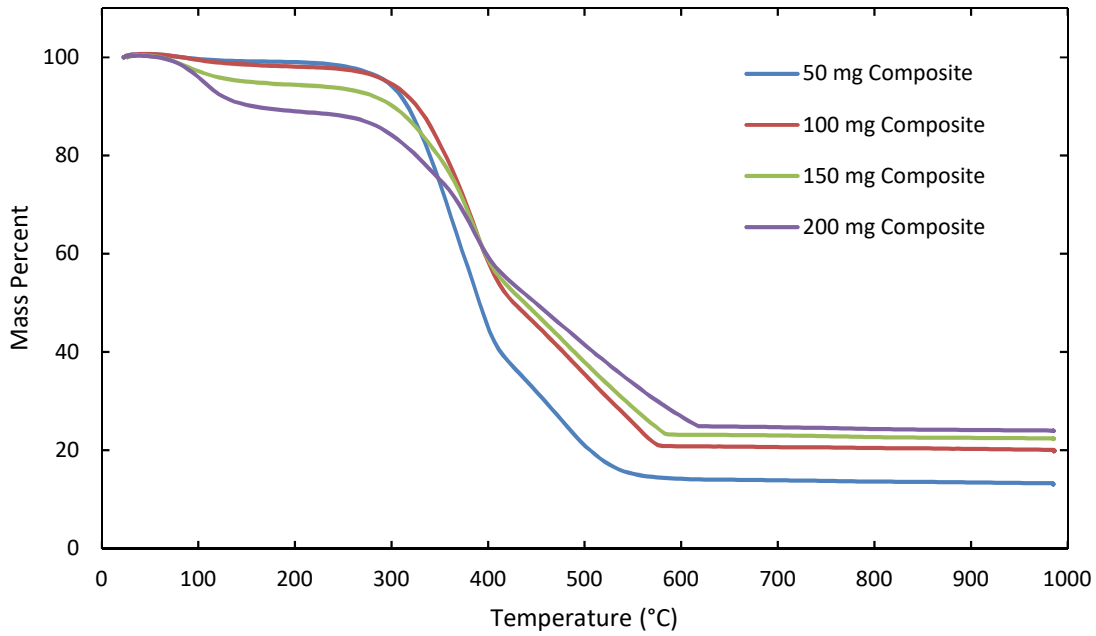

Figure 33 TGA curves for HEMA polyHIPE composites with different levels of MOF loading

Table 11 Data summary from TGA experiments with HEMA polyHIPE composites

Sample	MOF Content fromTGA
Polymer	0 %
50 mg Composite	37 %
100 mg Composite	57 %

150 mg Composite	67 %
200 mg Composite	76 %
UiO-66-NH_2	100 %

APPENDIX B. SUPPLEMENTAL DATA AND IMAGES FOR CHAPTER 4

B.1 TGA

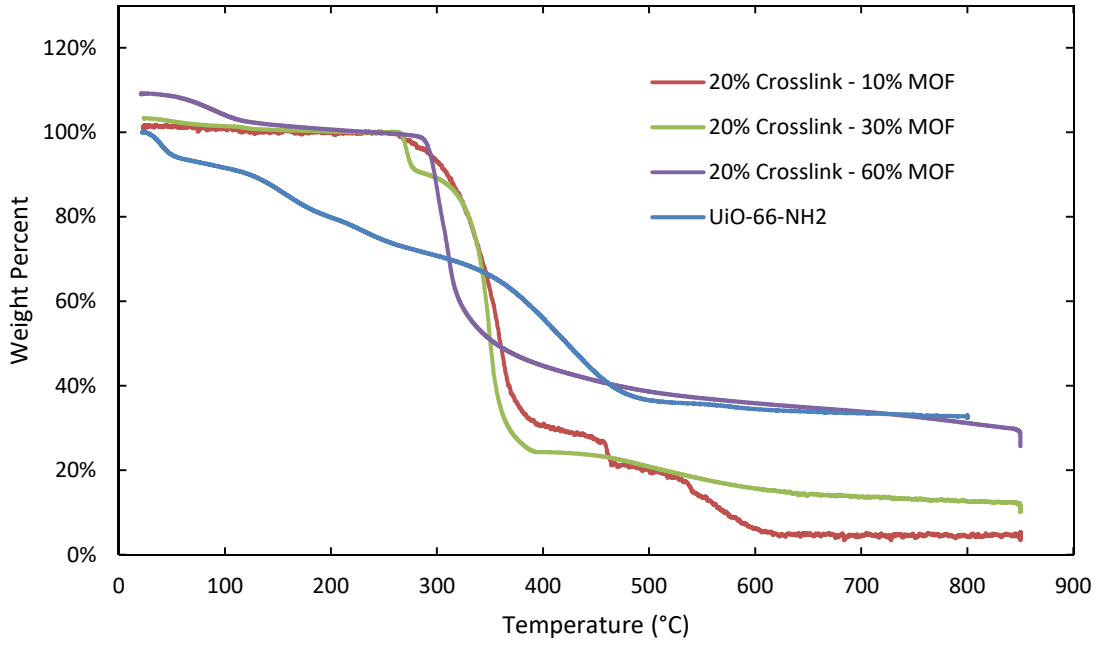

Figure 34 TGA curves for styrene polyHIPE composites with 20% crosslinker

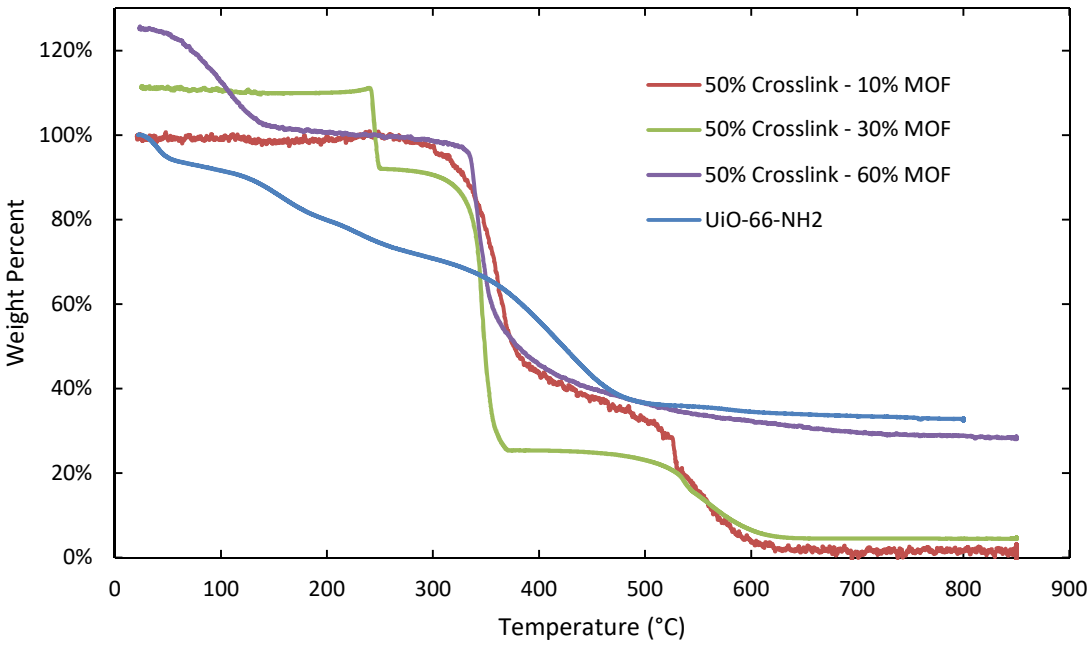

Figure 35 TGA curves for styrene polyHIPE composites with 50% crosslinker

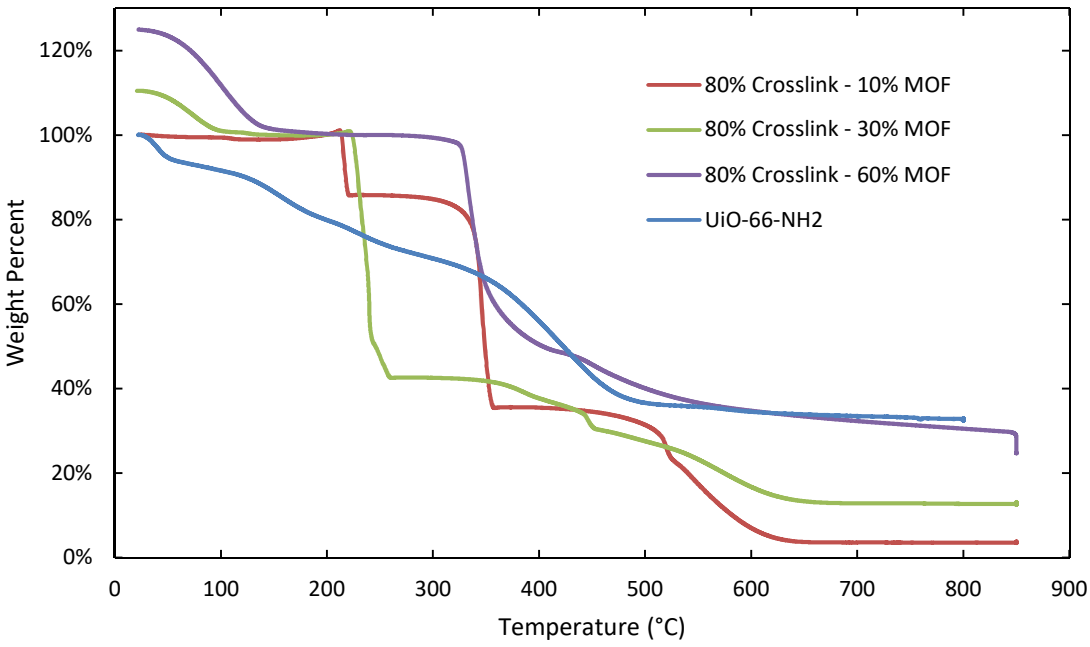

Figure 36 TGA curves for styrene polyHIPE composites with 80% crosslinker

B.2 Images

Figure 37 Styrene-based polyHIPE molded into an approximation of a honeycomb monolith. An example of shape retention and molding proposed in the main text

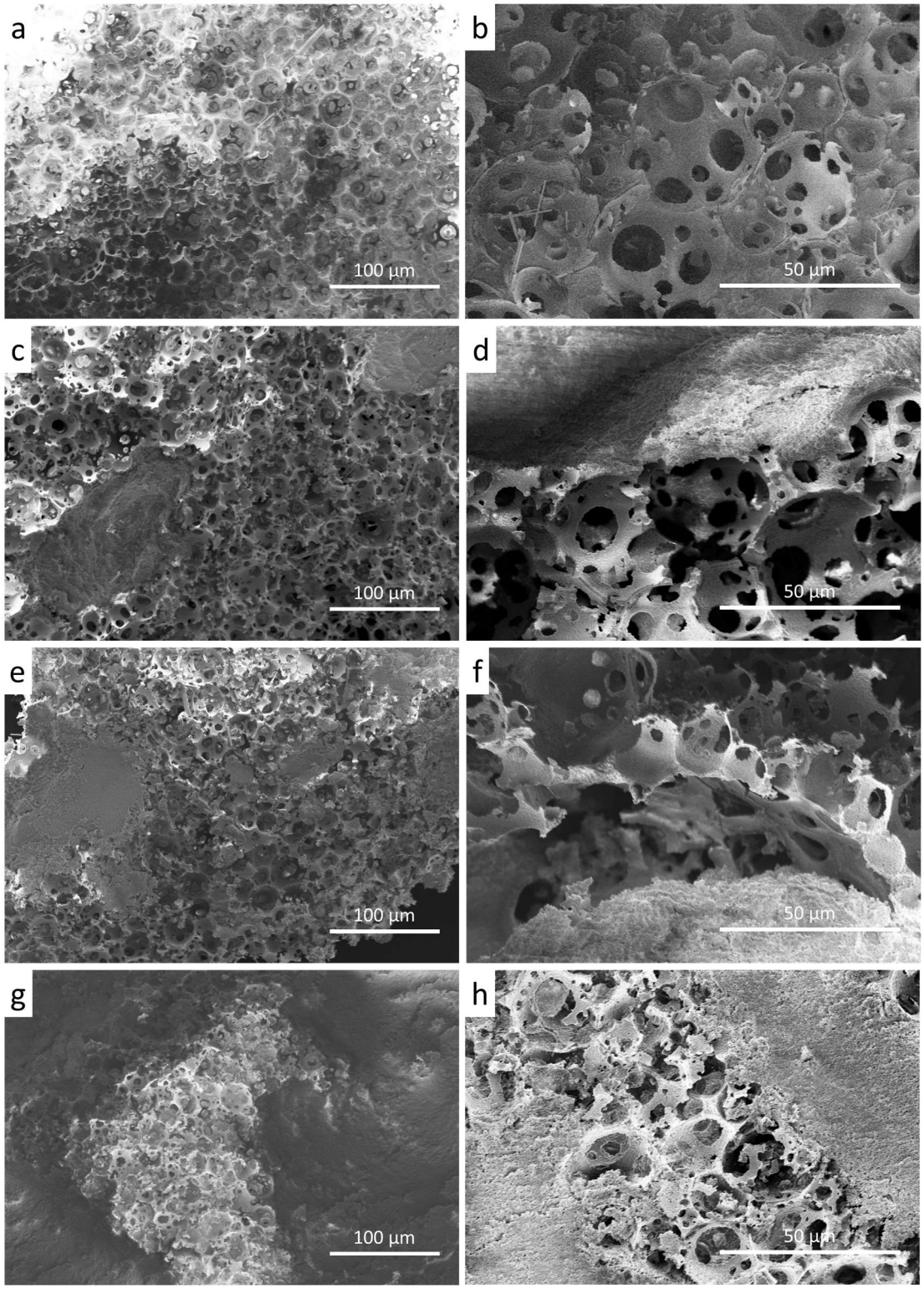

Figure 38 SEM images of UiO-66-NH_2 MOF@polyHIPE composites with 20% crosslinker. a, b: 0% MOF; c, d: 10% MOF; e, f: 30% MOF; g, h: 60% MOF

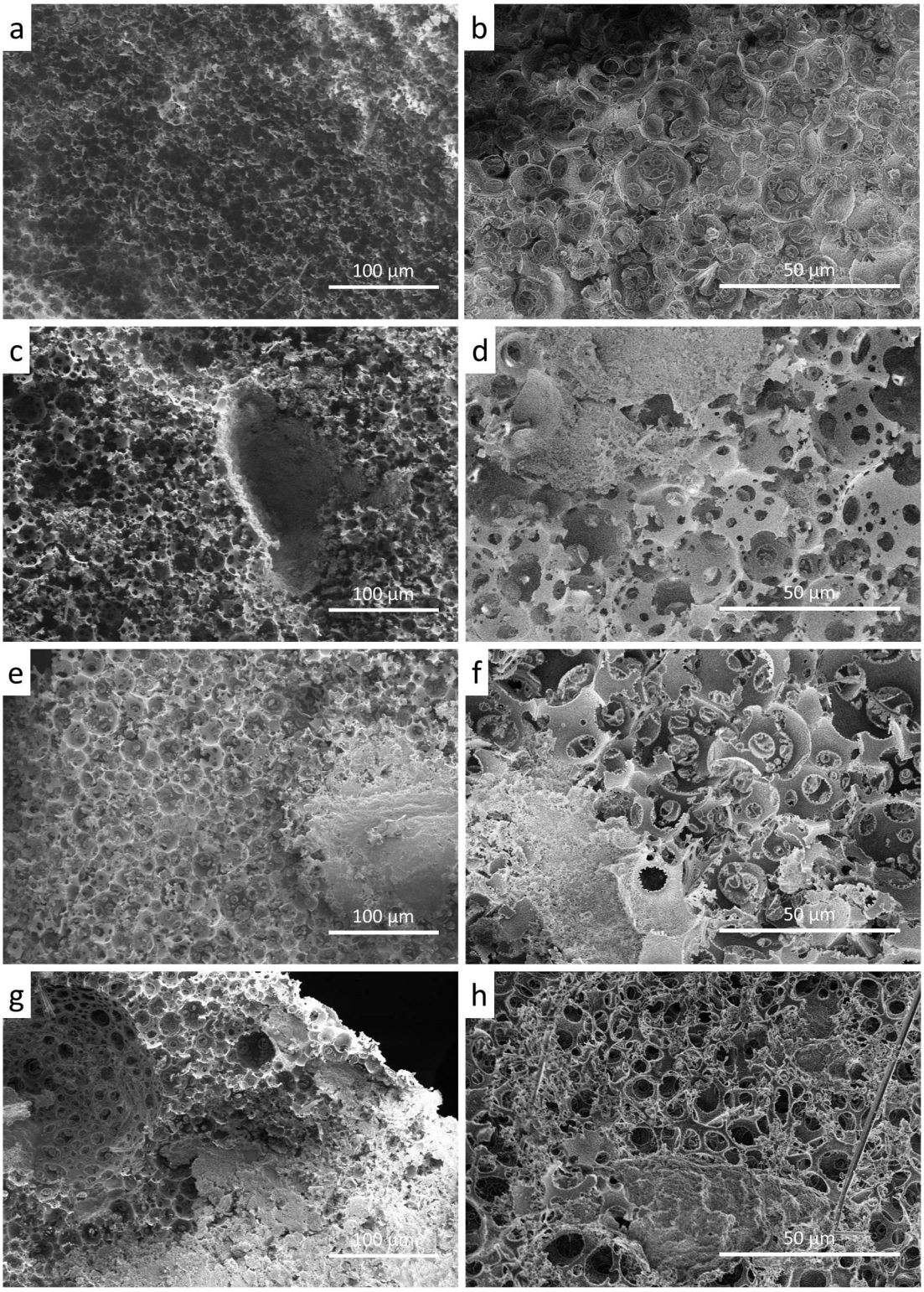

Figure 39 SEM images of UiO-66-NH_2 MOF@polyHIPE composites with 50% crosslinker. a, b: 0% MOF; c, d: 10% MOF; e, f: 30% MOF; g, h: 60% MOF

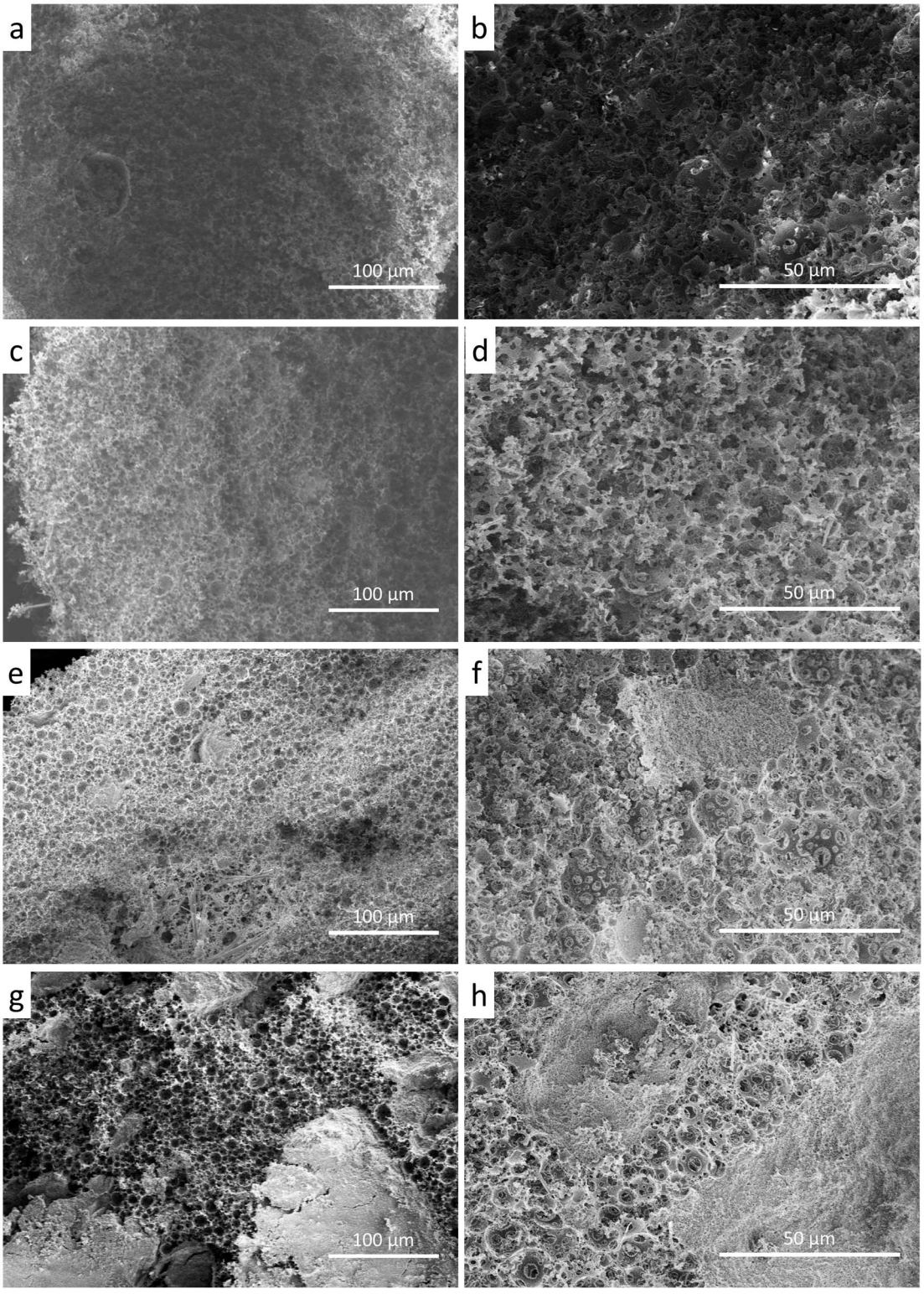

Figure 40 SEM images of UiO-66-NH_2 MOF@polyHIPE composites with 80% crosslinker. a, b: 0% MOF; c, d: 10% MOF; e, f: 30% MOF; g, h: 60% MOF

REFERENCES

1. Yang, Y.-C., Chemical Detoxification of Nerve Agent VX. *Accounts of Chemical Research* **1999,** *32* (2), 109-115.

2. DeCoste, J. B.; Peterson, G. W., Metal-Organic Frameworks for Air Purification of Toxic Chemicals. *Chemical Reviews* **2014,** *114* (11), 5695-5727.

3. Bobbitt, N. S.; Mendonca, M. L.; Howarth, A. J.; Islamoglu, T.; Hupp, J. T.; Farha, O. K.; Snurr, R. Q., Metal-organic frameworks for the removal of toxic industrial chemicals and chemical warfare agents. *Chemical Society reviews* **2017,** *46* (11), 3357-3385.

4. Hincal, F.; Erkekuglu, P., Toxic Industrial Chemicals (TICs) - Chemical Warfare Without Chemical Weapons. *FABAD Journal of Pharmaceutical Science* **2006,** *31* (4), 220-229.

5. Barea, E.; Montoro, C.; Navarro, J. A., Toxic gas removal--metal-organic frameworks for the capture and degradation of toxic gases and vapours. *Chemical Society reviews* **2014,** *43* (16), 5419-30.

6. Morrison, R. W., NBC Filter Performance. Edgewood Chemical Biological Center: Aberdeen Proving Ground, MD, 2001.

7. Center, U. A. E. C. B., Detail Specification: Carbon, activated, impregnated, copper-silver-zinc-molybdenum-triethylenediamine (ASZM-TEDA). Defense, D. o., Ed. 2002.

8. Espinal, L.; Poster, D. L.; Wong-Ng, W.; Allen, A. J.; Green, M. L., Measurement, Standards, and Data Needs for CO2 Capture Materials: A Critical Review. *Environmental Science & Technology* **2013,** *47* (21), 11960-11975.

9. Sircar, S., Basic Research Needs for Design of Adsorptive Gas Separation Processes. *Ind. Eng. Chem. Res.* **2006,** *45* (16), 5435-5448.

10. Ferey, G., Hybrid porous solids: past, present, future. *Chemical Society reviews* **2008,** *37* (1), 191-214.

11. Katz, M. J.; Mondloch, J. E.; Totten, R. K.; Park, J. K.; Nguyen, S. T.; Farha, O. K.; Hupp, J. T., Simple and Compelling Biomimetic Metal-Organic Framework Catalyst for the Degradation of Nerve Agent Simulants. *Angewandte Chemie-International Edition* **2014,** *53* (2), 497-501.

12. Jiang, J.; Yaghi, O. M., Brønsted Acidity in Metal–Organic Frameworks. *Chemical Reviews* **2015,** *115* (14), 6966-6997.

13. Zhou, F.; Lu, N.; Fan, B.; Wang, H.; Li, R., Zirconium-containing UiO-66 as an efficient and reusable catalyst for transesterification of triglyceride with methanol. *Journal of Energy Chemistry* **2016,** *25* (5), 874-879.

14. Rowsell, J. L. C.; Yaghi, O. M., Strategies for Hydrogen Storage in Metal–Organic Frameworks. *Angewandte Chemie International Edition* **2005,** *44* (30), 4670-4679.

15. Tagliabue, M.; Rizzo, C.; Millini, R.; Dietzel, P. D. C.; Blom, R.; Zanardi, S., Methane storage on CPO-27-Ni pellets. *Journal of Porous Materials* **2010,** *18* (3), 289-296.

16. Peterson, G. W.; Mahle, J. J.; DeCoste, J. B.; Gordon, W. O.; Rossin, J. A., Extraordinary NO2 Removal by the Metal–Organic Framework UiO-66-NH2. *Angewandte Chemie International Edition* **2016,** *55* (21), 6235-6238.

17. Darunte, L. A.; Oetomo, A. D.; Walton, K. S.; Sholl, D. S.; Jones, C. W., Direct Air Capture of CO2 Using Amine Functionalized MIL-101(Cr). *ACS Sustainable Chemistry & Engineering* **2016,** *4* (10), 5761-5768.

18. Pimentel, B. R.; Parulkar, A.; Zhou, E.-k.; Brunelli, N. A.; Lively, R. P., Zeolitic Imidazolate Frameworks: Next-Generation Materials for Energy-Efficient Gas Separations. *ChemSusChem* **2014,** *7* (12), 3202-3240.

19. Wales, D. J.; Grand, J.; Ting, V. P.; Burke, R. D.; Edler, K. J.; Bowen, C. R.; Mintova, S.; Burrows, A. D., Gas sensing using porous materials for automotive applications. *Chemical Society reviews* **2015,** *44* (13), 4290-4321.

20. Lu, G.; Hupp, J. T., Metal−Organic Frameworks as Sensors: A ZIF-8 Based Fabry−Pérot Device as a Selective Sensor for Chemical Vapors and Gases. *Journal of the American Chemical Society* **2010,** *132* (23), 7832-7833.

21. Wu, Y.-n.; Li, F.; Xu, Y.; Zhu, W.; Tao, C.-a.; Cui, J.; Li, G., Facile fabrication of photonic MOF films through stepwise deposition on a colloid crystal substrate. *Chemical Communications* **2011,** *47* (36), 10094-10096.

22. Deng, H.; Doonan, C. J.; Furukawa, H.; Ferreira, R. B.; Towne, J.; Knobler, C. B.; Wang, B.; Yaghi, O. M., Multiple Functional Groups of Varying Ratios in Metal-Organic Frameworks. *Science* **2010,** *327* (5967), 846-850.

23. Cmarik, G. E.; Kim, M.; Cohen, S. M.; Walton, K. S., Tuning the Adsorption Properties of UiO-66 via Ligand Functionalization. *Langmuir* **2012,** *28* (44), 15606-15613.

24. Jasuja, H.; Jiao, Y.; Burtch, N. C.; Huang, Y.-g.; Walton, K. S., Synthesis of Cobalt-, Nickel-, Copper-, and Zinc-Based, Water-Stable, Pillared Metal–Organic Frameworks. *Langmuir* **2014,** *30* (47), 14300-14307.

25. Eddaoudi, M.; Moler, D. B.; Li, H.; Chen, B.; Reineke, T. M.; O'Keeffe, M.; Yaghi, O. M., Modular Chemistry: Secondary Building Units as a Basis for the Design of Highly

Porous and Robust Metal−Organic Carboxylate Frameworks. *Accounts of Chemical Research* **2001,** *34* (4), 319-330.

26. Cavka, J. H.; Jakobsen, S.; Olsbye, U.; Guillou, N.; Lamberti, C.; Bordiga, S.; Lillerud, K. P., A New Zirconium Inorganic Building Brick Forming Metal Organic Frameworks with Exceptional Stability. *Journal of the American Chemical Society* **2008,** *130* (42), 13850-13851.

27. DeCoste, J. B.; Peterson, G. W.; Jasuja, H.; Glover, T. G.; Huang, Y.-g.; Walton, K. S., Stability and degradation mechanisms of metal-organic frameworks containing the Zr6O4(OH)4 secondary building unit. *Journal of Materials Chemistry A* **2013,** *1* (18), 5642-5650.

28. Burtch, N. C.; Jasuja, H.; Walton, K. S., Water Stability and Adsorption in Metal-Organic Frameworks. *Chemical Reviews* **2014,** *114* (20), 10575-10612.

29. Peterson, G. W.; DeCoste, J. B.; Fatollahi-Fard, F.; Britt, D. K., Engineering UiO-66-NH2 for Toxic Gas Removal. *Ind. Eng. Chem. Res.* **2014,** *53* (2), 701-707.

30. Schaate, A.; Roy, P.; Godt, A.; Lippke, J.; Waltz, F.; Wiebcke, M.; Behrens, P., Modulated synthesis of Zr-based metal-organic frameworks: from nano to single crystals. *Chemistry* **2011,** *17* (24), 6643-51.

31. Kim, M.; Cohen, S. M., Discovery, development, and functionalization of Zr(iv)-based metal-organic frameworks. *CrystEngComm* **2012,** *14* (12), 4096-4104.

32. DeCoste, J. B.; Demasky, T. J.; Katz, M. J.; Farha, O. K.; Hupp, J. T., A UiO-66 analogue with uncoordinated carboxylic acids for the broad-spectrum removal of toxic chemicals. *New Journal of Chemistry* **2015,** *39* (4), 2396-2399.

33. Piscopo, C. G.; Trapani, F.; Polyzoidis, A.; Schwarzer, M.; Pace, A.; Loebbecke, S., Positive effect of the fluorine moiety on the oxygen storage capacity of UiO-66 metal-organic frameworks. *New Journal of Chemistry* **2016,** *40* (10), 8220-8224.

34. Ren, J.; Ledwaba, M.; Musyoka, N. M.; Langmi, H. W.; Mathe, M.; Liao, S.; Pang, W., Structural defects in metal–organic frameworks (MOFs): Formation, detection and control towards practices of interests. *Coordination Chemistry Reviews* **2017,** *349* (Supplement C), 169-197.

35. Katz, M. J.; Moon, S.-Y.; Mondloch, J. E.; Beyzavi, M. H.; Stephenson, C. J.; Hupp, J. T.; Farha, O. K., Exploiting parameter space in MOFs: a 20-fold enhancement of phosphate-ester hydrolysis with UiO-66-NH2. *Chemical Science* **2015,** *6* (4), 2286-2291.

36. Jasuja, H.; Peterson, G. W.; Decoste, J. B.; Browe, M. A.; Walton, K. S., Evaluation of MOFs for air purification and air quality control applications: Ammonia removal from air. *Chemical Engineering Science* **2015,** *124*, 118-124.

37. Rezaei, F.; Webley, P., Structured adsorbents in gas separation processes. *Separation and Purification Technology* **2010,** *70* (3), 243-256.

38. Hashimoto, N.; Smith, J. M., Macropore Diffusion in Molecular Sieve Pellets by Chromatography. *Industrial & Engineering Chemistry Fundamentals* **1973,** *12* (3), 353-359.

39. Peterson, G. W.; DeCoste, J. B.; Glover, T. G.; Huang, Y. G.; Jasuja, H.; Walton, K. S., Effects of pelletization pressure on the physical and chemical properties of the metal-organic frameworks Cu-3(BTC)(2) and UiO-66. *Microporous and Mesoporous Materials* **2013,** *179*, 48-53.

40. Rezaei, F.; Sakwa-Novak, M. A.; Bali, S.; Duncanson, D. M.; Jones, C. W., Shaping amine-based solid CO2 adsorbents: Effects of pelletization pressure on the physical and chemical properties. *Microporous and Mesoporous Materials* **2015,** *204*, 34-42.

41. Fu, Y. Y.; Yang, C. X.; Yan, X. P., Incorporation of metal-organic framework UiO-66 into porous polymer monoliths to enhance the liquid chromatographic separation of small molecules. *Chemical Communications* **2013,** *49* (64), 7162-7164.

42. Moitra, N.; Fukumoto, S.; Reboul, J.; Sumida, K.; Zhu, Y.; Nakanishi, K.; Furukawa, S.; Kitagawa, S.; Kanamori, K., Mechanically stable, hierarchically porous Cu3(btc)2 (HKUST-1) monoliths via direct conversion of copper(ii) hydroxide-based monoliths. *Chemical Communications* **2015,** *51* (17), 3511-3514.

43. Li, Y. Y.; Perera, S. P.; Crittenden, B. D., Zeolite Monoliths for Air Separation: Part 1: Manufacture and Characterization. *Chemical Engineering Research and Design* **1998,** *76* (8), 921-930.

44. Li, Y. Y.; Perera, S. P.; Crittenden, B. D., Zeolite Monoliths for Air Separation: Part 2: Oxygen Enrichment, Pressure Drop and Pressurization. *Chemical Engineering Research and Design* **1998,** *76* (8), 931-941.

45. Li, G.; Singh, R.; Li, D.; Zhao, C. X.; Liu, L. Y.; Webley, P. A., Synthesis of biomorphic zeolite honeycomb monoliths with 16 000 cells per square inch. *Journal of Materials Chemistry* **2009,** *19* (44), 8372-8377.

46. Darunte, L. A.; Terada, Y.; Murdock, C. R.; Walton, K. S.; Sholl, D. S.; Jones, C. W., Monolith-Supported Amine-Functionalized Mg2(dobpdc) Adsorbents for CO2 Capture. *ACS Applied Materials & Interfaces* **2017**.

47. Hong, W. Y.; Perera, S. P.; Burrows, A. D., Manufacturing of metal-organic framework monoliths and their application in CO2 adsorption. *Microporous and Mesoporous Materials* **2015,** *214*, 149-155.

48. Küsgens, P.; Zgaverdea, A.; Fritz, H.-G.; Siegle, S.; Kaskel, S., Metal-Organic Frameworks in Monolithic Structures. *Journal of the American Ceramic Society* **2010,** *93* (9), 2476-2479.

49. Adatoz, E.; Avci, A. K.; Keskin, S., Opportunities and challenges of MOF-based membranes in gas separations. *Separation and Purification Technology* **2015,** *152*, 207-237.

50. Qiu, S.; Xue, M.; Zhu, G., Metal-organic framework membranes: from synthesis to separation application. *Chemical Society reviews* **2014,** *43* (16), 6116-6140.

51. Tanh Jeazet, H. B.; Staudt, C.; Janiak, C., Metal-organic frameworks in mixed-matrix membranes for gas separation. *Dalton Transactions* **2012,** *41* (46), 14003-14027.

52. DeCoste, J. B.; Denny, J. M. S.; Peterson, G. W.; Mahle, J. J.; Cohen, S. M., Enhanced aging properties of HKUST-1 in hydrophobic mixed-matrix membranes for ammonia adsorption. *Chemical Science* **2016,** *7* (4), 2711-2716.

53. Moreton, J. C.; Denny, M. S.; Cohen, S. M., High MOF loading in mixed-matrix membranes utilizing styrene/butadiene copolymers. *Chemical Communications* **2016,** *52* (100), 14376-14379.

54. Su, N. C.; Sun, D. T.; Beavers, C. M.; Britt, D. K.; Queen, W. L.; Urban, J. J., Enhanced permeation arising from dual transport pathways in hybrid polymer-MOF membranes. *Energy & Environmental Science* **2016,** *9* (3), 922-931.

55. Küsgens, P.; Siegle, S.; Kaskel, S., Crystal Growth of the Metal—Organic Framework Cu3(BTC)2 on the Surface of Pulp Fibers. *Advanced Engineering Materials* **2009,** *11* (1-2), 93-95.

56. da Silva Pinto, M.; Sierra-Avila, C. A.; Hinestroza, J. P., In situ synthesis of a Cu-BTC metal–organic framework (MOF 199) onto cellulosic fibrous substrates: cotton. *Cellulose* **2012,** *19* (5), 1771-1779.

57. Zhao, J.; Losego, M. D.; Lemaire, P. C.; Williams, P. S.; Gong, B.; Atanasov, S. E.; Blevins, T. M.; Oldham, C. J.; Walls, H. J.; Shepherd, S. D.; Browe, M. A.; Peterson, G. W.; Parsons, G. N., Highly Adsorptive, MOF-Functionalized Nonwoven Fiber Mats for Hazardous Gas Capture Enabled by Atomic Layer Deposition. *Advanced Materials Interfaces* **2014,** *1* (4), n/a-n/a.

58. Chen, G.; Koros, W. J.; Jones, C. W., Hybrid Polymer/UiO-66(Zr) and Polymer/NaY Fiber Sorbents for Mercaptan Removal from Natural Gas. *ACS Applied Materials & Interfaces* **2016,** *8* (15), 9700-9709.

59. Lively, R. P.; Chance, R. R.; Mysona, J. A.; Babu, V. P.; Deckman, H. W.; Leta, D. P.; Thomann, H.; Koros, W. J., CO2 sorption and desorption performance of thermally cycled hollow fiber sorbents. *International Journal of Greenhouse Gas Control* **2012,** *10*, 285-294.

60. Ostermann, R.; Cravillon, J.; Weidmann, C.; Wiebcke, M.; Smarsly, B. M., Metal-organic framework nanofibers viaelectrospinning. *Chemical Communications* **2011,** *47* (1), 442-444.

61. Lu, A. X.; McEntee, M.; Browe, M. A.; Hall, M. G.; DeCoste, J. B.; Peterson, G. W., MOFabric: Electrospun Nanofiber Mats from PVDF/UiO-66-NH2 for Chemical Protection and Decontamination. *ACS Applied Materials & Interfaces* **2017,** *9* (15), 13632-13636.

62. Peterson, G. W.; Lu, A. X.; Epps, T. H., Tuning the Morphology and Activity of Electrospun Polystyrene/UiO-66-NH2 Metal–Organic Framework Composites to Enhance Chemical Warfare Agent Removal. *ACS Applied Materials & Interfaces* **2017**.

63. Cameron, N. R., High internal phase emulsion templating as a route to well-defined porous polymers. *Polymer* **2005,** *46* (5), 1439-1449.

64. Silverstein, M. S.; Cameron, N. R., PolyHIPEs — Porous Polymers from High Internal Phase Emulsions. In *Encyclopedia of Polymer Science and Technology*, John Wiley & Sons, Inc.: 2002.

65. Hainey, P.; Huxham, I. M.; Rowatt, B.; Sherrington, D. C.; Tetley, L., Synthesis and ultrastructural studies of styrene-divinylbenzene Polyhipe polymers. *Macromolecules* **1991,** *24* (1), 117-121.

66. Ruckenstein, E.; Hong, L., Binding catalytic sites to the surface of porous polymers and some catalytic applications. *Chemistry of Materials* **1992,** *4* (1), 122-127.

67. Zhang, H.; Cooper, A. I., Synthesis of monodisperse emulsion-templated polymer beads by oil-in-water-in-oil (O/W/O) sedimentation polymerization. *Chemistry of Materials* **2002,** *14* (10), 4017-+.

68. Krajnc, P.; Štefanec, D.; Pulko, I., Acrylic Acid "Reversed" PolyHIPEs. *Macromolecular Rapid Communications* **2005,** *26* (16), 1289-1293.

69. Schwab, M. G.; Senkovska, I.; Rose, M.; Koch, M.; Pahnke, J.; Jonschker, G.; Kaskel, S., MOF@PolyHIPEs. *Advanced Engineering Materials* **2008,** *10* (12), 1151-1155.

70. O'Neill, L. D.; Zhang, H.; Bradshaw, D., Macro-/microporous MOF composite beads. *Journal of Materials Chemistry* **2010,** *20* (27), 5720-5726.

71. Pinto, M. L.; Dias, S.; Pires, J., Composite MOF Foams: The Example of UiO-66/Polyurethane. *ACS Applied Materials & Interfaces* **2013,** *5* (7), 2360-2363.

72. Le Calvez, C.; Zouboulaki, M.; Petit, C.; Peeva, L.; Shirshova, N., One step synthesis of MOF-polymer composites. *Rsc Advances* **2016,** *6* (21), 17314-17317.

73. Zhu, H.; Zhang, Q.; Zhu, S., Assembly of a Metal–Organic Framework into 3 D Hierarchical Porous Monoliths Using a Pickering High Internal Phase Emulsion Template. *Chemistry – A European Journal* **2016,** *22* (26), 8751-8755.

74. Wickenheisser, M.; Janiak, C., Hierarchical embedding of micro-mesoporous MIL-101(Cr) in macroporous poly(2-hydroxyethyl methacrylate) high internal phase emulsions with monolithic shape for vapor adsorption applications. *Microporous and Mesoporous Materials* **2015,** *204*, 242-250.

75. Kovačič, S.; Štefanec, D.; Krajnc, P., Highly Porous Open-Cellular Monoliths from 2-Hydroxyethyl Methacrylate Based High Internal Phase Emulsions (HIPEs): Preparation and Void Size Tuning. *Macromolecules* **2007,** *40* (22), 8056-8060.

76. Wang, Z.; Cohen, S. M., Postsynthetic modification of metal-organic frameworks. *Chemical Society reviews* **2009,** *38* (5), 1315-1329.

77. Hintz, H.; Wuttke, S., Solvent-Free and Time Efficient Postsynthetic Modification of Amino-Tagged Metal–Organic Frameworks with Carboxylic Acid Derivatives. *Chemistry of Materials* **2014,** *26* (23), 6722-6728.

78. Tanabe, K. K.; Wang, Z.; Cohen, S. M., Systematic Functionalization of a Metal−Organic Framework via a Postsynthetic Modification Approach. *Journal of the American Chemical Society* **2008,** *130* (26), 8508-8517.

79. Binks, B. P., Particles as surfactants—similarities and differences. *Current Opinion in Colloid & Interface Science* **2002,** *7* (1–2), 21-41.

80. Hunter, T. N.; Pugh, R. J.; Franks, G. V.; Jameson, G. J., The role of particles in stabilising foams and emulsions. *Advances in Colloid and Interface Science* **2008,** *137* (2), 57-81.

81. Yang, F.; Liu, S.; Xu, J.; Lan, Q.; Wei, F.; Sun, D., Pickering emulsions stabilized solely by layered double hydroxides particles: The effect of salt on emulsion formation and stability. *Journal of Colloid and Interface Science* **2006,** *302* (1), 159-169.

82. Hua, Y.; Zhang, S.; Zhu, Y.; Chu, Y.; Chen, J., Hydrophilic polymer foams with well-defined open-cell structure prepared from pickering high internal phase emulsions. *Journal of Polymer Science Part A: Polymer Chemistry* **2013,** *51* (10), 2181-2187.

83. Perrin, E.; Bizot, H.; Cathala, B.; Capron, I., Chitin Nanocrystals for Pickering High Internal Phase Emulsions. *Biomacromolecules* **2014,** *15* (10), 3766-3771.

84. Rezaei, F.; Webley, P., Optimum structured adsorbents for gas separation processes. *Chemical Engineering Science* **2009,** *64* (24), 5182-5191.

85. Crittenden, B.; Patton, A.; Jouin, C.; Perera, S.; Tennison, S.; Echevarria, J. A. B., Carbon monoliths: A comparison with granular materials. *Adsorption-Journal of the International Adsorption Society* **2005,** *11*, 537-541.

86. López-Maya, E.; Montoro, C.; Rodríguez-Albelo, L. M.; Aznar Cervantes, S. D.; Lozano-Pérez, A. A.; Cenís, J. L.; Barea, E.; Navarro, J. A. R., Textile/Metal–Organic-Framework Composites as Self-Detoxifying Filters for Chemical-Warfare Agents. *Angewandte Chemie International Edition* **2015,** *54* (23), 6790-6794.

87. Meilikhov, M.; Yusenko, K.; Schollmeyer, E.; Mayer, C.; Buschmann, H.-J.; Fischer, R. A., Stepwise deposition of metal organic frameworks on flexible synthetic polymer surfaces. *Dalton Transactions* **2011,** *40* (18), 4838-4841.

88. Sinha-Ray, S.; Yarin, A. L.; Pourdeyhimi, B., Meltblowing: I-basic physical mechanisms and threadline model. *Journal of Applied Physics* **2010,** *108* (3).

89. Amid, H.; Mazé, B.; Flickinger, M. C.; Pourdeyhimi, B., Hybrid adsorbent nonwoven structures: a review of current technologies. *Journal of Materials Science* **2016,** *51* (9), 4173-4200.

90. Huang, Z.-M.; Zhang, Y. Z.; Kotaki, M.; Ramakrishna, S., A review on polymer nanofibers by electrospinning and their applications in nanocomposites. *Composites Science and Technology* **2003,** *63* (15), 2223-2253.

91. Casasola, R.; Thomas, N. L.; Trybala, A.; Georgiadou, S., Electrospun poly lactic acid (PLA) fibres: Effect of different solvent systems on fibre morphology and diameter. *Polymer* **2014,** *55* (18), 4728-4737.

92. Luo, C. J.; Stoyanov, S. D.; Stride, E.; Pelan, E.; Edirisinghe, M., Electrospinning versus fibre production methods: from specifics to technological convergence. *Chemical Society reviews* **2012,** *41* (13), 4708-4735.

93. Medeiros, E. S.; Glenn, G. M.; Klamczynski, A. P.; Orts, W. J.; Mattoso, L. H. C., Solution blow spinning: A new method to produce micro- and nanofibers from polymer solutions. *Journal of Applied Polymer Science* **2009,** *113* (4), 2322-2330.

94. Sinha-Ray, S.; Zhang, Y.; Yarin, A. L.; Davis, S. C.; Pourdeyhimi, B., Solution blowing of soy protein fibers. *Biomacromolecules* **2011,** *12* (6), 2357-2363.

95. Da Silva Parize, D. D.; De Oliveira, J. E.; Foschini, M. M.; Marconcini, J. M.; Mattoso, L. H. C., Poly(lactic acid) fibers obtained by solution blow spinning: Effect of a greener solvent on the fiber diameter. *Journal of Applied Polymer Science* **2016,** *133* (18).

96. Rajgarhia, S. S.; Benavides, R. E.; Jana, S. C., Morphology control of bi-component polymer nanofibers produced by gas jet process. *Polymer* **2016,** *93*, 142-151.

97. Daristotle, J. L.; Behrens, A. M.; Sandler, A. D.; Kofinas, P., A Review of the Fundamental Principles and Applications of Solution Blow Spinning. *ACS Applied Materials & Interfaces* **2016,** *8* (51), 34951-34963.

98. Kolbasov, A.; Sinha-Ray, S.; Joijode, A.; Hassan, M. A.; Brown, D.; Maze, B.; Pourdeyhimi, B.; Yarin, A. L., Industrial-Scale Solution Blowing of Soy Protein Nanofibers. *Ind. Eng. Chem. Res.* **2016,** *55* (1), 323-333.

99. Hong, D.-Y.; Hwang, Y. K.; Serre, C.; Férey, G.; Chang, J.-S., Porous Chromium Terephthalate MIL-101 with Coordinatively Unsaturated Sites: Surface Functionalization, Encapsulation, Sorption and Catalysis. *Advanced Functional Materials* **2009,** *19* (10), 1537-1552.

100. Wisser, D.; Wisser, F. M.; Raschke, S.; Klein, N.; Leistner, M.; Grothe, J.; Brunner, E.; Kaskel, S., Biological Chitin–MOF Composites with Hierarchical Pore Systems for Air-Filtration Applications. *Angewandte Chemie International Edition* **2015,** *54* (43), 12588-12591.

101. Lin, J.; Ding, B.; Yu, J.; Hsieh, Y., Direct Fabrication of Highly Nanoporous Polystyrene Fibers via Electrospinning. *ACS Applied Materials & Interfaces* **2010,** *2* (2), 521-528.

102. Megelski, S.; Stephens, J. S.; Chase, D. B.; Rabolt, J. F., Micro- and Nanostructured Surface Morphology on Electrospun Polymer Fibers. *Macromolecules* **2002,** *35* (22), 8456-8466.

103. Casper, C. L.; Stephens, J. S.; Tassi, N. G.; Chase, D. B.; Rabolt, J. F., Controlling Surface Morphology of Electrospun Polystyrene Fibers: Effect of Humidity and Molecular Weight in the Electrospinning Process. *Macromolecules* **2004,** *37* (2), 573-578.

104. Kosuri, M. R.; Koros, W. J., Defect-free asymmetric hollow fiber membranes from Torlon®, a polyamide–imide polymer, for high-pressure CO2 separations. *Journal of Membrane Science* **2008,** *320* (1–2), 65-72.

105. van de Witte, P.; Dijkstra, P. J.; van den Berg, J. W. A.; Feijen, J., Phase separation processes in polymer solutions in relation to membrane formation. *Journal of Membrane Science* **1996,** *117* (1), 1-31.

106. Qi, Z.; Yu, H.; Chen, Y.; Zhu, M., Highly porous fibers prepared by electrospinning a ternary system of nonsolvent/solvent/poly(l-lactic acid). *Materials Letters* **2009,** *63* (3), 415-418.

107. Yu, X.; Xiang, H.; Long, Y.; Zhao, N.; Zhang, X.; Xu, J., Preparation of porous polyacrylonitrile fibers by electrospinning a ternary system of PAN/DMF/H2O. *Materials Letters* **2010,** *64* (22), 2407-2409.